UNIVERSITY OF TWENTE.

Deltares

Wave-driven dynamics of Shoreward Propagating Accretionary Waves in the Nearshore

Lianne van der Weerd

19th of October, 2012

Graduation committee

Dr. Ir. J.S. Ribberink	(University of Twente)
Dr. K.M. Wijnberg	(University of Twente)
Dr. Ir. J.J. van der Werf	(Deltares and University of Twente)
Ir. D.J.R. Walstra	(Deltares)

Deltares

Title
Wave-driven dynamics of Shoreward Propagating Accretionary Waves in the Nearshore

Pages
118

Keywords
Nearshore bar, nearshore processes, Delft3D, SPAW, Duck (North Carolina, USA), nourishment, humplike nourishments.

Summary
A new phenomenon in the evolution of nearshore topography is a small-scale natural mode of shoreface nourishments observed by Wijnberg and Holman (2007). It is referred to as Shoreward Propagating Accretionary Waves (SPAWs) and is a bar-like feature shed of from the nearshore bar. It is observed to transit the through between bar and shore as an intact form. This study identified which nearshore processes control the shoreward propagation of a SPAW phenomenon after it has been initiated.

The wave-driven flow field and related initial sediment transport patterns were simulated with a three-dimensional Delft3D model with a high spatial and temporal resolution. Based on statistics of SPAWs observed near Duck (North Carolina, USA) (Wijnberg and Holman, 2007) a schematized bathymetry was defined and typical wave conditions were selected (H_s=0.56 m and T_p=8.2 s). Additional to this base case, the influence on initial sedimentation and erosion patterns was assessed of different water levels, SPAW size and location, and nearshore bar geometry.

Results showed that under typically prevailing wave conditions the process of wave transformation (i.e. increasing wave skewness and asymmetry) over the SPAW is important to generate onshore sediment transports over the feature. Near-bed transport processes in the direction of wave propagation due to wave asymmetry were dominant in all cases. These processes consisted of (i) bed load transport due to waves and currents, and (ii) suspended load due to wave asymmetry. Furthermore, the process of local wave breaking (i.e. energy dissipation), generates a horizontal circulation current around the SPAW. Since near-bed transport is dominant for our cases with a low wave height, it was shown that the generated circulation pattern did hardly influence sediment transport patterns over the SPAW. The onshore transports over the SPAW result in a shoreward displacement of the SPAW, consistent with SPAW observations in nature. This pattern persisted for different water levels, different SPAW sizes and location, and different nearshore bathymetry.

References

Version	Date	Author	Initials	Review	Initials	Approval	Initials
1	Oct. 2012	Van der Weerd	A.J.				

State
final

Preface

This report is the final step for me to finish the Master Water Engineering and Management at the University of Twente. It was carried out at the unit Marine and Coastal Systems at Deltares where I experienced an ambitious and work friendly atmosphere. This study introduced me to interesting aspects of nearshore processes. Also I learned a lot about modelling, interpreting results, planning a research, and reading and writing a scientific report. For the modelling part a challenging aspect was to deal with setbacks. Sometimes it felt like an Old Dutch game of "Ganzenbord", in which you can get the frustrating task to go back to start and begin all over. Nevertheless, also attempts that did not work were worth it, since it always gives you new insights. All in all, doing this Master Thesis was a good opportunity to learn a lot.

I would like to acknowledge the Field Research Facility in Duck (North Carolina, USA) for using the bathymetry and wave conditions data for Duck. Also I would like to acknowledge Larry Hsu and Jebbe van der Werf for sharing their Delft3D model of the SandyDuck cases. Furthermore, I would like to acknowledge Kathelijne Wijnberg and Rob Holman for providing me SPAW observation data that I could use during this study.

Many persons supported me which I would all like to thank, starting with my supervisors. Jan Ribberink, he showed his contagiously enthusiasm for the field of study already in the 2nd year of the Bachelor. During this research he gave me insight in the value of this study within literature. Another person was Dirk-Jan Walstra, I could always pass by to ask questions regarding modelling and he was always able to put things in perspective when it seemed like the model was not working at all. Also Jebbe van der Werf was always there to help. Thank you for all the valuable discussions, patience and help while doing this research. And finally, I would like to thank Kathelijne Wijnberg for all her enthusiasm about the topic and the trust you put into me, her patience and last-minute reading through pieces of work. I enjoyed working with all of you very much, and you all certainly encouraged and taught me a lot! Also I would like to thank Dano Roelvink for his help on interpreting modelling results and his suggestions to improve the model schematization. And Maarten van Ormondt for his help on modelling issues, but also for providing me the Muppet tool to produce fancy figures. And off course, I should not forget the other Deltares employees which I could bother at any time to ask a question. Also the students were good company during my time at Deltares, with the nice coffee break at 3 'o clock, dinners and Friday afternoon drinks.

Besides all the persons from the University and Deltares, also I would like to thank Nienke for being my "afstudeerbuddy", for her good comments and questions which improved the report. Renske for giving me mental support even though she was in Zambia and Renée for her positive notes, her patience to listen to the stories about modelling issues, and her ability to put things in perspectives. Last but not least, my parents, sister and brother for being there, no matter what.

I hope you enjoy reading the report, please let me know your opinion!

Lianne van der Weerd

Delft, 19 October 2012

Summary

A new phenomenon in the evolution of nearshore topagrophy, is a small-scale natural mode of shoreface nourishments observed by Wijnberg and Holman (2007). It is formed during a natural process in which a small bar-shaped feature separates at the landward side from a nearshore bar, then propagates onshore, and eventually merges with the beach. This phenomenon, also referred to as Shoreward Propagating Accretionary Wave (SPAW), is observed at several beaches. The feature represents a locally significant onshore sediment flux. SPAWs observed at Duck (USA) have an average length of 126 +/- 60 m and a width of 30 +/- 10 m, which gives an indication of the scale of the feature. At present, it is unclear which processes explain this phenomenon. Knowing more about SPAW dynamics is important for two main reasons; (i) it will improve current knowledge about nearshore morphodynamics, and (ii) the onshore propagation process of a SPAW has possible relevance for sand nourishment techniques, which in The Netherlands currently focus on large scale nourishments.

The objective of this study is to identify which nearshore processes control the shoreward propagation of a SPAW phenomenon after it has been initiated. Besides that, the influence of water depth, SPAW size and location, and nearshore bar topography of the feature on SPAW dynamics are investigated.

Investigating SPAW dynamics was done by studying wave-driven flow fields and related initial sediment transport patterns. Starting with formulating a hypothesis for the wave-driven flow field and sediment transport patterns based on literature. It was hypothesized that a horizontal circulation current would develop in the wave-driven flow field, and that the sediment transport over the SPAW would be onshore directed due to non-linear wave transformation. To test this hypothesis, a schematized 3-dimensional Delft3D model was set up for the beach Duck (North Carolina, USA).The model schematization is based on earlier schematizations made by Hsu et al. (2006, 2008), Van der Werf (2009) and Treffers (2009). It was adjusted by refining the grid, in order to have a better resolution around the SPAW. Additionally, model input such as bathymetry and typical wave conditions (H_s=0.56 m and T_p=8.2 s) were based on a representative SPAW event at Duck, since most observations are done at this site.

Results show that wave height varied locally since waves break over the feature, by which energy is dissipated. These variations in wave height induce cross-shore and longshore gradients in radiation stress, which generates local set-up (or relative set-down). These variations in water level cause longshore pressure gradients, which induce currents. As a result, a horizontal circulation current develops around the SPAW tips, which is onshore directed over the crest and offshore directed around the SPAW. The Eulerian flow pattern was dominated by the undertow, induced by wave breaking at the coast. The modulated wave-driven flow field accross a SPAW was such that near-bed sand transport processes were dominant and onshore directed. These processes consisted of (i) bed load transport due to waves and currents, and (ii) suspended load transport due to wave assymetry. The sediment transport contributions result in a shoreward displacement of the SPAW, namely erosion occurs seaward and sedimentation occurs just landward of the feature. Results are consistent with the formulated hypothesis based on literature, and with SPAW observations done by Argus video systems and also with previous estimates of sediment fluxes (Wijnberg and Holman, 2007).

The shoreward displacement pattern persisted for different water levels, different SPAW size and location, and different nearshore bar geometry. Water levels influenced the wave-driven flow field which made them differ from the base case, whereas sediment transport patterns were similar. The latter is due to the fact that near-bed sediment transport is dominant. SPAW location was observed to influence the wave-driven flow field; for SPAWs located closer to the bar a stronger horizontal circulation cell developed over the full length of the SPAW crest. Consequently, sediment transports were higher over the full lenght of the SPAW crest for this case, whereas for a SPAW located closer to shore sediment transport was concentrated at the tips. Compared to the base case for a wider SPAW a stronger horizontal circulation current developed. For a longer SPAW, the horizontal circulation current developed around the tips, for the centre of the longer SPAW no effects of the horizontal circulation currents were seen. The change of local geometry of the nearshore bar, largely influenced the flow-field. For this case the depth averaged flow field differed from the base case, since velocities were mainly directed through the location of the lowered bar. Nevertheless, the still sediment transport was onshore directed over the SPAW. A remarkable result was that the onshore directed sediment transports at the tips of the SPAW were directed slightly to the middle of the SPAW, because the suspended sediment transport component is directed from the sides to the middle of the feature.

In conclusion, the numerical simulation has shown that the consistent onshore directed propagation of SPAWs can be explained by the SPAW induced modulation of the wave-driven flow field and related transport patterns.

Contents

Appendices

1 Introduction

The Dutch coast is exposed to erosion. In 1990, a coastal policy was adopted to maintain the Dutch coastline position by applying beach, shoreface and dune nourishments. Since then, several nourishments have been done at different locations in the Netherlands with currently a total yearly volume of 12 Mm^3 (De Ronde, 2008). The performed nourishment strategies are mainly large scale. For example in Egmond aan Zee in the summer of 1999, a shoreface nourishment was done at the outer bank of approximately 2 km long and 200 m wide, backed by a beach nourishment (Van Duin et al., 2004).

Interestingly, at a smaller-scale a natural mode of shore nourishments has been observed. This phenomenon is named a Shoreward Propagating Accretionary Wave (i.e. SPAW) and was described for the first time by Wijnberg and Holman (2007). A SPAW is formed during a natural process in which a small bar shaped feature separates at the landward side from a nearshore bar, then propagates onshore, and eventually merges with the beach. SPAWs observed at Duck (North Carolina, USA) have an average length of 126 +/- 60 m and a width of 30 +/- 10 m, which indicates the scale of the feature (Wijnberg and Holman, 2007). This feature is the main focus of this study, and is described in more detail in paragraph 2.1.

1.1 Relevance of this research

Knowing more about SPAW dynamics is important for two main reasons; (i) it will improve current knowledge about nearshore morphodynamics, and (ii) the possible relevance for sand nourishment techniques. These are explained in more detail in this paragraph.

Firstly, much is still unknown about nearshore and shallow water processes, and we are only partly aware of the range of morphologic behaviour that can occur in the nearshore zone. In morphological studies the SPAW feature is not yet addressed so far. This is due to the fact that there is a lack of long-term, high resolution data sets on nearshore morphology, because it is hard to obtain them with conventional surveying techniques that require physical presence in the surf zone. There is in general a lack of understanding of the complex interaction processes between waves, currents, sediment transport, and bed levels, especially in the highly dynamic surf zone. Additionally, specifically for SPAWs it is hard to include them in a bathymetric measuring campaign, because they are very local and unpredictable features. Investigating mechanisms causing a SPAW to propagate onshore through a trough, while in the same time approximately maintaining its shape, can contribute to a better understanding of cross-shore transport processes in the nearshore environment (Wijnberg and Holman, 2007).

Secondly, the mobility of sediment in the nearshore is high, waves and currents induce sediment transport in the nearshore. Due to non-linearity in both sediment transport processes and surf zone hydrodynamics, unexpected gradients in sediment transport across the nearshore topography can occur. This can result in unexpected bathymetric changes, such as the formation of SPAWs (Wijnberg and Holman, 2007). Since SPAWs are submerged volumes of sand which will eventually merge with the beach, they can be a large input of sediment on the beach or the intertidal area (Almar et al., 2010 and Capo et al., 2009). This implies that SPAWs merging at the beach nourish the beach. Since SPAWs represent a consistently onshore directed sediment flux, gaining more insight in their dynamics can be of interest for the design of artificial shoreface nourishments.

1.2 Research objective and questions

As described above there is still much to discover about the newly discovered SPAW phenomenon. Therefore, the objective of this research is to identify which nearshore processes control the shoreward propagation of the SPAW phenomenon after it has been initiated.

This report addresses several questions in order to fulfil the objective:

- What is the effect of a SPAW on the wave-driven flow field and related initial sediment transport pattern, and what is the resulting initial morphologic development of a SPAW:
  - According to a conceptual model developed using theory of shallow water processes?
  - According to simulations done with the numerical process-based model Delft3D?
  - Which differences between the conceptual idea and numerical simulations are present; and what can be possible explanations for them?

- How are the wave-driven flow field, the related initial sediment transport over a SPAW, and the resulting initial morphologic development, affected by:
  - Water depth above the SPAW?
  - Morphometric characteristics of a SPAW?
    - Size (width and length of a SPAW)
    - Location (closer to bar or shore)
    - Local bathymetry

1.3 Methodology

In order to answer the above described research questions we followed several steps; firstly we formulated a hypothesis for the hydrodynamic flow field around a SPAW and the initial sediment transport pattern based on literature. To test this hypothesis, a schematized 3-dimensional Delft3D model was set up for Duck (North Carolina, USA). This model is based on earlier schematizations made by Hsu et al. (2006, 2008), Van der Werf (2009) and Treffers (2009). The model was adjusted by refining the grid, in order to have a better resolution around the SPAW. With the Delft3D model several cases were run, to investigate the effect of wave height, water level, and morphometric characteristics of the SPAW on the flow field and initial sediment transport around the SPAW. We considered particularly relative effects of the reference case without a SPAW and a situation with a SPAW. Based on modelling results, we drew conclusions and formulated recommendations for future research.

1.4 Outline of the report

Information on SPAWs, theory about nearshore processes and literature about nearshore nourishments is described in Chapter 2. Followed by a presentation of the Delft3D model schematization is presented, and key-decisions made during the modelling process are discussed in Chapter 3. Then in Chapter 4 the modelling results are presented for the base case, which has a SPAW configuration based on an average SPAW event, a low wave height and an average water level. Subsequently, the influence of varying water levels, wave height, and Delft3D-versions are discussed in Chapter 5. Then influences of varying morphodynamic characteristics of a SPAW are briefly discussed in Chapter 6. Followed by a discussion of the obtained results and modelling approach, an overview of the main conclusions and recommendations based on this study in Chapter 7.

2 Shoreward Propagating Accretionary waves and nearshore processes

The nearshore area consists of a shoaling zone in which water depth decreases, a surf zone where waves break and a swash zone in which waves run up the beach. Especially the interaction between the Shoreward Propagating Accretionary Wave (abbreviated SPAW; i.e. a bed feature lying in between the inner and outer bars) and nearshore processes are of interest to gain more insight in the expected SPAW dynamics.

This chapter zooms in on the phenomenon of Shoreward Propagating Accretionary Waves and relevant processes in the nearshore area. In Section 2.1 it is first defined what is meant by a SPAW. It is explained how it initiates, evolves and how it is measured. Then SPAW observations are briefly described. Subsequently, in Section 2.2 relevant nearshore processes are discussed. This is followed by a description of current nourishment strategies and a study on humplike nourishments in Section 2.3. This chapter concludes with a hypothesis on the wave-driven flow field and related initial sediment transport pattern around a SPAW in Section 2.4.

2.1 Shoreward Propagating Accretionary Wave (SPAW)

2.1.1 Definition of a SPAW

Shoreward Propagating Accretionary Waves (SPAWs) were described for the first time by Wijnberg and Holman (2007). They defined a SPAW as an isolated, spatially non-repetitive bathymetric feature that is generated on the landward side of a nearshore bar. The feature systematically propagates onshore across the trough as an intact form (Figure 2.1 and 2.2). When arriving at the beach, these small bars merge with the beach (i.e. see the protrusion at March 13, 1994 in Figure 2.2). They referred to the feature as a wave, because of similarities between the observed phenomenon and a solitary wave in fluid dynamics. Namely, both phenomena are single, isolated perturbations which approximately maintain their shape when propagating. In both cases the latter involves a net displacement of material in the direction of propagation.

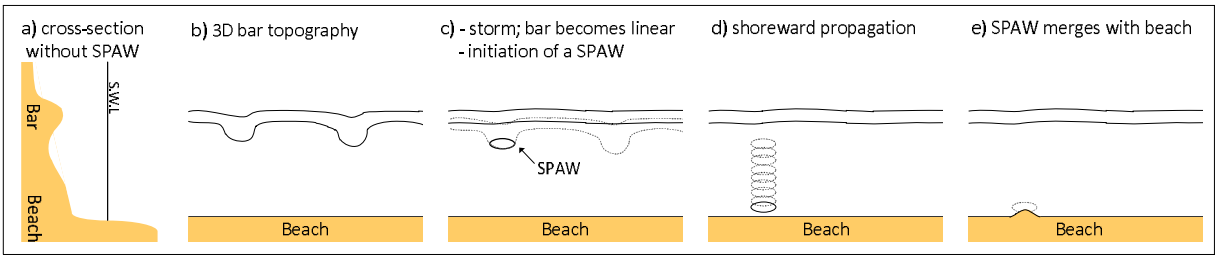

Figure 2.1. Conceptual sketch of SPAW initiation and migration

2.1.2 Initiation of a SPAW

Although the initiation of SPAWs is not investigated in much detail yet, Wijnberg and Holman (2007) observed that a three-dimensional bar pattern with onshore protruding features favoured the initiation of SPAWs. The three-dimensionality will rapidly become linear when wave conditions become more energetic (i.e. storm events, figure 2.1c) (Wright and Short, 1984; Lippmann and Holman, 1990). In case the onshore protruding part is separated from the main bar a SPAW is formed.

2.1.3 Evolution of a SPAW

After initiation, observed SPAWs transit the trough and eventually merge with the beach (figure 2.1 d and e). Wijnberg and Holman (2007) indicate two probable flow-topography mechanisms playing a role for the onshore propagation of SPAWs; local feedback (or self-organisation) and non-local feedback. The former comprises direct interaction between the SPAW topography and overlying fluid motion, which might be the cause for a SPAW to systematically migrate onshore and approximately maintain its shape as it propagates onshore. The non-local feedback involves effects of nearshore topography on the fluid motion in down-wave direction. For example, the breaker bar fulfils a filtering function for the variation in offshore wave height; namely, waves break over the breaker bar resulting in more constant hydrodynamic conditions shoreward of the bar and thus across the SPAW. The filtering mechanism may explain the observation of Wijnberg and Holman (2007) that no relationship was found between mean offshore wave conditions and average onshore propagation speed over the life time of a SPAW. Additionally, no relation was found between the average onshore propagation speed and initial cross-shore position of the feature. This indicates that the initial water depth does not influence the migration speed of a SPAW.

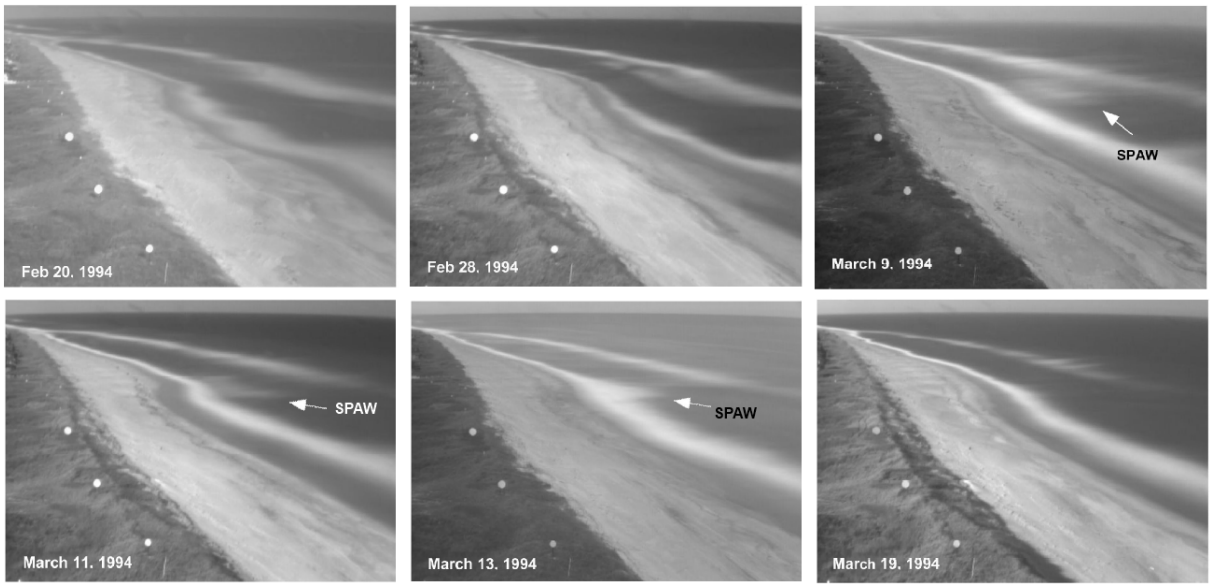

Figure 2.2. Sequence of time-exposure images near Duck (USA), white areas represent wave breaking. Peaks in cross shore intensity indicate the presence of a sand bar or SPAW (Wijnberg and Holman, 2007).

2.1.4 Methodology for observing SPAWs

Since SPAWs are a reasonably newly discovered phenomena not many are observed yet. The observation procedure as applied by Wijnberg and Holman (2007) on three beaches is described in this paragraph followed by a brief summary of observed SPAWs in the next paragraph.

The observations were done based on video time-exposure imagery (i.e. Argus images), taken over about a 10 minute time span. Generally every hour a time-exposure image is taken. The technique is based on the fact that waves break when entering a shallower part, thus clearly it is only applicable when wave conditions are such that waves break over a bar. White areas represent wave breaking, and peaks in cross shore intensity indicate the presence of a sand bar (Lippman and Holman, 1990). The visual signal created by breaking waves is a function of local water depth, incident wave conditions, but also includes properties of hydrodynamic process of wave breaking itself. A SPAW is actually a submerged

volume of sand and can be observed as an isolated, patch of foam in between the nearshore bar and the shoreline (Figure 2.2). It should be noted that observers should compare successive visual signals to see if patterns persists over time.

Observers first scanned the long time series of time-exposure images by eye to check for SPAW features. Then they determined the starting and ending date of the event. The starting date is defined as the first day on which the SPAW separated from its parent bar (Figure 2.1 c). However choosing this date involves uncertainty, because SPAWs initiate during high energetic conditions, in which many waves break. The ending date is defined as the day on which no noticeable traces are left on the shore line (Figure 2.1 e). For a uniform coast this implies the hump at the merging location is gone. The SPAW migration speed is approximated by dividing the initial cross-shore distance from the coast by the events duration (number of days from starting date to ending date). Finally, they determined the cross-shore SPAW position at initiation and dimensions (i.e. the width and length of the foam patch) from the images as described in the next paragraph. The above described procedure was followed independently by three independent operators, to reduce the arbitrariness in indicating SPAW events, and omit dubious cases.

2.1.5 Methodology for determining SPAW dimensions

The size of a SPAW was estimated by developing an outermost equal intensity contour on the time-exposure image (i.e. an equal intensity of white patches at the image) (Figure 2.3). When the SPAW is not fully separated from the outer bar, the outermost contour was picked showing contractions around the feature. It should be noted that this is only a proxy method for two reasons. Firstly, the images show the shallower part of the SPAW where waves are breaking; and secondly, the image intensity itself is not a direct measure for depth, thus an equal intensity contour does not necessarily relate to a single depth contour.

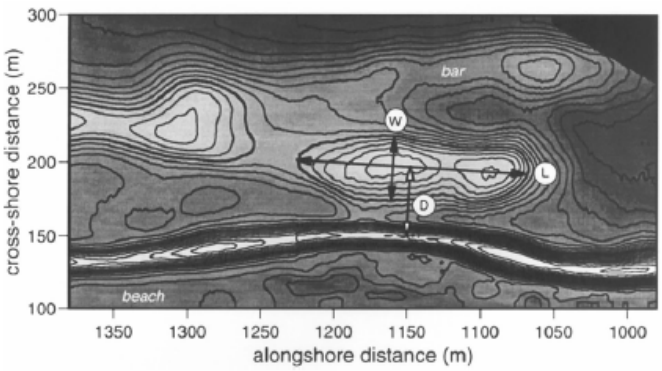

Figure 2.3. Definition sketch of morphometric measurements on contoured time-exposure image (contour based pixel intensity). W = SPAW width (cross-shore), L = SPAW length (alongshore), D = SPAW initial cross-shore distance (adopted from Wijnberg and Holman, 2007).

Since only video time-exposure observations were present it was not possible to estimate the height of a SPAW (i.e. the crest to trough elevation distance) and the development in height when migrating onshore. Nevertheless, since the feature separates from the main bar we expect it will have a similar height as the parent bar just after its initiation. This approximation is also reinforced in the fact that waves break over the SPAW, which indicates the SPAW having a sufficient height (Wijnberg and Holman, 2007). Also a SPAW observation captured by accident in a bathymetric survey at the Duck study site (USA) confirms this assumption (Figure 2.4). The height of the parent bar and SPAW are similar; the features height is approximately 0.7 m.

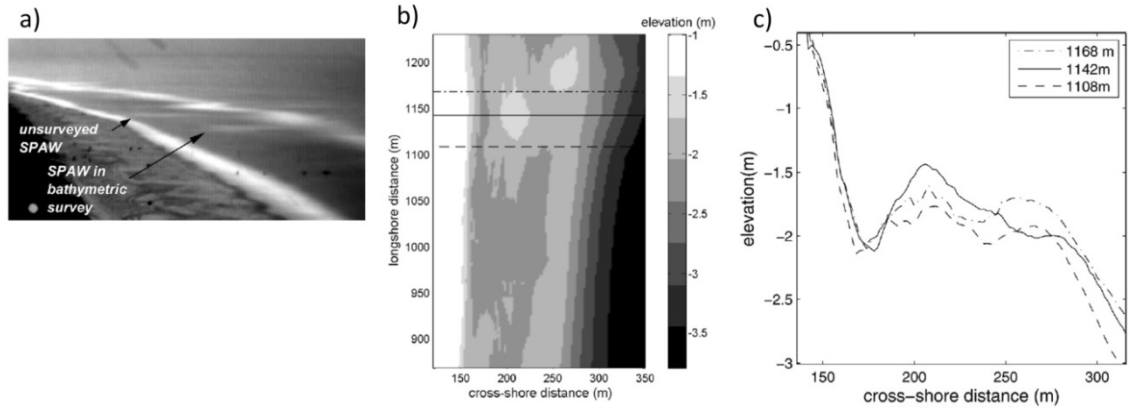

Figure 2.4. Captured SPAW event during bathymetric survey at Duck beach 6 September, 1994. (a) The surveyed SPAW in the time-exposure video images; (b) Indications of bathymetric survey showing three transects; (c) measured cross-shore profiles for the three transects (adopted from Wijnberg and Holman, 2007).

2.1.6 SPAW observations

Wijnberg and Holman (n.p.) studied three beaches (Duck, North Carolina, USA; Agate Beach, Oregon, USA; and Palm Beach, New South Wales, Australia) with noticeably different hydrodynamics and morphologic settings (Table 1).

On all three beaches they observed SPAWs that were shed of from the inner bank and eventually merged with the coast; this can be an indication that the phenomenon may be part of the normal range of nearshore bar behaviour. Almar et al. (2010) also observed a SPAW feature at Le TrucVert beach (France). This was actually a SPAW shed of the outer bar which propagates onshore and eventually merged with the inner bar. Additionally, at Egmond beach (The Netherlands) SPAWs were observed, but these observations were not reported in literature (Personal communication with K.M. Wijnberg). This study focuses on Duck (USA), since most SPAW events were observed here (19 in total). Besides that, this site is analyzed often and many hydrodynamic data are available.

Table 1. Summary of characteristics for beaches on which SPAWs are observed.

Sites	Slope	Environment (dominated)	Bar system	Sediment Sand	Average wave height/period
Palm Beach	1:50	Swell	One	Medium	1.6 m / 10 s
Duck	1:12.5	Swell	One or two	Medium	1 m / 8s
Le TrucVert	1:20	Wave	Two	Medium	1.4 m / 6.5 s
Agate beach	1:70	Swell	Triple	Medium	2 m / 11s
Egmond aan Zee	1:30 - 1:50	Wave	Two or three	Medium	1 m / 5 s

Observed SPAWs had length scales in the order of tens to hundreds of meters, with an average length at Duck beach of 126 +/- 60 m (Wijnberg and Holman, 2007). The maximum observed SPAW length is 375 m at Agate Beach (Australia), and the minimum observed SPAW length is 39 meter at Duck (Wijnberg and Holman, n.p.). The widths are in the order of tens of meters, with an average of 30 +/- 10 m at Duck beach (Wijnberg and Holman, 2007). The height of a SPAW at Duck is assumed to be approximately 0.7 m, based on a bathymetric survey at Duck (one time only). Therefore, the average volume of sand in a SPAW at Duck is estimated to be roughly 1900 m^3. Onshore migration rates for observed SPAWs at Duck are on average 3.1 m/day with a standard deviation of 0.8 m/day. The dimensions, in alongshore and cross-shore direction are much smaller than the current artificial nourishments as applied at the Dutch coast as mentioned in the introduction.

2.2 Relevant nearshore processes

The nearshore zone is an area in which many processes take place, each having a specific impact on the hydro- and morphodynamics. We expect some processes to be of importance for SPAW migration. And we believe that since observations show that the development of SPAW is dominantly cross-shore, the dynamics are essentially wave-driven. The relevant processes are discussed in this paragraph, subdivided in topics about waves (2.2.1), currents (2.2.2) and sediment transport (2.2.3).

2.2.1 Waves

Wind offshore can disturb the water surface and eventually develop waves. Wind generated waves are important as energy-transfer agent. Linear airy wave theory can be applied, assuming that wave height is much smaller than wave length and water depth ($H \gg L$ and $H \gg h$). This paragraph discusses topics related to waves, such as wave energy, radiation stress, shoaling, refraction, and wave deformation (skewness and asymmetry).

2.2.1.1 Wave energy

Waves transport energy, consisting of two parts. Firstly kinetic energy by the motion of fluid particles; and secondly potential energy possessed by the particles because they are displaced from their mean (equilibrium) position (Park, 1999). The total energy per unit area E [J/m^2] is directly related to the wave height H and is given by

$$E = \frac{1}{8}\rho g H^2 \tag{2.1}$$

In which ρ is the density of water [kg/m^3]. The wave energy is not a constant since it is energy density, and it varies with wave height. However, energy must be conserved within a system, so the flux of energy is considered to be approximately constant. This flux is called wave power (P), the rate at which energy is carried along by waves, and is given by

$$P = ECn = EC_g \tag{2.2}$$

Where C is the phase velocity of an individual wave [m/s], n depends on the region of application, and C_g is the group speed [m/s]. As the equation of wave power already suggested, for other conditions than shallow water conditions (i.e. n = 1) energy of waves travel at a different speed as individual waves. This velocity is referred to as group speed. Wave groups are composed of waves of close frequencies and directions. For shallow water conditions only water depth determines wave speed ($c_s = \sqrt{gh}$), so all waves will travel at the same speed.

2.2.1.2 Shoaling transformation and refraction of waves

When waves approach the shore two phenomena are present which influences wave amplitude and direction, namely shoaling and refraction (Figure 2.5). Both are interesting for SPAW dynamics, since shoaling influences wave height, and refraction might occur locally around the SPAW.

Shoaling is the process for which wave height increases when waves approach the shore. This can be explained by the fact that when entering shallower water the depth decreases and thus wave velocities decreases. Nevertheless, when ignoring energy losses (e.g. by friction and wave breaking), the wave energy flux should approximately remain constant. Thus when celerity decreases, wave energy should increase, hence wave height increases.

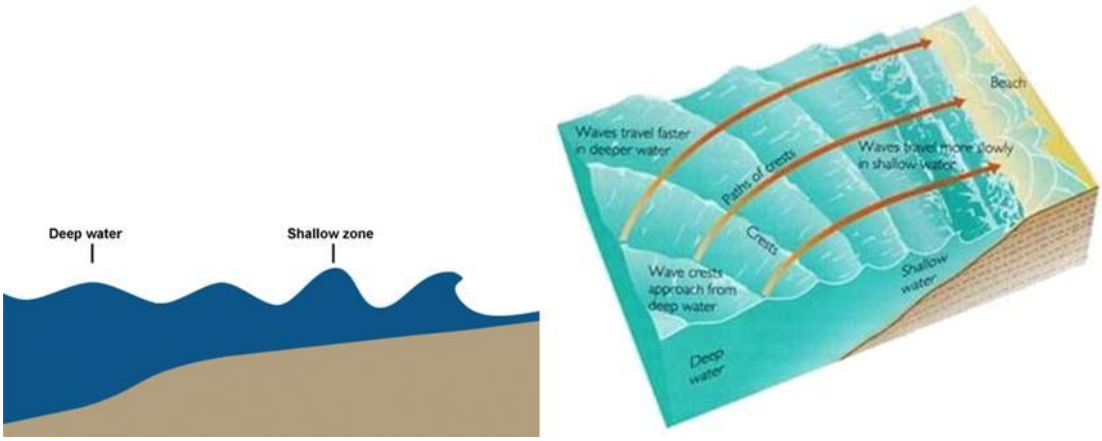

Figure 2.5. Left: Schematization of shoaling process (Source: https://www.meted.ucar.edu/). Right: Schematization of refraction process(Source: homepages.cae.wisc.edu.jpg).

Refraction is the process for which the angle of wave incidence decreases when entering shallower water for waves approaching the shore oblique to the coast. In shallow water the water depth determines the velocity of a wave. When approaching the coast from an angle the crest propagates much slower in shallower than in deeper water. Thus waves tend to turn and eventually have crests parallel to the shore (i.e. in that case the whole wave travels at the same speed for a uniform coast). Since wave energy in most cases has to spread over a wider area, wave heights generally reduces by refraction (Masselink and Hughes, 2003).

2.2.1.3 Radiation stress and wave set-up/set-down

The concept of radiation stress was firstly described by Longuet-Higgins and Stewart (1964) and is explained in Appendix A.1. They defined radiation stress as "*the excess flow of momentum due to the presence of waves"*.

For the most general situation (waves propagating perpendicular to the coast) the radiation stresses are:

$$S_{xx,deep} = \frac{1}{2}E \qquad S_{xx,shallow} = \frac{3}{2}E \qquad (2.3)$$

$$S_{yy,deep} = 0 \qquad S_{yy,shallow} = \frac{1}{2}E \qquad (2.4)$$

In which S_{xx} and S_{yy}refer to radiation stress in respectively in and normal to the direction of wave propagation. E refers to the wave energy. Subscripts deep and shallow refer to deep and shallow water.

In a spatially non-uniform situation with varying wave characteristics and/or water depth a resulting net wave force is present due to gradients in radiation stress. The wave force vector, $\vec{R}$ in the direction of wave propagation can be calculated by:

$$R_x = -\frac{\partial S_{xx}}{\partial x} - \frac{\partial S_{xy}}{\partial y} \qquad R_y = -\frac{\partial S_{yx}}{\partial x} - \frac{\partial S_{yy}}{\partial y} \qquad (2.5)$$

Radiation stress in water waves plays an important role in a variety of oceanographic phenomena. One of the most important wave driven effects occurs when waves encounter a sloping beach. Changes in bottom topography influence wave forms and result in changes in radiation stress, which subsequently lead to changes in mean water surface level, referred to as wave set-up and set-down. Variations in radiation stress can induce wave-driven mean flows.

For the nearshore zone on beaches two distinctive regions can be identified: seawards of the breaker (wave set-down) and shoreward of the breaker (wave set-up). Firstly, waves shoal in the nearshore zone seawards of the breaker line, which increases wave height and thus wave energy. Therefore the gradient in radiation stress is positive in flow direction. This leads to a lowering of the mean water level, referred to as wave set-down. Secondly, inside the breaker lines wave energy decreases shoreward, due to strongly decreasing wave heights by energy dissipation due to wave breaking and friction. This leads to negative gradients in radiation stress, resulting in increasing mean water-level in onshore direction, defined as wave set-up.

2.2.1.4 Wave asymmetry and skewness

In shallow water also non-linear interactions take place, and the wave form starts to deform from its sinusoidal wave shape. The shoaling process results not only in increasing wave height, but the wave also deforms during the process. Two typical transitions take place which are referred to as skewness and asymmetry (Figure 2.6) (Bosboom and Stive, 2011). The processes are important for SPAW dynamics, since they are important for sediment transport in the nearshore.

Skewness refers to the gradual peaking of wave crests and flattening of troughs; this results in a long, flat trough and narrow peaked crests. The second-order stokes theory is a theory which can be applied as a non-linear wave theory. The second order for the surface elevation (η) can be written as:

$$\eta = \hat{\eta}_1 \cos(\omega t - kx) + \hat{\eta}_2 \cos 2(\omega t - kx) \qquad (2.6)$$

The term $\omega t - kx$ refers to the phase of the harmonic. The first term represents linear wave theory (first order) with certain amplitude ($\hat{\eta}_1$), the second term refers to the second harmonic with double frequency (second-order Stokes for short waves). The amplitude of the second term ($\hat{\eta}_2$) is generally small compared to the first order (Figure 2.6 – left).

Since the wave form is skewed, also orbital velocities become skewed. They become larger in the crest where orbital velocities are in direction of water movement, i.e. onshore. And become lower in the trough, where orbital velocities are directed offshore. However also the duration of onshore/offshore orbital velocities is different since the wave form is skewed. The duration of onshore directed orbital motion is smaller (narrow peaked crest), and the duration of the offshore directed motion is larger (long flat trough). This has implications for sediment transport under a wave.

a) Wave skewness (Stokes wave) *b) Wave asymmetry*

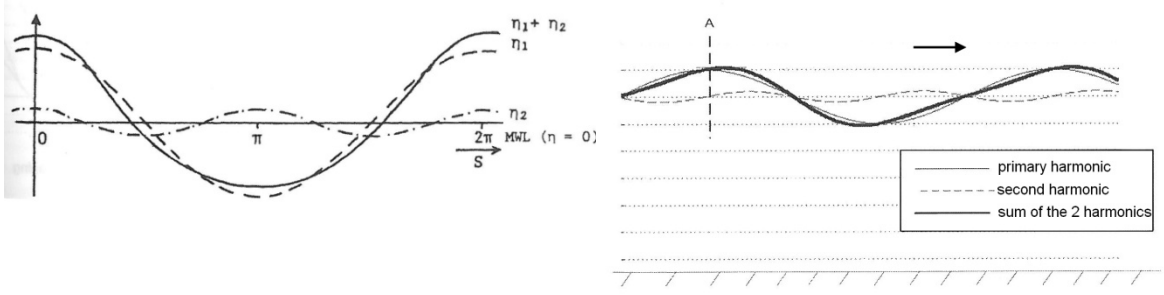

Figure 2.6. Wave skewness and asymmetry. a) the first and second order Stokes components result in a skewed wave. b) Pitched forward shape, showing asymmetry (adopted from Bosboom and Stive, 2011).

Asymmetry refers to the relative steepening of the face until breaking occurs, resulting in a pitched-forward wave shape. This is caused by the crest moving faster than the trough since velocity depends directly on water depth.

Both processes, skewness and asymmetry, interact with each other and take place in different stages. Shoaling waves become first gradually more skewed, and when approaching the surf-zone the harmonics shift phases which lead to an increase in wave asymmetry, and eventually a decrease in skewness.

2.2.2 Currents

In this paragraph currents in the nearshore are explained, such as the wave-generated cell circulation and tides.

2.2.2.1 Wave-generated cell circulation

Cell-circulation systems can develop in the nearshore due to longshore variations in wave height and wave set-up. A well-known phenomenon is a rip current, which is a strong, narrow current that flows seaward through the surf zone (Figure 2.7 - left). But also cell circulation can be formed around a nourishment area, as hypothesized by Van Duin (2004).

The occurrence of horizontal cell-circulation can be explained by the concept of radiation stress. The shoreward component of the radiation stress induces set-down offshore of breaker lines and set-up onshore of breaker lines (Appendix A.2). Haas et al. (1998) studied horizontal currents in the nearshore (Figure 2.7 - right). He observed that wave break over the bars, which generates a set up shoreward of the bars. Within the channels in between the bars, waves are not breaking as much, thus the mean water level is lower in and shoreward of the channel. This induces a longshore pressure gradient from the bars directed to the channels. This gradient drives the currents toward the channels, creating feeder currents for the rips. Another interesting circulation-cell is generated close to the shore. Since waves through the channels did not break yet when arriving at the coast, these waves will be larger and therefore break sooner when arriving at the coast. This will generate more wave set-up at this location and hence a longshore pressure gradient will drive flow away from the channels creating a secondary or recirculation cell close to the shoreline. Whether circulation cells will develop depends on whether waves are breaking or not.

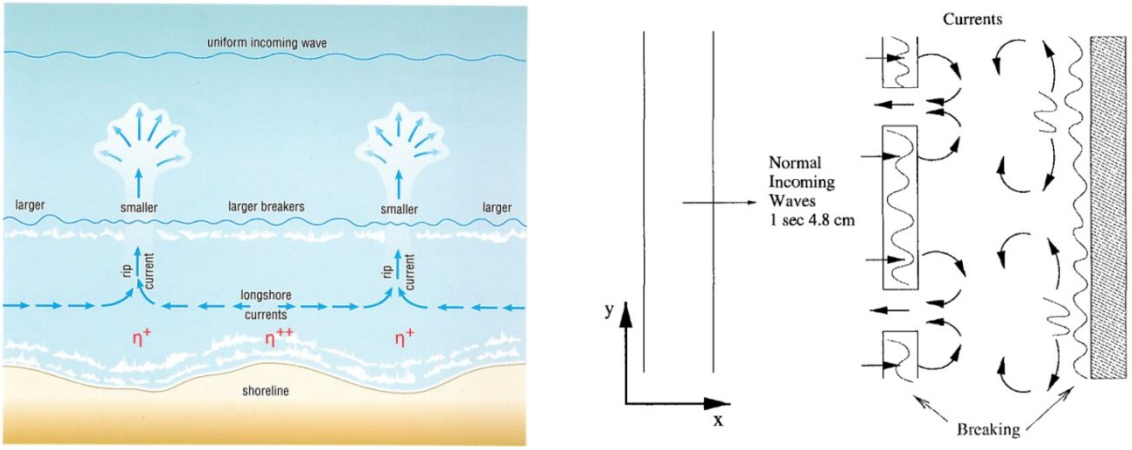

Figure 2.7. Wave induced horizontal cell-circulation systems. Left: Plan view of a section of a coastline showing rip currents (adopted from Park, 1999). Right: Schematic diagram of a wave-averaged flow adopted from the experiment of Haas et al. (1998), η^{++} indicates high wave set-up, η^{+} indicates low wave set-up.

Alongshore variation in wave set-up can be caused by variations in wave height along a crest, for example if one section of the crest encounters shallow water before another; this is determined by offshore bathymetry. Also it can be caused by sheltering effects due to for instance headlands, or by engineering structures such as jetties and breakwaters (Komar, 1998).

A SPAW or a nourishment is also a submerged amount of sand in the nearshore zone on which waves are observed to break; therefore a similar kind of flow circulation pattern as observed in the experiment of Haas et al. (1998) (Figure 2.7 - right) is expected around a SPAW.

2.2.2.2 Undertow

Breaking waves transport mass shoreward between the wave crest and trough. The coast is a closed boundary, thus continuity requires a zero net transport (otherwise, water is increasingly pilling up the coast). In order to have a net velocity below wave trough level to compensate for the flux above wave trough level a return current develops. For non-breaking waves there is a relatively small return current. For breaking waves much water is transported shoreward, thus a large return current develops, this specific current is referred to as undertow (Bosboom and Stive, 2011). It can be considered to be a vertical circulation current inside the breaker zone having a surface current towards the coast between wave and trough level, and a seaward current below trough level.

In the surf zone relative high sediment concentrations occur, due to wave breaking. This implies an undertow is important for seaward directed sediment transport, since it has a relatively high offshore directed velocity in the lower and middle part of the water column. The undertow is thought to be responsible for severe beach erosion during heavy storms.

2.2.2.3 Tides

The tide is a long wave developed by the influence of the moon and sun on seas and oceans, tidal ranges (difference between high and low water levels) differ per location, but can be more than 10 m. Two characteristics of tides are distinguished, the vertical and horizontal tide (Bosboom and Stive, 2011).

The vertical tide is the vertical rise and fall of the water level. High tide refers to high elevated water levels and low tide to low water levels. This difference in water level influences the location where waves break, and therefore it influences the flow-field and related sediment transport and nearshore morphology. For a nearshore bar or a SPAW this may imply for example that waves break over it when it is low tide, but do not break over it during high tide. Due to which sediment transport patters are expected to be different during high and low tide. In this study vertical tide is taken into account by simulating different water levels during runs.

The horizontal tide or tidal current refers to horizontal movement of water associated with changing tidal water levels. This component of the tide is not taken into account in this study, since SPAW movement is observed to be dominated by cross-shore movements we do not expect this longshore component to be essential in explaining SPAW dynamics.

2.2.3 Sediment transport

The interaction between hydrodynamics and sediment is complex and not yet well understood. A SPAW is a submerged amount of sand which migrates due to sediment transport gradients. Much sediment is in motion in the nearshore zone. In general, movement of sediment particles depends on the characteristics of transported material (grain size,

shape, density, fall velocity, pore content), and the ambient flow conditions. Two main modes of transport are distinguished:

- Bed load; particles are sliding, rolling, shifting and making small jumps over the seabed while they stay close to the bed.
- Suspended load; particles are lifted from the bed and transported in suspension by the (moving) water. Particles are kept in suspension by fluid turbulence.

The total sediment load is the sum of the bed and suspended load. Sediment particles will start moving as bed load when a critical shear stress is exceeded. Bed load transport is mainly determined by the bed shear stress (τ_b) that acts on the sediment particles. Therefore bed load formulas are among other parameters (such as diameter and density) expressed in terms of the bed shear stress supplemented with a bed-slope correction factor.

Suspended transport rate (Q_{ss}) is calculated by taking the sediment flux (defined as the sediment concentration multiplied by the horizontal velocity), and integrate it over water depth (from top of the bed load layer to the water level) (Eq. 2.7). In Delft3D the wave-related part of the suspended sediment transport is classified as near-bed load transport (Van Rijn, 2007; Appendix B.6). Suspended load does not always respond instantaneously to hydrodynamic conditions especially fine grains experience phase lag effects: sediment pickup and settling requires times due to which phase differences between velocities and suspended sand concentrations can occur.

$$\underbrace{\langle Q_{ss} \rangle}_{\substack{time\ averaged\ sediment \\ transportrate}} \cong \underbrace{\int_a^h UC dz}_{current-related\ part} + \underbrace{\int_a^h \langle \tilde{u}\tilde{c} \rangle dz}_{wave-related\ part} \qquad (2.7)$$

In which Q_{ss} = instantaneous suspended transport rate [m^3/s/m], U time averaged fluid velocity at height z [m/s], C time-averaged concentration at height z [m^3/m^3], $\tilde{u}$ oscillating fluid component [m/s], $\tilde{c}$ oscillating concentration component [m^3/m^3], a is top of bed load layer, h is instantaneous water level $h = h_0 + \eta$.

Wave action, as well as current action (e.g. horizontal circulation, undertow, and tides) takes place in the nearshore. The presence of waves leads to (i) additional stirring (e.g. by wave breaking) resulting in an increased current-related sediment transport and more suspended sediments in the upper part of the flow, also (ii) an additional wave-related transport component in the direction of wave propagation is generated by waves. The effects related to wave asymmetry are dominantly occurring in the nearshore zone as stated by Van Rijn (2007).

Both currents and waves induce sediment transport, in longshore as well as cross-shore direction. In cross-shore direction (the direction of wave propagation) a net sediment transport can take place, due to the presence of waves and currents. For example three possible interactions are:

- The presence of waves may result in a wave-averaged net sediment transport, particularly during the peaks of a wave period much sediment is entrained. When the oscillatory velocity signal is symmetric, no net sediment transport takes place. However, for deformed waves in the shoaling area a positively skewed velocity signal is present. This induces a net sediment transport in the direction of wave propagation because sediment load is related to the velocity in a non-linear way (it still holds that $\langle \tilde{u} \rangle = 0$).
- Similar processes occur in case of a current superimposed on a sinusoidal velocity signal; this also deforms the velocity signal such that a net sediment transport in the

direction of the current develops, which is larger than the transport for the current alone.

- Another possibility is that a vertical circulation cell develops in the nearshore due to the undertow, this wave-generated current transports much sediment offshore because it is offshore directed in the lower part of the water column. Since sediment concentration is non-uniformly distributed over the vertical the highest sediment concentrations occurs in the lower part of the water column. This undertow is dominating during storm conditions, during which much sediment is transported offshore.

In longshore direction, transport depends amongst others on hydrodynamics in the breaker zone and on sediment properties. The longshore transport is enhanced due to waves because waves stir up sediments, after which the longshore current transports it.

In general, bed level changes can be estimated using the mass balance equation. Assuming there are no local inputs or abstractions of sediment, and no sediment can vanish, the mass balance of sediment is:

$$(1-p)\frac{\partial z_b}{\partial t} + \frac{\partial S_x}{\partial x} + \frac{\partial S_y}{\partial y} = 0 \qquad (2.8)$$

In which z_b is the bed level above a certain horizontal datum (m), S_x the sediment transport rate (volume in solid grains) in x,y-direction (m^3/s/m), and p the porosity (-).

The basic problem is that the net transport in this zone is a delicate balance of various onshore and offshore-directed transport processes which are all of the same order of magnitude. Thus the net result in these conditions is by definition uncertain and almost unpredictable. Van Rijn (2007) also states that our knowledge of sediment transport in the nearshore zone close to the beach is still very limited and more research is necessary.

2.3 Nourishment strategies

Nourishments can be done at different scales and cross-shore locations; it can be done at a beach or dune face (sub aerial) or on the shoreface to the subaqueous part of the profile. Shoreface nourishment locally prevents the coast from erosion due to two main effects: the lee and the feeder effect (Figure 2.8). Firstly, the lee effect (Figure 2.8 – left) contains the fact that large waves will break over nourishments and decrease the wave-driven longshore current shoreward of the nourishment. A decreasing longshore current results in decreasing longshore sediment transport capacity; hence sediment is trapped shoreward of the nourishment. Since the nourishment acts as a blockade, updrift deposition and downdrift erosion shoreward of the nourishment is expected. Since SPAWs are only small humps (average width and length of respectively 20 and 126 m at Duck (USA)), we do not expect the lee effect to be large.

Secondly, the feeder effect (Figure 2.8 – right) includes onshore movement of nourished sand particles. Since large waves break at the seaward side of shoreface nourishment, the remaining shoaling waves generate more onshore transport as a result of wave non-linearity. The smaller waves in the lee side generate less stirring of the sediment and a decreasing wave-induced return flow (undertow). Due to the fact that waves break over the nourishment, wave set-up is generated directly shoreward of the berm. This induces horizontal cell-circulation current patterns (especially on the tips of the berm) (Koster, 2006; Ojeda et al., 2008; Van Rijn and Walstra, 2004).

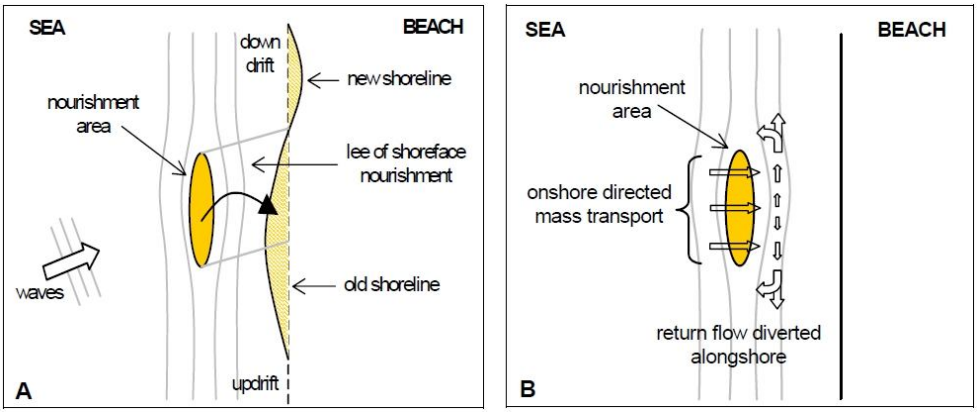

Figure 2.8. Expected effects as a consequence of the placement of a shoreface nourishment (adopted from Van Rijn en Walstra, 2004). Showing the lee effect (left) and the feeder effect (right).

Van Rijn and Walstra (2004) concluded that based on observations at Egmond aan Zee, Terschelling and Delfland the final sand budget in the nourishment zone had increased after implementing nourishment. Also they found an amount in the order of 50 – 70% of the initially nourished sand is still in the nourished nearshore section after 3-5 years. The lifetime of shoreface nourishment is about 2-10 years. The supply of sand from the feeder berm to the beach takes place on a relatively long time scale (10 years or so), so the feeder berm needs additional nourishments as well in order to stay effective.

2.3.1 Humplike nourishment study (Koster, 2006)

Koster (2006) investigated an alternative design for shoreface nourishments. It was suggested to use humplike nourishments instead of the conventional method of elongated bars. Hypothesising that humplike nourishments cause more onshore transport than longer bars, because positive effects of horizontal circulation cells at the crest of the bar is better used. Koster tested the efficiency of humplike nourishments using the numerical model Delft3D. And he invested the effectiveness of different hump lengths, gap widths, water depth, wave angles and wave heights. It turned out that indeed humplike nourishment seemed potentially more efficient than bar nourishments. The crests of all nourishments had a flat surface width of 50 meter. A hump length of 200 m with a gap width of 300 – 500 m gave the best results, since longer humps started to behave like elongated nourishment and shorter humps use too much amount of sand in relation with the efficient hump length. However, it should be noted that the study was done with a highly simplified bathymetry and boundary conditions.

The study of Koster is very interesting in relation to studying SPAW behaviour, since it is also about relatively small nourishment compared to the current nourishment strategies. Nevertheless, there are significant differences between both studies. Firstly the location, Koster (2006) studies Egmond aan Zee, whereas this study focuses on Duck (USA). Both bathymetries are schematized, however Koster (2006) does not include alongshore bars (i.e. a plane bottom profile), whereas this study does (paragraph 3.4.3). Also locations and sizes of the submerged mount of sand (either nourishment or a SPAW) are different. The nourishment is located further offshore than the SPAW respectively at 600 and 200 m offshore. SPAWs are generally located in the nearshore zone onshore of the breaker bar. The nourishment is much higher than the SPAW, respectively 3 and 0.9 m. The location and height of the humps also imply that water depth above the humplike nourishment is much higher. Nevertheless, the insights of Koster are useful, because mechanisms for a SPAW are expected to be quite similar.

2.4 Hypothesis about SPAW behaviour

A Shoreward Propagating Accretionary Wave is a consistently onshore migrating morphological feature observed in nature. We investigated the dynamics of SPAWs after initiation using the process-based Delft3D software package. In previous paragraphs relevant nearshore processes and theory about nourishments have been discussed. Based on this literature, we formulated the following hypothesis for shoreward propagation of a SPAW consisting of two parts:

1. We expect increased onshore sediment transports over the SPAW due to the development of a horizontal circulation pattern around the SPAW which is onshore directed over the SPAW crest (Figure 2.9). This circulation is generated by local shoaling/deshoaling and wave-breaking over the SPAW inducing gradients in radiation stress. These result in a local wave set-down directly seaward of the SPAW due to shoaling, and wave set-up directly shoreward of the SPAW due to deshoaling and/or wave breaking. This local wave set-up/set-down induces longshore pressure gradients, which drives the local horizontal circulation current which we expect to be present in the flow-field.

2. We expect sediment transport to be higher above the SPAW due to non-linear wave transformation over the SPAW caused by a different bathymetry. This results in waves becoming skewed and more asymmetric over the feature. Also we expect waves to break over the SPAW (since it has approximately the same height of the bar), which leads to more turbulence and more sediment in suspension. When waves are more asymmetric and skewed, the onshore sediment transport is expected to be higher than around the SPAW.

The first part of the hypothesis is checked by looking at flow-fields around the SPAW. The second part is checked by analyzing sediment transport patterns and the different components of sediment transport (i.e. near-bed load and suspended load) that develop around a SPAW.

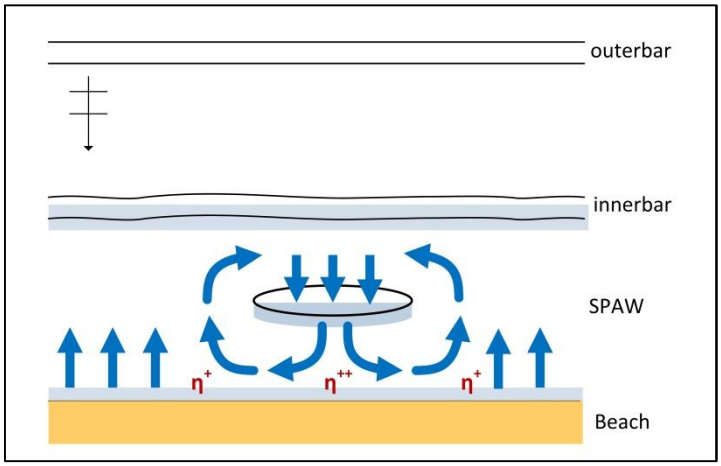

Figure 2.9. Top view of hypothesized horizontal cell circulation induced by local pressure gradients by wave-breaking. η+ indicate areas of set up, η+ indicate areas of large set-up. Blue arced areas indicate wave breaking.

3 Delft3D model for modelling SPAW dynamics

To investigate the flow field around a SPAW, a three-dimensional Delft3D model is set up for Duck beach (USA). The input for the model (e.g. bathymetry, SPAW dimensions and wave height) is based on a chosen representative SPAW event that occurred at Duck Beach in 1994. This Chapter discusses key-decisions made when setting up the Delft3D model schematization, also the model schematization itself is discussed.

In Section 3.1 the modelling approach is explained, followed by some general information about Delft3D in Section 3.2. Section 3.3 describes the field site, a representative SPAW event on which the model is based, and measured conditions during the average SPAW event. Subsequently, in Section 3.4 the Delft3D model schematization for the representative SPAW event at the Duck Beach study site as applied in this study is discussed. From grids, bathymetry, initial and boundary conditions to the parameter settings, and the implementation of the roller model in Delft3D.

3.1 Modelling approach

This study focuses on studying the hydrodynamic field that develops across and around a SPAW feature. A schematized modelling approach was chosen, in order to investigate autonomous effects of a SPAW. However, the schematized input is based on realistic wave conditions which could have occurred during the representative SPAW event.

Schematizations are the following:

- One average SPAW event is chosen, representative for most SPAW events. An average SPAW event is taken as a basis, since also morphometric characteristics of the SPAW will be varied.
- The bathymetry is based on measurements during a chosen representative SPAW event period (paragraph 3.3.2), but is assumed alongshore uniform. With an alongshore uniform bathymetry results are not influences by interaction with small alongshore variations in bathymetry.
- For offshore wave data the schematized JONSWAP spectrum is imposed, instead of a measured 2D-(direction and frequency) wave spectrum. Waves are chosen to approach the coast perpendicular; this reduces side effects of directional spreading and longshore currents.
- Hydrodynamic characteristics are highly schematized; we assumed a constant significant wave height and water level instead of a time series. This facilitates the analysis of results, since we can analyze the influence of changes in certain parameters. Also computational time would become too long if a time series of several hours should be computed.
- Wind is excluded from the simulation, since we do not expect wind to have very large impact in the flow fields around a SPAW. Wind generally can induce additional currents. Also another reason to exclude wind was that the model showed unexpected non-uniformities in model outputs.
- Horizontal tide is excluded from the simulation. It is expected that this longshore component is not essential in explaining SPAW dynamics, which was dominated by cross-shore movements.

This schematized approach facilitates interpretation of results, since these are not disturbed by other factors than the presence of a SPAW. Also an advantage is that due to the schematizations the reference case (i.e. without a SPAW) should be alongshore uniform, this

knowledge is used by deciding whether confidence could be put in the model. Although simulations provide a good general impression of SPAW dynamics, it is important to realize during the analysis that the modeled situation is highly schematized. The actual hydrodynamic field around a SPAW is a summation of all effects of different hydrodynamic conditions (wave angle, wave height, water level above SPAW etc.) and local bathymetry.

3.2 Delft3D software

Modeling of almost all runs was done with Delft3D-FLOW (Version 4.00.04.757, August 23, 2011), and Delft3D-WAVE (Version 3.04.01.757, Aug 23 2011). One run was done as a sensitivity analysis with a test-version of Delft3D-FLOW (Version 5.00.08.1832, Sep 13 2012) in combination with Delft3D-WAVE (Version 4072ABCDE). Paragraph 3.4.7 describes the choice to use version 4 as well as a test-version of Delft3D.

Delft3D is a process-based morphodynamic model developed to simulate phenomena occurring in water environments. The model schematization used in this study is based on earlier schematizations made by Hsu et al. (2006, 2008), Van der Werf (2009) and Treffers (2009). These models were hydrodynamically calibrated for the SandyDuck97 cases. The focus of these studies was to investigate longshore wave driven currents. Since no measurements of the flow-field and sediment transports (such as the SandyDuck97 cases) are present for periods in which SPAWs occur, it is not desirable to develop a new model for Duck (USA) to investigate SPAW dynamics.

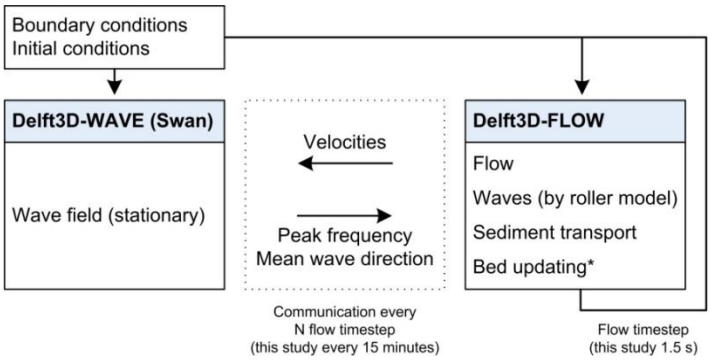

*Figure 3.1. Structure of Delft3D in stationary mode, *the bed updating is only done in the last time step.*

For the model schematization the WAVE and FLOW modules are used. More information can be found in Appendix B.3 and B.4. Delft3D-FLOW calculates the flow field, the wave parameters (e.g. wave height) using the Roller model, the sediment transport field and the initial morphological evolution. Delft3D-WAVE calculates the short wave field using the SWAN wave model. These two modules are coupled in an online morphodynamic way (Figure 3.1), which implies Delft3D-FLOW makes several computations before the wave field is updated.

This schematization applies the roller model to compute wave heights, as it was shown to improve predictions for the wave height and longshore current velocities (Hsu et al., 2006).The effect of including the roller model is that regions of wave-set up are shifted shoreward as well as the wave-driven currents, because wave energy dissipation is delayed. The peak frequency and mean wave direction as computed by SWAN are used as input for the roller model.

Delft3D utilises the two-layer concept introduced by De Vriend and Stive (1987) in which it is assumed that onshore mass transport of water occurs between wave top and trough, which is compensated by an offshore directed undertow below the wave trough. Delft3D considers

phase-averaged wave properties, only mass flux below the wave trough is considered through the application of the shallow water equations in a generalized lagrangian mean (GLM) framework (Walstra et al., 2000). The relation between the GLM velocity and the Eulerian-mean velocity is the Stokes drift (i.e. the wave-induced mass-flux in direction of wave-propagation):

$$\vec{u}^E = \vec{u}^L - \vec{u}^S \quad (3.1)$$

In which $\vec{u}^E$ the ordinary Eulerian-velocity vector, $\vec{u}^L$ is the GLM-velocity vector, and $\vec{u}^S$ is the Stokes drift vector. The Stokes drift is analytically computed from the wave theory Dean and Dalrymple (1991). Delft3D output is normally given in Eulerian velocity, to be able to compare computational results with measurements.

Sediment transport is calculated online, during the FLOW module. The transport formulation TRANSPOR2004 of Van Rijn (2007) was used. This is an updated version of TRANSPOR1993 (Van Rijn, 1993). In TRANSPOR2004 the bed-shear stress is based on a new bed roughness predictor. Also the reference concentration function has been recalibrated using laboratory and field data for combined steady and oscillatory flow (Van Rijn, 2007a). Transport is divided into suspended and near-bed load transport. The suspended load is calculated using GLM velocities. In contrary, the bed load is computed using the bed shear stress, which originates from Eulerian velocities (Walstra et al., 2000). The near-bed load consists of three components, namely:

1. Bed-load due to currents (S_{bc}), acting in the direction of the (Eulerian) near-bed current.
2. Bed-load due to waves (S_{bw}), acting in the direction of wave propagation.
3. Suspended load due to wave asymmetry effects (S_{sw}), acting in the direction of wave propagation.

More information about the sediment transport calculations is given in Appendix B.6.

3.3 Field site, choice representative SPAW event and data description

Wijnberg and Holman measured SPAW events at three different beaches. This study focuses on Duck (North Carolina, USA), since most SPAW events were observed here (19 in total). Also, this site is analyzed often and many hydrodynamic data are available.

3.3.1 Duck Field site description

The Duck study area is located in North Carolina (USA) near the CERC Field Research Facility (FRF). The FRF is located at about the middle of Currituck Spit, a 100 km long unbroken stretch of shoreline facing the Atlantic Ocean (Figure 3.2). It is a predominantly steep beach (1:12.5) and it is fronted by one or two nearshore bars (usually an outer storm bar in water depths of about 4.5 m and an inner bar in water depths between 1.0 and 2.0 m). The mean annual wave height is about 1 m and its period is 8 s; the spring tide range is about 1.5 m (Leffler et al. 1992). It is a swell-dominated area. The area of interest in the view of the camera starts about 200 m north of the pier and extends 1 km alongshore. In cross-shore direction it extended from the inner nearshore bar to the shoreline. The analysed period for SPAWs spans from October 7, 1986 until December 1996. A gap existed in the data between 10th of August, 1992 and 28th of January, 1993 (Wijnberg and Holman, 2007).

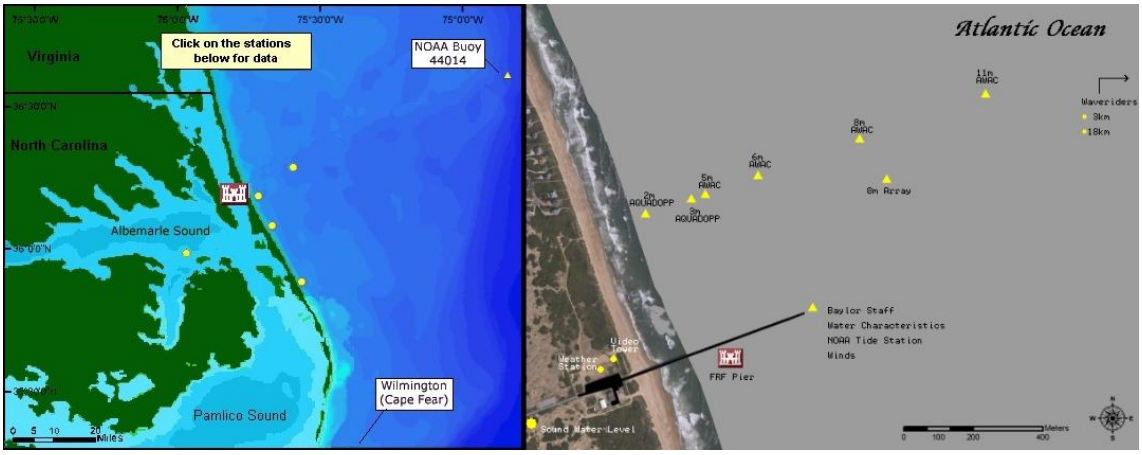

Figure 3.2. Field Research Facility Duck (FRF), the castle in the left figure represents the measuring pier (right figure), adopted from http://www.frfusace.army.mill/.

3.3.2 Representative SPAW event

In this study a representative SPAW event is chosen to represent the SPAW for all runs. It had average SPAW characteristics, from which realistic wave conditions and bathymetry were used for the model schematization. As mentioned in chapter 2, SPAWs have an average length of 126 (stdev 60m), an average width of 30 (stdev 10 m), and an average migration speed of 3.1 m/day (stdev 0.8 m/day). Two events are approximately the same as the average event. The SPAW event of 22nd of April 1994 to 5th of May 1994 (Length =131 m, Width = 18 m, Migration speed =2.9 m/day) is chosen to be representative. Although the width deviates slightly more than the standard deviation, the other characteristics are average. The other SPAW event which reassembles an average event is measured between the 4thof June1988 to 19th of June 1988 (Length = 134 m, Width =24 m, Migration speed =2.3 m/day). This event was not chosen, because no wave data are available for that period.

3.3.3 Conditions during average SPAW event

At FRF many (hydrodynamic) measurements were carried out. The model of Hsu et al. (2006) was calibrated on Duck94; Van der Werf (2009) and Treffers (2009) used the SandyDuck97 data. The conditions during the SPAW event (22nd of April to 5th of May 1994) are visualized in Figure 3.3 and 3.4.

Winds were measured at the end of the pier at an elevation of 19.36 m referred to National Geodetic Vertical Datum (NGVD) presently using an RM Young Marine anemometer at an interval of 34 minutes. The NGVD is 0.42 m above Mean Low Water (MLW). The wind direction is defined nautically; 0˚ denotes wind coming from the North and is positive in clockwise direction.

Directional wave data are taken from the Senso-metric 8m Array (1 km offshore). The FRF's 8m Array consists of 15 pressure gauges mounted approximately 0.5 m off the bottom at the 8-m contour line about 900 m offshore and to the north of the research pier (Figure 3.2). Directional information is computed from these gauges using an iterative maximum likelihood estimator. Directions are defined nautical (same as wind directions), i.e. 90˚ represent waves propagating straight onshore. Directional wave data show that on average waves approach the coast approximately straight onshore.

Wave heights are generally low, and wave periods are long (Figure 3.4). This is typical for a swell-dominated beach. When considering significant wave heights during SPAW events in

1994, there is a tendency for SPAWs to initiate after a storm and propagate during calmer conditions (Figure 3.4 and red shaded periods in Figure 3.5) this was also observed by Wijnberg and Holman (2007).

The tidal data (z_{tide}) are taken from the National Oceanic and Atmospheric Administration (NOAA) primary tide station located at the seaward end of the FRF pier. The z-axis (vertical) is positive upwards and relative to NGVD. The vertical tide is measured every 6 minutes. The data show that the dominant M_2-tide has average amplitude of approximately 0.5 m.

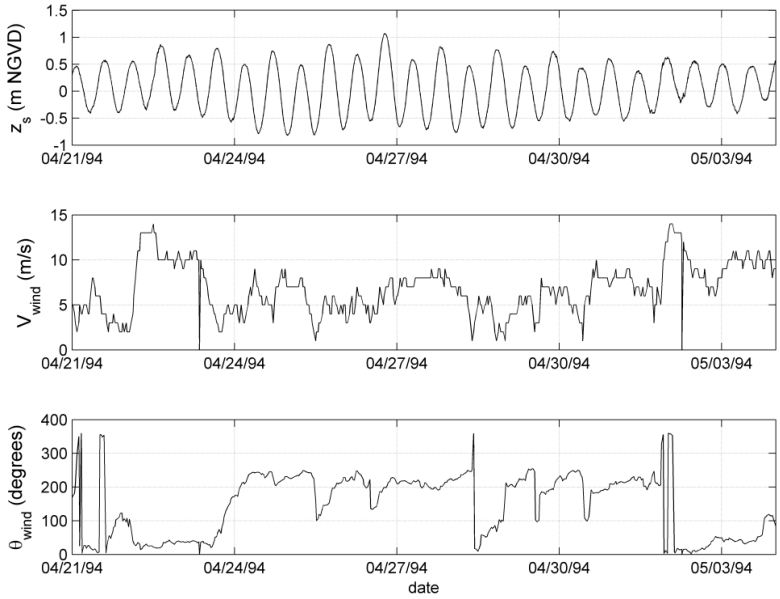

Figure 3.3. Water elevation, wind speed, and wind direction during the representative SPAW event. The wind direction is defined nautically and positive in clockwise direction.

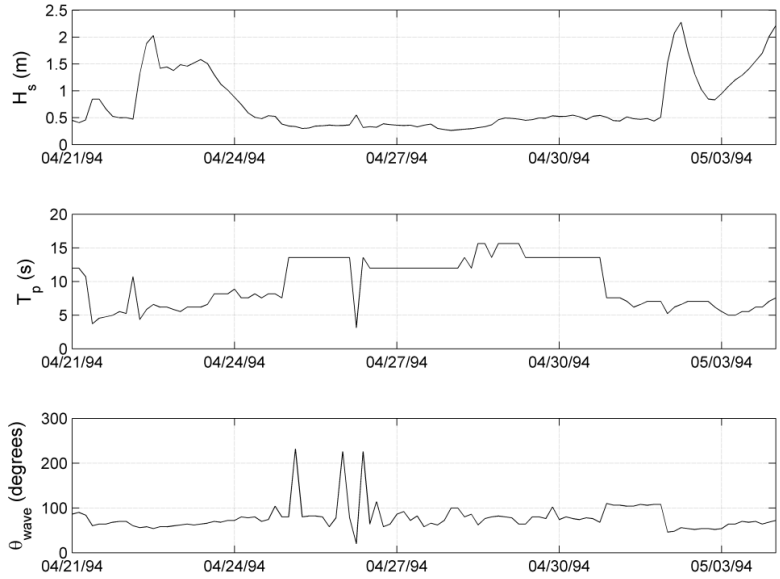

Figure 3.4. Significant wave height, peak period and mean wave direction during average SPAW event. The wave direction represents the angle in degrees counter clock-wise from shore normal.

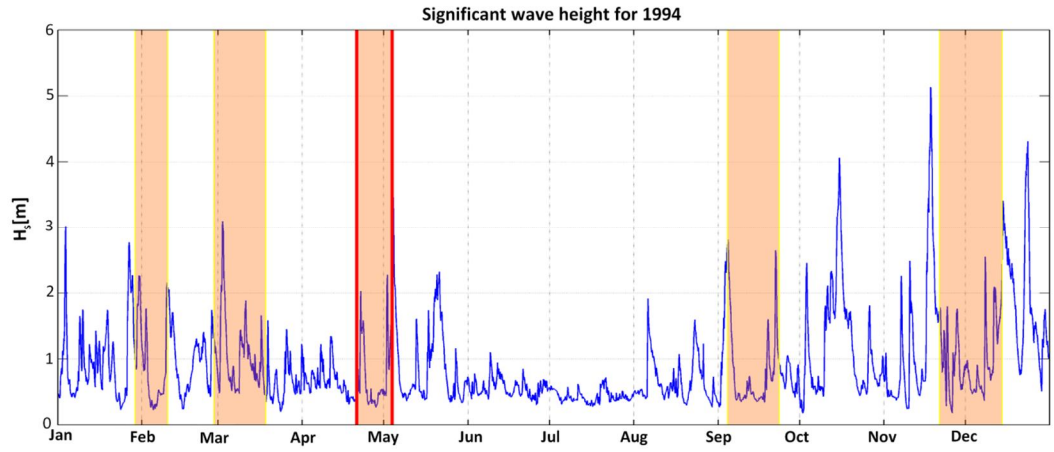

Figure 3.5. Significant wave height for the year 1994. Shaded areas represent SPAW events, the event with red lines is the average SPAW event.

3.4 Delft3D model

3.4.1 Horizontal Delft3D computational grid

The rectangular FLOW grid has 187 cells in m-direction (cross-shore) and 301 in n-direction (longshore) (Figure 3.6). This corresponds to a modelled area of 850 x 1500 m. We choose a longshore distance of 1500 m to be able to use the same model schematization for SPAWs with lengths up to a maximum of approximately 500 m. The flow grid has a high resolution nearshore and coarser offshore since the nearshore zone is the main area of interest. A short investigation on differences in grid-resolution on- and offshore showed that making the grid coarser offshore had no significant impact on results.

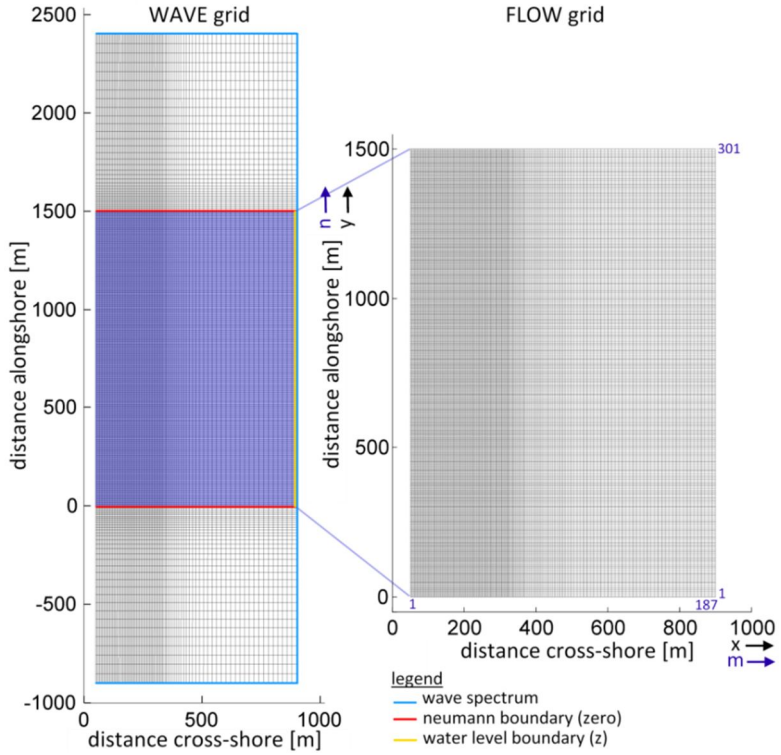

Figure 3.6. Computational grid for Delft3D model, showing WAVE grid (left) including boundary conditions (paragraph 3.2.3) and FLOW grid (right).

The maximum grid resolution is high compared to other Delft3D studies; this is necessary because SPAW dimensions are relatively small. The model has a grid-step size of 2,5 m in cross-shore and 5 m in longshore direction, which implies that for a SPAW with a width of 25 m eleven depth points are located over the SPAW. It would not be feasible to refine the grid further, because otherwise the time step should be even smaller and consequently the computational time would become much longer.

The WAVE grid is two times coarser than the FLOW grid in order to save computational time. Since the model applies the roller model (paragraph 3.4.6 and Appendix B.4), only the peak frequency and mean wave direction field are used from SWAN. The WAVE grid is larger than the FLOW grid in alongshore direction (i.e. extended by the cross-shore distance, 900 m), to compensate for boundary effects. This ensures that boundary conditions of the FLOW grid are realistic wave conditions.

3.4.2 Vertical grid

The model is three dimensional for investigating three dimensional effects of a SPAW on the flow field. This was done by implementing a vertical grid. It is recommended to choose the bed layer thickness in the order of 2% of the water depth (Deltares, 2011). Another factor to take into account is the variation factor, i.e. the difference in thickness of subsequent layers. The Delft3D flow manual suggests a variation factor in the range of 0.7 – 1.4. When this variation factor becomes too large, it can induce numerical errors.

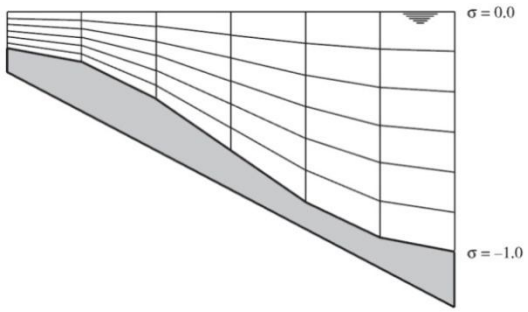

3.7. Vertical grid schematization showing σ-coordinate system with 6 layers(Deltares, 2011), in this study a schematization with 20 layers was applied.

Since the main areas of interest for turbulence and sediment transport are those near the surface and the bed, the resolution is chosen higher in the lower and higher part of the water column (log-log distribution). 20 layers were used in the vertical, since computational time is not a very large issue (only 2 hrs have to be simulated, which takes about 17 hrs computational time with current settings). The distribution uses σ-layers (Appendix B.2) and is symmetric in the vertical: starting at the bottom and at the surface with 2% of the water depth and getting coarser to the middle of the water column having subsequent layers of 2.2, 2.8, 3.3, 4, 4.8, 5.8, 6.9, 8.3, 9.9 % of the water depth.

3.4.3 Bathymetry

Bathymetric surveys at the FRF are conducted monthly over a series of 26 shore perpendicular “profile lines”, from the dunes to approximately 950 m offshore. They are conducted using a Coastal Research Amphibious Buggy (CRAB).

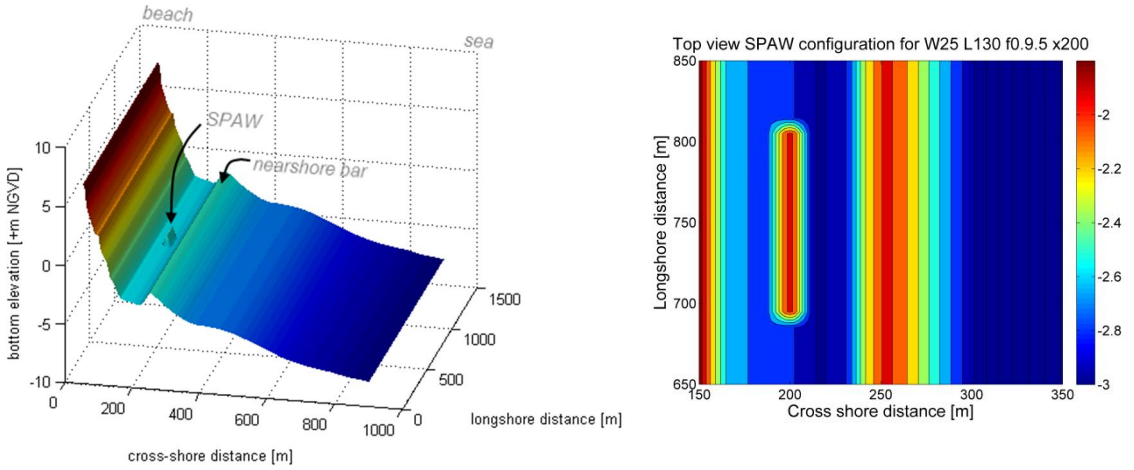

Figure 3.8. ***Base case:*** *Schematic alongshore uniform bathymetry including a SPAW (left), and top view of SPAW configuration zoomed in at SPAW location (right). The axis and colouring of both figures do not have the same scale.*

We analyzed bathymetric measurements on the 6th of April 1994 and chose a representative transect (Appendix C) and extended it uniformly along the coast (Figure 3.8). One nearshore breaker bar is located at a cross shore distance of 250 meter. The model is based on a highly schematized alongshore uniform bathymetry, in order to investigate the autonomous effect of a SPAW. On top of the uniform bathymetry, SPAWs are schematized as described in the following paragraph.

3.4.3.1 SPAW configuration

Since a SPAW is only captured once in a bathymetric survey, uncertainty is involved in modelling a SPAW event. In this study the SPAW top is assumed to be at the same height as the top of the nearshore bar (Figure 3.9 - left), this is confirmed by the one observation which was done (Figure 2.4). Also it is observed that waves break over the SPAW, this indicates that SPAWs should have a similar height as the bar. The slopes of SPAWs are assumed to be of maximum 1:10; because if slopes are steeper, the feature is not likely to occur in real life due to the angle of repose of sand. Additionally, a slope of 1:10 approximately resembles the shoreward slope of the bar.

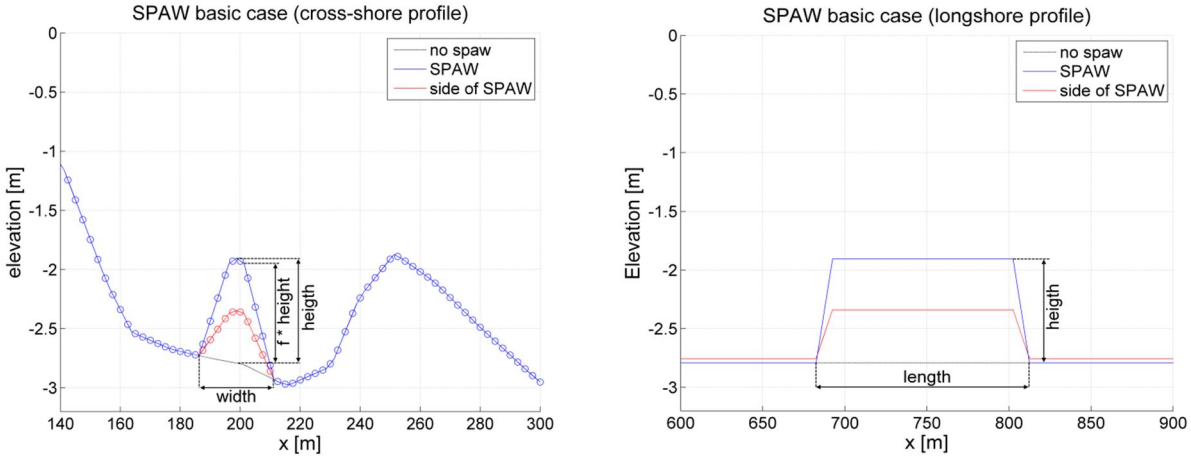

Figure 3.9. Cross-sections of SPAW, showing cross-shore (left) and longshore (right) configuration. Circles indicate water depth points.

The height of a SPAW is defined as the distance from top to original bottom at that location. Despite the high resolution not much depth points are located over the SPAW. The grid-resolution in cross-shore direction is 2.5 m; so for a SPAW of 25 m wide, 11 points are located over the SPAW. Therefore the shape is modelled relatively simple. It is modelled as a triangle with a flattened top; the height of the depth points close to the top are a factor (f) times the height of a SPAW (Figure 3.9 - left).

In longshore direction the grid-resolution is 5 m. applying a 1:10 slope implies that only one depth point is located at the sloping side of the SPAW. For cross-shore grid points at the slope the shape is defined in the same way as for the middle, only the height is taken as the half of the height of the top of the SPAW (Figure 3.9 -red line).

Delft3D applies a staggered grid; this has implications for the SPAW schematizations. It was chosen to specify the depth in the cell-centres (in water level points), using the key value DPSOPT = DP. For calculations in the velocity points depth was interpolated as the mean of two adjacent velocity points (DPUOPT = MEAN_DPS).

3.4.3.2 SPAW Base case

For the base case scenario a SPAW was configured as follows: Width (W) = 25 m, Length (L) = 130 m, factor for flattened top (f) = 0.95. As can be noted, the width deviates from the width of the chosen representative SPAW event. This is due to the fact that the height, slope and width are linked. The slopes would become too steep when modelling the SPAW with a width of 18 meter. Since determining the sizes of a SPAW is uncertain, adjusting the width seems acceptable. The SPAW is located at a cross-shore distance of 198.75 m, in between the coast and bar. And at a longshore distance of 750 m, in the middle of the domain.

3.4.3.3 SPAW scenarios

In the last part of this study (Chapter 6) SPAW configurations are varied to investigate the sensitivity of results to morphometric characteristics of SPAWs. Since the available time was not sufficient to run many cases, it was chosen only to run one specific case of each scenario. This will give a first impression of the response of the wave-induced flow field around a SPAW to morphometric characteristics of the SPAW. Running cases with SPAWs at different locations, gives insight in the expected morphodynamic behavior of a SPAW. Because if a SPAW shows a shoreward displacement for all locations; it can be expected that during a morphodynamic run the SPAW will propagate onshore.

Five SPAW configurations were tested (lower part in Table 2), in which the width, length, location and local bathymetry were changed. In scenario 5 the local bathymetry was adjusted (Figure 3.10), because it could be seen in the conducted bathymetric survey at Duck that the bar was lowered seaward of the SPAW. The bathymetry and a top view of the bathymetry for each scenario are shown in Appendix F.

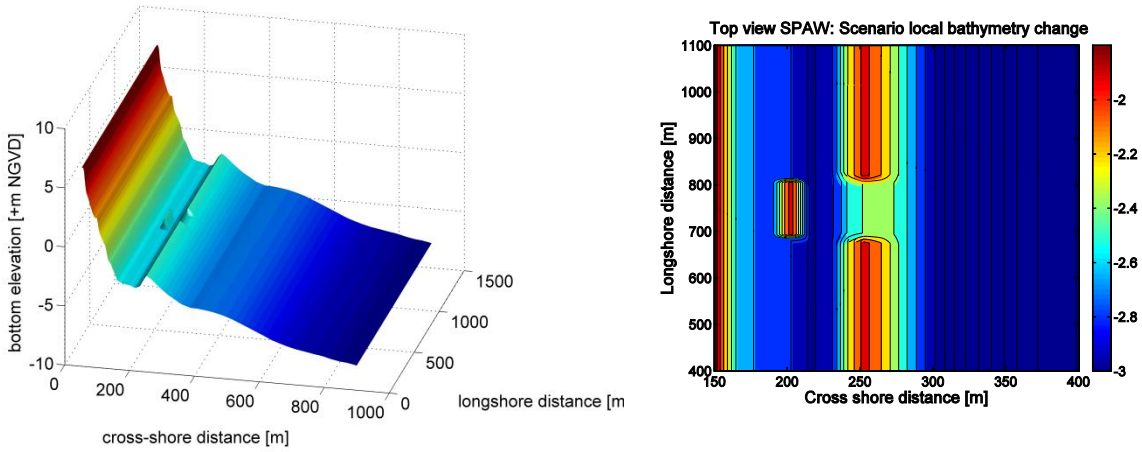

Figure 3.10. ***Scenario with local bathymetry change:*** *Schematic alongshore uniform bathymetry including a SPAW (left), and top view of SPAW configuration zoomed in at SPAW location (right). The axis and colouring of both figures do not have the same scale.*

Table 2. SPAW configurations for base case and different scenarios

	Hs [m]	Z [m]	Width [m]	Length [m]	Location [m]	Remarks
Base case	0.56	0	25	130	198.75	
S1: varying water levels	0.56	-0.5, 0, 0.5	25	130	198.75	
S2: varying wave heights	2.23	0	25	130	198.75	
S3: longer SPAW	0.56	0	25	400	198.75	
S4: wider SPAW	0.56	0	60	130	198.75	
S5: closer to shore	0.56	0	25	130	175	
S6: closer to bar	0.56	0	25	130	225	
S7: local bathymetry change	0.56	0	25	130	198.75	Bar lowered

3.4.4 Initial and boundary conditions

Flow and transport boundary conditions are required at an open boundary, representing the influence of the area outside the modelled area. In this model we used three types of boundary conditions (Figure 3.6, left). For the FLOW-module Neumann boundaries are combined with water level boundaries. A Neumann boundary of zero is imposed at the lateral boundaries perpendicular to the coast; it implies that alongshore water level gradient is zero (no horizontal tide). These boundaries need to be used in combination with a water level boundary at the seaward boundary, to make the solution of the mathematical boundary value problem well-posed. For the WAVE-module 2D-(directional and frequency) wave spectra are imposed at all boundaries. For sediment transport no boundary conditions are specified, an equilibrium sediment concentration at the boundaries is calculated. This provides the model area of sediment. As initial condition 0 kg/m^3 is imposed. The initial sediment layer thickness at the bed is set to 5 m (default).

3.4.5 Conditions applied in Delft3D modelling

As mentioned in the paragraph above, Delft3D requires wave and water level information at the model boundaries. The imposed conditions (i.e. tide, significant wave height, water level, and wave spectra) are based on the measured data during the 1994 representative SPAW event, and are discussed in this paragraph.

3.4.5.1 Tide (Water level, z_{tide})

A fixed water level (z_{tide}) was imposed at the offshore boundary which represents high/low tide states of the vertical tide. Since the dominant M_2-tide has an average amplitude of approximately 0.5 m (Figure 3.3) water levels of -0.5 m, 0 m and +0.5 m are imposed to investigate the influence of vertical tide. The different water elevations are implemented in Delft3D by adapting the offshore boundary condition. The water level of 0 meter is used in the base case.

The horizontal tide component is not taken into account in this study, since it is expected that this longshore component does not have much impact on dominantly cross-shore SPAW dynamics.

3.4.5.2 Significant wave height and peak period

Two significant wave heights are chosen in order to represent the extremes which occur during SPAW occurrence. As explained in the introduction there is a tendency that the SPAW initiates after a storm and propagates during calmer conditions, this is confirmed by the significant wave height data measured during SPAWs for 1994 (Figure 3.5). For this reason a low and high significant wave height were chosen, respectively H_s =0.56 m and H_s =2.23 m. The low wave height is used in most cases, since it is the prevailing wave condition during the SPAW events.

We also took SandyDuck97 data (Van der Werf, 2009; Appendix E) into account when choosing values for the significant wave height, since for the representative SPAW event no spectral wave data are available whereas for the SandyDuck97 there is. H_s and T_p were chosen so that the combination occurred during the average SPAW event and the SandyDuck97 experiments. Thus we used 2D-spectral wave data from '97 to investigate whether the JONSWAP spectrum resembles a realistic wave spectrum at Duck Beach (USA).

We searched for a time in the SandyDuck97 data at which the mean wave direction (θ_{Tmean}) was around 90˚ (i.e. waves coming from the East) in order to minimize effects of oblique incoming waves and directional spreading. Also T_p was chosen such that it was very similar for both wave heights, to exclude the effect of wave period. A relatively long wave period was chosen to represent swell occurring at Duck. Applied conditions to represent hydrodynamics during an average SPAW event are summarized in Table 3.

Table 3. Conditions from SandyDuck97 to represent average SPAW event hydrodynamics.

	H_s [m]	T_P[s]	θ_{Tmean}[˚]	V_{wind}[m/s]	θ_{wind}[˚]	Z_{tide}[m]		
10/18/1997 19:00:00	2.23	8.1	80*	11.9	26.9	-0.5	0	0.5
09/27/1997 01:00:00	0.56	8.2	90	4.16	75.37	-0.5	0	0.5
** in the simulation a θ_{Tmean} of 90˚ was used for generating the JONSWAP spectrum*								

3.4.5.3 Wave spectra

For the WAVE module wave spectra were imposed at all boundaries, we applied uniform boundary conditions along all boundaries. This can either be 2D (directional and frequency)-wave spectra obtained from data or a parametric specified spectrum such as JONSWAP, Pierson-Moskowitz or Gauss. In this study we use a parametric specified spectrum, because it has the advantage that it is a regular spectrum, with no natural irregularities at different frequencies and directions. This helps by interpreting results, since patterns become clearer and are not disturbed by variances in the spectra.

We choose a JONSWAP spectrum which stands for Joint North Sea Wave Observation Project (Hasselman et al., 1973). They found that a wave spectrum is never fully developed and continues developing through non-linear wave-wave interactions when waves are propagating. In Delft3D a JONSWAP spectrum can be generated, requiring significant wave height and peak period as input. The peak enhancement factor is set to 3.3 and the direction spreading is 4 (default Delft3D).

JONSWAP is developed for the North Sea which has a different wave climate than the Atlantic Ocean (respectively wave and swell dominated). However, since we give input data for the spectrum that is based on a swell dominated beach it was seen to represent the measured spectrum quite well (Figure 3.11). The main differences between the two spectra is (i) that for the measured spectrum also more energy is found at higher frequencies and (ii) the measured spectrum has a *mean* wave direction of 90˚, instead of the having the peak at that direction. Therefore the 1D-spectra for a direction of 90˚ how similar patterns, but have a different maximum energy density (Figure 3.11 - bottom).

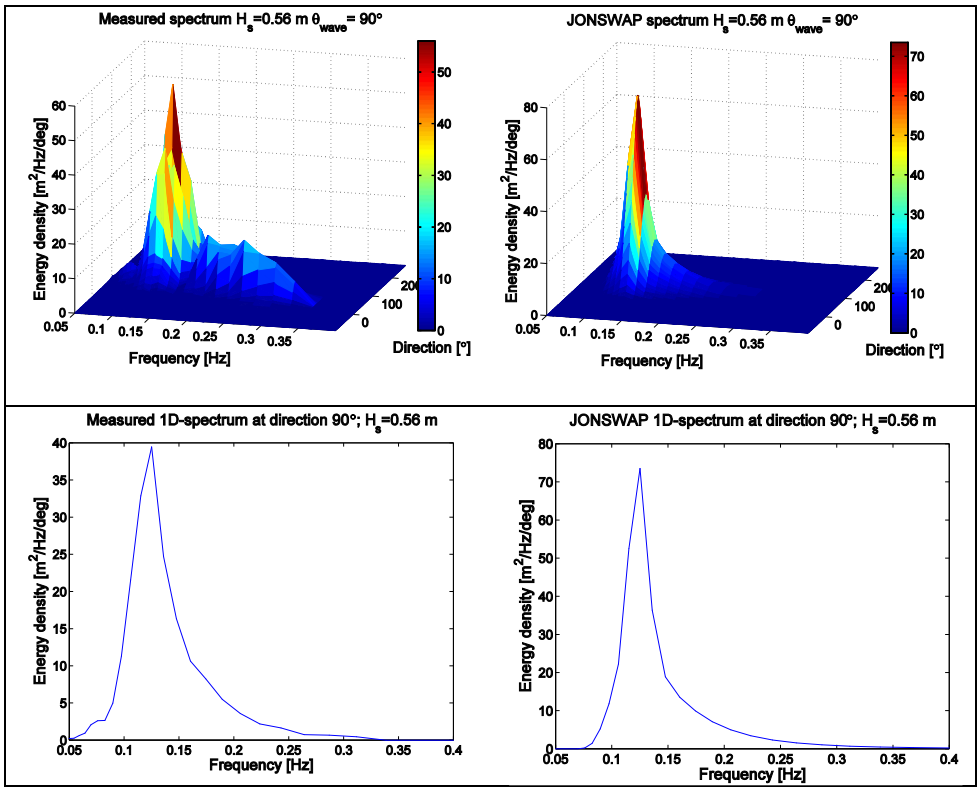

Figure 3.11. Wave spectra for the low wave height. Measured wave spectrum for the low wave height (left) and JONSWAP wave spectrum as applied in this study (right). Top figures are 2D-wave spectra (directional and frequency), and bottom figures are 1D-wave spectra (frequency) for the mean wave direction. Note that the scaling is different for all plots.

3.4.6 Parameter settings

Since no measured data of the flow-field and sediment transports are available for calibrations within the period of interest (22nd of April 1994 to 5th of May 1994) the parameter settings as used by Van der Werf (2009) and Treffers (2009) are applied, and some were slightly adjusted based on expert knowledge or sensitivity analysis. The parameter settings are summarized in Table 4. For parameters not mentioned in this paragraph, we used default Delft3D settings.

Table 4. Parameters for the Delft3D model to simulate SPAW behaviour.

Parameter		Default Delft3D	Van der Werf (2009)	This study
Simulation time	[min]	-	60	120
Time step	[s]	-	6	1.5
Nr. of vertical layers	[-]	-	-	20
Reflection parameter	[s^{-2}]	0	100	100
Water density	[kg/m^3]	1000	1025	1025
Chézy roughness coefficient	[$m^{0.5}/s$]	65	60	60
Background horizontal viscosity	[m^2/s]	1	0	0.1
Background horizontal diffusivity	[m^2/s]	10	0	0.1
Model for 3D-turbulence	[-]	-	k-ε model	k-ε model
Threshold depth	[m]	0.1	0.2	0.2
Smoothing time	[min]	60	15	15
Interval wave computation	[min]	-	30	15
Roller	[-]	No	Yes	Yes
Cstbnd	[-]	No	Yes	Yes
Gamdis	[-]	0.55	Ruessink et al. (2003)	Ruessink et al. (2003)
Mean sediment diameter (d_{50})	[mm]	-	-	0.2

The *simulation time* for the model in this study was taken twice as long as Van der Werf (2009). Trial runs showed that after 60 minutes of simulation time, results were not yet fully in equilibrium. Extending the simulation time with 60 minutes gave more steady results (Appendix D).

The *time step* in this study is 1.5 seconds, which is much smaller than that of Van der Werf (2009). We have increased the grid resolution significantly, to ensure enough grid cells were located over the SPAW. Therefore a smaller timestep is necessary to ensure accurate results, see also the time step analysis reported in Appendix D.

A *reflection parameter (alpha)* was set for the water level boundary; a higher value of alpha makes the open offshore boundary less reflective for short wave disturbances propagating from inside the model. This kind of disturbances can especially occur at the start of the computation. Alpha is set to 100 (similar to Van der Werf, 2009) in order to let initial disturbances propagate out the model quickly.

The *Chézy value* was set at a value of 60 $m^{0.5}/s$, similar to Van der Werf (2009) and Treffers (2009). They calibrated the model on data. Treffers showed that 60 $m^{0.5}/s$ agreed better with longshore measurements than 55 $m^{0.5}/s$. Van der Werf (2009) showed that the Chézy value did not influence significant wave height much, but it did influence longshore currents which was the main focus of their study.

The *background horizontal viscosity and diffusivity coefficients* represent a series of complicated hydrodynamic phenomena. Decreasing horizontal eddy viscosity reduces horizontal mixing. These coefficients are so called calibration parameters, so their value is normally determined in the calibration process. However, no SPAW data for calibration are available; therefore we choose parameters based on expert knowledge. The horizontal eddy viscosity depends on the flow and the grid size used in the simulation, for detailed models with grid sizes typically as tens of meters of less, the values should be in the range of 1 to 10

m^2/s (Deltares, 2011). Since this study applies an extremely detailed grid, the value was set to 0,1 m^2/s (Personal communication with Walstra and Roelvink). Treffers (2009) showed that the default value of Delft3D as well as a value of zero did give good agreement with measurements for the external forcing (wave height and water level). For longshore currents agreement it was better if the background horizontal viscosity was set to zero. In this case only wave-breaking induced horizontal viscosity is added by the roller model to the system.

A *model for 3D turbulence* can be selected for a 3D simulation to determine the vertical turbulent eddy viscosity and turbulent eddy diffusivity additional to the background values. For this study the k-epsilon turbulence model was applied, this model relates the vertical mixing length and vertical eddy viscosity to actual flow properties. Therefore this model is assumed to give a more realistic distribution of the velocity (Treffers, 2009).

The *threshold depth* is the depth above which a grid cell is considered wet. Also, it affects currents since in Delft3D the roller stress is turned off at twice the threshold depth. In very shallow water, say depth less than 0.4 m, Delft3D occasionally generates large currents, due to unrealistic roller or wave forces (Hsu et al., 2006). Setting the threshold depth at 0.2 m avoids this problem.

The *smoothing time* is taken similar to Van der Werf (2009). It represents the time interval used at the start of a simulation for a smooth transition between boundary and initial conditions. In the model schematization the offshore water level boundary matches the initial condition, therefore a smoothing time of 15 minutes is sufficient.

The *interval of wave computation* is set to 15 minutes, which is slightly smaller than the interval set by Van der Werf (2009). Trial runs showed that when reducing the interval, the model results were stabilizing quicker.

The *roller model* (Appendix B.4) is used in this schematization to compute wave heights, as it was shown to improve predictions of wave height and longshore current velocities (Hsu et al., 2006). The effect of including the roller model is that regions of wave-set up are shifted shoreward as well as the wave-driven currents, because wave energy dissipation is delayed. The peak frequency and mean wave direction as computed by SWAN are used as input for the roller model. The term *Cstbnd* should be used when applying the roller model; it switches advection terms containing normal gradients off. Advection terms at the offshore boundaries may generate an artificial boundary layer along the boundary, which is not desired. Additionally, dissipation of wave energy is calculated within the roller model; *Gamdis* is used for specifying a user defined gamma (γ) value used for calculating dissipation of wave energy formula. The parameter represents the significant wave height to depth ratio associated with depth induced breaking, i.e. the maximum height that can occur at a given depth. This γ can either be constant or variable γ (Ruessink et al., 2003). The latter is used in this study, since Hsu et al. (2006) showed that this expression improved wave height prediction. Compared to a typical fixed γ -value (0.5-0.8), the variable gamma leads to higher waves in deeper water and lower waves in more shallow water (Van der Werf, 2009).

For the *mean sediment diameter* a uniform value of 0.2 mm was taken. Larson and Kraus (1993) obtained from 209 sediment samples that coarser material is present close to the shore and decreases rapidly with distance offshore. About 200 m from the shoreline the grain size is almost constant. Although the scatter in the data is wide, the median grain size in the offshore part of the profile is slightly less than 0.2 mm, whereas the material at the shoreline is generally coarser.

3.4.7 Roller model implementation

A three-dimensional Delft3D model which applies the Roller model was used (Appendix B.5). The roller model as applied in Delft3D-FLOW has been introduced to delay transfer of wave energy to the current. When using roller equations, the wave set-up and longshore and cross-shore flow are shifted shoreward.

3.4.7.1 Roller model formulation (Delft3D Manual)

The roller model formulations are described in the Delft3D-FLOW manual (Deltares, 2011). The short wave balance reads:

$$\frac{\partial E}{\partial t} + \frac{\partial}{\partial x}\left(EC_g \cos(\propto)\right) + \frac{\partial}{\partial y}\left(EC_g \, sin(\propto)\right) = -D_w \tag{3.2}$$

In which E is the short wave energy, C_g is the group velocity, $\propto$ the wave direction, and D_w the dissipation of wave energy. The latter is described by the expression of Roelvink (1993). Wave energy is reduced and transformed into roller energy if wave break. It is located in down-wave region after wave breaking. This roller energy is modelled to propagate at twice the local celerity of the carrier waves and is rapidly dissipated in shallow regions. The energy that is lost from the organised wave motion is converted to roller energy through the roller energy balance:

$$\frac{\partial E_r}{\partial t} + \frac{\partial}{\partial x}\left(2E_r C_g \cos(\propto)\right) + \frac{\partial}{\partial y}\left(2E_r C_g \, sin(\propto)\right) = D_w - D_r \tag{3.3}$$

In which D_r is the roller energy dissipation, this is a function of the roller energy:

$$D_r = 2\beta g \frac{E_r}{C} \tag{3.4}$$

In which β is a user-defined coefficient of approximately 0.1 (default Delft3D) and g the acceleration of gravity. The above described time- and space-varying wave and roller energy cause a variation in radiation stresses (vertically averaged), through the following relations:

$$S_{xx} = \left(\frac{C_g}{C}(1 + \cos^2(\alpha)) - \frac{1}{2}\right)E + 2\,cos^2(\alpha)\,E_r \tag{3.5}$$

$$S_{xy} = S_{yx} = \sin(\alpha)\cos(\alpha)\left(\frac{C_g}{C}E + 2E_r\right) \tag{3.6}$$

$$S_{yy} = \left(\frac{C_g}{C}(1 + \sin^2(\alpha)) - \frac{1}{2}\right)E + 2\,sin^2(\alpha)\,E_r \tag{3.7}$$

In which S denotes radiation stress, which is subdivided in a depth-uniform stress and a surface stress as a result of the roller on the top of the water column. These surface stresses are always directed to the coast (since they are a result of wave breaking), and are the shear stresses related to the roller. The surface stress is formulated as a roller force ($F_{r,x/y}$):

$$F_{r,x} = \frac{D_r}{C}\cos(\alpha) \qquad F_{r,y} = \frac{D_r}{C}\sin(\alpha) \tag{3.8}$$

Then the depth-invariant part of the radiation stresses, the organized wave forces ($F_{w,x/y}$), follow from the total radiation stress gradient minus the roller force:

$$F_{w,x} = -\left(\frac{\partial S_{xx}}{\partial x} + \frac{\partial S_{xy}}{\partial y}\right) - F_{r,x} \qquad F_{w,y} = -\left(\frac{\partial S_{xy}}{\partial x} + \frac{\partial S_{yy}}{\partial y}\right) - F_{r,y} \tag{3.9}$$

When assuming a uniform coast, a steady flow, and wave-dominance (i.e. tidal flow can be neglected in the near-shore zone) the equation of motion reduces to:

$$\underbrace{g\frac{\partial \xi}{\partial x}}_{1} = \underbrace{\frac{F_x}{\rho h}}_{2} - \underbrace{\frac{\langle \tau_{bx} \rangle}{\rho h}}_{3} \tag{3.10}$$

In which the terms represents (1) the water level slope, (2) wave forcing (in this case the roller plus the wave force) and (3) bed-shear stress. When considering merely cross-shore flow and not sediment transport the bed shear stress term can be neglected. Then equation 3.9 reduces to:

$$g\frac{\partial \xi}{\partial x} = \frac{F_x}{\rho h} \tag{3.11}$$

As described earlier in Chapter 2 and Appendix A.2 stresses as induced by wave force (i.e. gradients in radiation stresses) are compensated by a slope in water level (i.e. wave set-up or set-down). Since the roller force is only directed in direction of propagation (x-direction), the force will induce a wave set-up only and no set-down.

3.4.7.2 Roller model implementation in Delft3D-FLOW

During the analysis it turned out that in the current Delft3D-FLOW version 4.00.04.757 roller forces are indeed calculated by Eq. 3.7. However organized wave forces are not calculated by Eq. 3.8, but are always set to zero for the whole domain when using a stationary roller model. This implies that wave set-down due to shoaling and the wave-set up due to wave height decrease by deshoaling/breaking induced by the organized wave force is not incorporated in the current Delft3D version. Only the roller force is calculated and used for calculating water level gradient. This might influence the flow-field around the SPAW.

In order to investigate effects of incorporating wave forces in the calculation a test-version of Delft3D was made (Sep 13th, 2012) in which wave forces are calculated as described in the manual. Runs were done with this test version for H_s=0.56 meter and different water levels. Unfortunately, runs for the average and high water levels (z = 0 m and z=+0.5 m) gave unstable results for the current settings in the model schematization. Since the time span for this study was limited, no time was left to investigate why these results became unstable for the test-version. This is an interesting topic to investigate in more detail in future research. The results for the lower water level (z = -0.5 m) were stable, and were used to compare results of the current and test-version of Delft3D (paragraph 5.3).

4 SPAW dynamics for the base case

SPAW behaviour is observed in nature and can be seen as a natural way of beach nourishment (Chapter 2). A SPAW is located in the nearshore zone, in which waves break and nearshore processes are complex. Waves interact with the bottom, which results in gradients in radiation stresses, by which pressure gradients develop. These gradients on their turn generate currents in longshore and cross-shore direction. And finally, they interact with waves again, resulting in a complex hydro-morphodynamic system.

In this Chapter, SPAW dynamics for the base case scenario are analysed. The base case applies SPAW dimensions of the representative SPAW events, and a low wave height (H_s=0.56 m; T_p=8.2 s) and an average water level (z=0 m). The low wave height is chosen since it is dominant in periods when SPAWs occur, as there is a tendency for SPAWs to initiate after a storm and propagate during calmer conditions (paragraph 3.3.3). All runs in this Chapter were done with the current version of Delft3D (i.e. version 4.00.04.757 in which wave forces are set to zero). The situation without a SPAW is referred to as the *reference situation*. It has the same conditions as the SPAW case, but only a different bathymetry.

In Section 4.1 an overview is given of transects on which results are presented. The analysis of the base case was done in the sequence of analysing the following parameters: wave heights development (Section 4.2), water level development (Section 4.3), cross-shore and longshore velocities (Section 4.4), and resulting sediment transport patterns (Section 4.5). Some minor non-uniformity was found in modelling results, and is discussed in Section 4.6. The Chapter concludes with a summary of important insights in Section 4.7.

4.1 Transects for analysing

Different transects are used in the analysis to show local changes in parameters (Figure 4.1), it also visualizes directions and magnitudes of currents in more detail. Longshore transects are chosen on top of the bar, and seaward, on top, and just landwards of the SPAW; referred to as “Top bar” (purple), “Seaward” (green), “Top SPAW” (blue), and “Landwards” (red). The cross-shore transects are chosen southward, at the tip and in the middle of the SPAW; referred to as “Side SPAW” (red), “Tip SPAW” (green), and “Centre SPAW” (blue). The centre of the SPAW is located at a cross-shore distance of 198 m and a longshore distance of 750 meter. The top of the bar is located at a cross-shore distance of 251 meter.

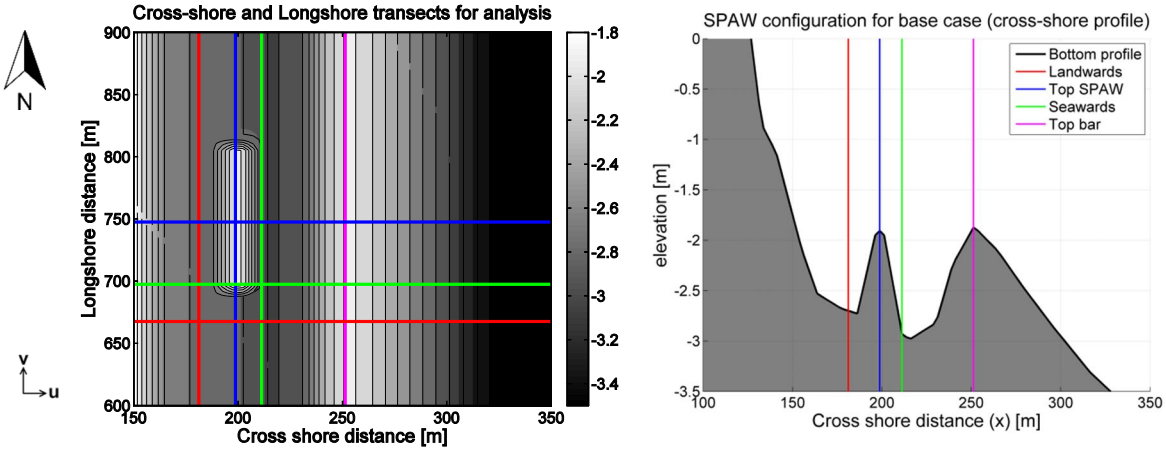

Figure 4.1. Transects on which simulation outputs are plotted. Left: top view of longshore and cross-shore transects. Right: Side view of longshore transects. The colours match with the colouring in plots of results.

In the analysis, especially relative differences between the situation with a SPAW and the reference situations (i.e. without a SPAW) are of importance. Therefore, also differences between the two situations are plotted several times. These plots always show differences between situations with a SPAW minus the reference situation. So if the difference is positive, the SPAW case showed an increase relative to the reference case.

Be aware that in the plots cross-shore velocity (U) and sediment transports are *positive* (negative) for values in *offshore* (onshore) direction. The longshore velocity (V) is *positive* (negative) in *northward* (southward) direction. Also note that plots zoom in at the SPAW location and do not visualize the total modelled area.

4.2 Significant wave height development

Variations in wave height show several aspects (Figure 4.2 and 4.5). Firstly, significant wave height increases at the bar (shoaling) and decreases landward of the bar (deshoaling and wave-breaking) for both reference and SPAW situation. A little bit of wave breaking takes place over the bar, as can be seen in the presence of a roller force at the bar location (i.e. x=251 m in Figure 4.3). Since no difference is visible between the reference and SPAW situation at the bar, the SPAW does hardly influence wave heights in seaward direction.

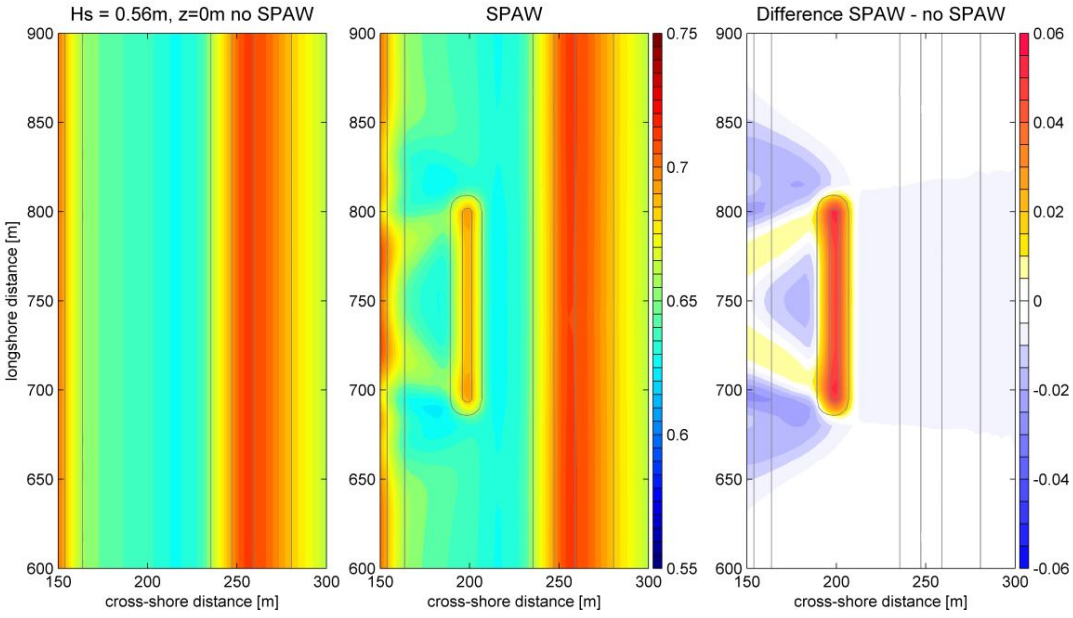

Figure 4.2. Top view of significant wave height, showing reference situation (left), situation with a SPAW (middle) and the difference (right). The background colouring represents magnitude in meters, contour lines show bottom contours. Note that the figures are zoomed at the SPAWs location.

Secondly, the SPAW case shows increasing wave heights over the SPAW due to shoaling effects (Figure 4.2 and 4.5). Some waves break over the feature, since landward of it wave height is slightly reduced compared to the reference situation. This indicates a loss of energy due to wave breaking. Also small roller forces develops over the feature (i.e. around x=198 m in Figure 4.3).

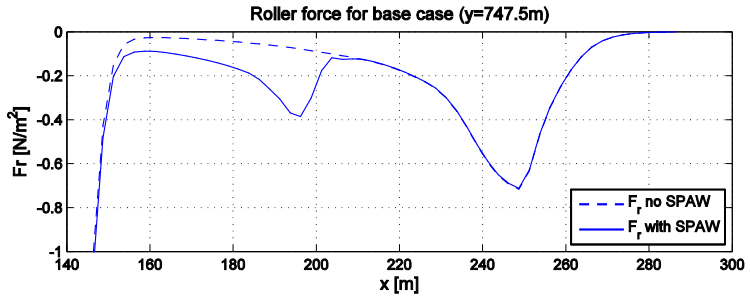

Figure 4.3. Cross-shore variation in roller (F_r) force over the middle of the SPAW. A negative force is directed onshore. The SPAW is located at x=198 m and the top of the bar is located at x=251 meter.

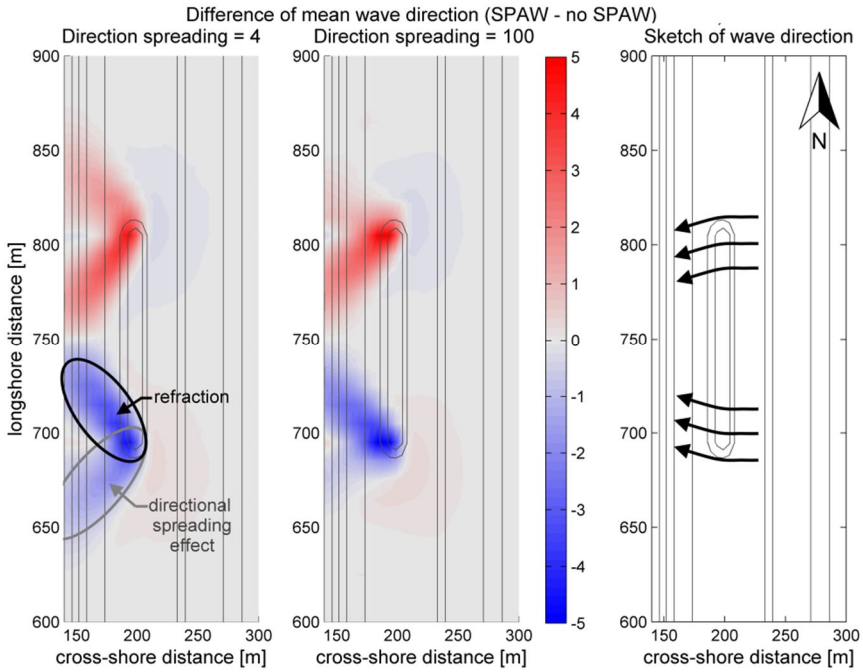

Figure 4.4. Mean wave direction differences for two directional spreading coefficients. Showing refraction, reflected by difference in mean wave direction landward of the SPAW. Besides this, a directional spreading effect north and south of the SPAW can be seen, which is especially visible with a lower directional spreading coefficient (left). Background colouring shows magnitudes in meter, a negative value implies that the wave is directed slightly to the North compared to the reference situation. Contour lines show SPAW bathymetry.

Thirdly, it can be observed that the presence of a SPAW affects wave direction, due to refraction and directional spreading effects (Figure 4.2 and Figure 4.4). Waves are refracted around the SPAW just landward of it. The effect of directional spreading is visible north and southwards of the SPAW. The feature can be seen as a submerged breakwater for waves over which still some waves can pass. Although for this study mean wave direction is set to 90 degrees, waves enter the domain with a certain directional spreading depending on the directional spreading coefficient. A low value for this coefficient corresponds to a spectrum with a larger directional spreading, whereas a high value corresponds to a narrow spectrum for the directions. Delft3D default for this coefficient for a JONSWAP spectrum is 4. To explain the directional spreading effect, an example is given: at the North side of the SPAW, waves coming from southeast are partly “blocked” by the feature. These waves are not in the wave field on the northern side landwards of the SPAW anymore. Due to this filtering mechanism, waves at this northern side of the SPAW are slightly directed more to the south

(i.e. a positive difference in Figure 4.4). For the southern part, the same process takes place for wave approaching from northeast. When increasing the directional spreading coefficient (i.e. less directional spreading), directional spreading effect decreases whereas the effect of refraction is similar.

The longshore variation in significant wave height also shows effects of above described differences in wave direction (Figure 4.5). The wave height at the SPAW tip is slightly higher due to refracted wave energy. Also the effect of refracted waves can be seen just landward of the feature (Figure 4.5, right), for which a decrease in wave height is visible around the SPAW tips (i.e. at approximately y=690 and y=810 m wave energy is reduced). A local increase just landward of the SPAW in wave height due to refracted wave energy, is visible at a quarter of the SPAW for the landward transect (i.e. at approximately y=710 and y=790 m in Figure 4.5, right).

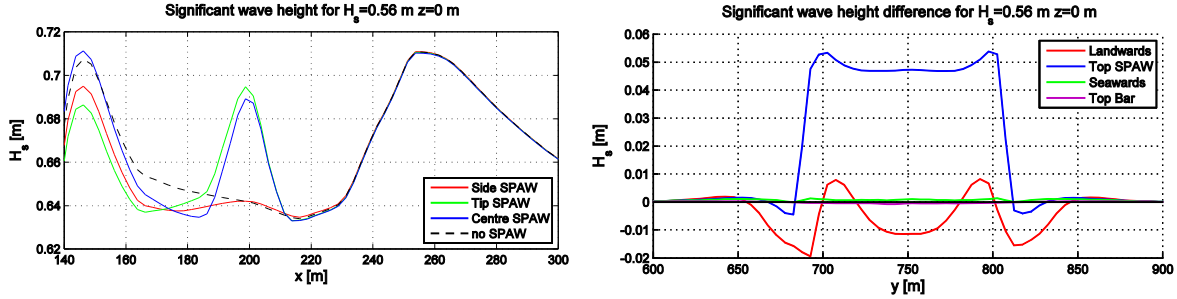

Figure 4.5. Left: Cross-shore variation in H_s on different longshore transects for the SPAW situation. Right: Alongshore variation in H_s on different cross-shore transects, showing differences.

4.3 Water level development

Variations in significant wave height and dissipation induce gradients in radiation stress. These induce set-up and set-down (paragraph 2.2.1.3), resulting in longshore pressure gradients and mass-fluxes, generating circulation currents. For the current version of Delft3D wave forces are set to zero, so no wave set-down and additional set-up by the wave forces is computed. Since roller forces are directed shoreward, they only induce set-up.

In the reference situation wave set-up develops offshore, and increases significantly around the bar location (x=255 m). Also a rapid wave set-up is seen at the shore; at these locations waves are breaking (Figure 4.6 and 4.7).

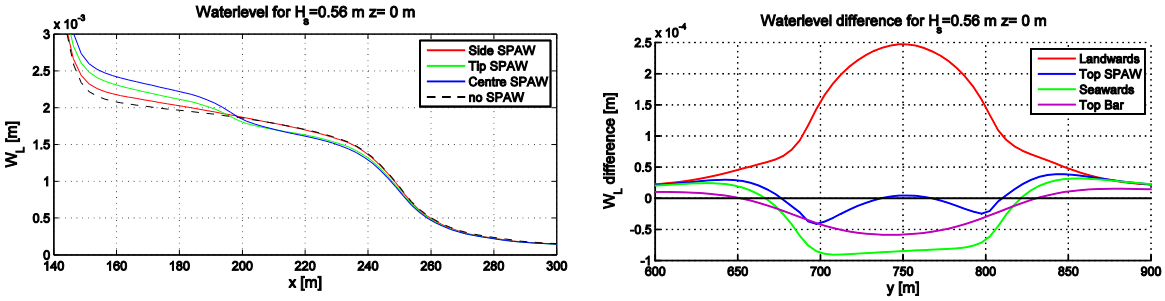

Figure 4.6. Left: Cross-shore variation in water level on different longshore transects for a SPAW situation. Right: Alongshore variation in water level on different cross-shore transects, showing differences.

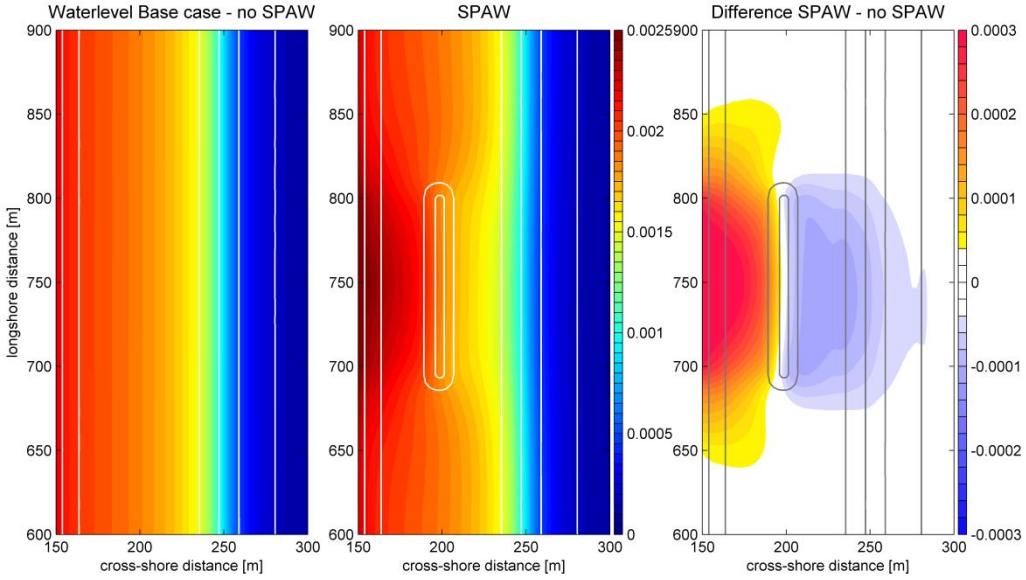

Figure 4.7. Top view of water level, showing reference situation (left), situation with a SPAW (middle) and the difference (right). Background colouring represents magnitude of water level in meters, contour lines show bottom contours.

For the SPAW situation there is less set-up seaward of the SPAW, leading to locally slightly lower water levels (Figure 4.7). In contrary, landward of it an increase in set up is visible, since some waves break over the feature generating set-up. These local areas of set-up and relative set-down generate a horizontal circulation current. Water flows from high pressures to low pressures, so pressure gradients induce currents. At the landward side, water is higher in the middle then at the sides, consequently water will flow from the center to the sides. In contrary, seawards of the SPAW water is lower at the center then at the sides, so water flows from the side to the center. This induced a horizontal circulation in the flow-field as seen in Figure 4.8 (right figure). Longshore variations show a special water level gradient above the SPAW, with lower water level at the tips of the SPAW (i.e. blue line in right Figure 4.6). This pattern can be an effect of the horizontal circulation pattern induced by the wave generated longshore pressure gradients land- and seawards of the SPAW. In order to close the circulation at the crest of the SPAW water should flow from the tips to the middle and from the tips to the sides of the SPAW.

4.4 Velocity patterns

Local gradients in water levels and mass-fluxes can generate local horizontal circulation currents. It is important to note that cross-shore current (U) is defined positive in offshore direction. Longshore currents (V) are positive in Northern direction. Unless stated otherwise, figures show Eulerian velocities.

The reference situation (no SPAW) shows a longshore depth-averaged uniform velocity field as expected (Figure 4.8). Since waves enter the domain perpendicular to the coast; longshore velocities are approximately zero in the whole domain for the reference situation. The cross-shore velocity is larger over the bar. Since water depth is smaller above the bar, velocities should be higher in order to transport the same mass of water.

An undertow is visible near the coast (around x=140 m), this is generated by (breaking) waves. Delft3D utilises the two-layer concept introduced by De Vriend and Stive (1987) in which it is assumed that onshore mass transport of water occurs between wave top and

trough, which is compensated by an offshore directed undertow below the wave trough. Since Delft3D considers phase-averaged wave properties, only mass flux below the wave trough is considered through the application of the shallow water equations in a generalized lagrangian mean (GLM) framework (Walstra et al., 2000). In contrast to the GLM-velocities, which include the onshore directed stokes drift; Eulerian velocities include the wave induced undertow. For closed coast applications this typically results in offshore directed Eulerian flows as can be seen from these simulations.

Figure 4.8 shows a top view of depth-averaged velocities for the situation without, with and the differences between these two cases. The latter clearly show that differences show a horizontal circulation cell pattern around the SPAW. Caution is needed by interpreting this plot since it only shows *differences* in magnitude and direction and not the velocity pattern in case of a SPAW.

Figure 4.9 shows depth-averaged Eulerian and GLM velocities, the only difference between these plots is that from the GLM velocities the onshore directed stokes drift is subtracted in order to obtain Eulerian velocities. The figures show that indeed a horizontal circulation cell develops due to the presence of a SPAW (see GLM-velocities); however for Eulerian velocities this flow-field is dominated by the undertow.

With respect to Figure 4.8, 4.9, 4.10 and 4.11 several aspects are worth mentioning:

- A horizontal circulation current around the SPAW tips is generated due to the SPAW presence. This is visible in the GLM velocities and also the difference plot in Eulerian velocities; for the wave conditions and water depths for this base case the depth averaged Eulerian flow-field is dominated by the undertow. The circulation pattern is also visible in longshore depth averaged Eulerian velocities (Figure 4.10). Namely, seaward of the SPAW these are directed southwards (negative), but landward of the SPAW these are directed northwards (positive) on the northern part of the SPAW (y>750 m).
- For the SPAW case depth averaged Eulerian velocity over the feature is offshore directed (Figure 4.9 and 4.11), only the magnitude is smaller compared to the reference case due to the generated circulation current. Also land- and seaward of the SPAW velocity is directed less offshore, due to the horizontal circulation.
- At the SPAW crest the magnitude of cross-shore depth averaged velocity is higher than land- and seaward of the SPAW to transport the same mass of water over the reduced water depth at the feature (Figure 4.11).
- At the tips (i.e. longshore distance y=690 and y=810 m) depth averaged velocity is smaller than at the middle of the SPAW (i.e. longshore distance y=750 m). This also reflects the influence of the cell-circulation which is larger at the tips than in the middle of the SPAW (Figure 4.8).

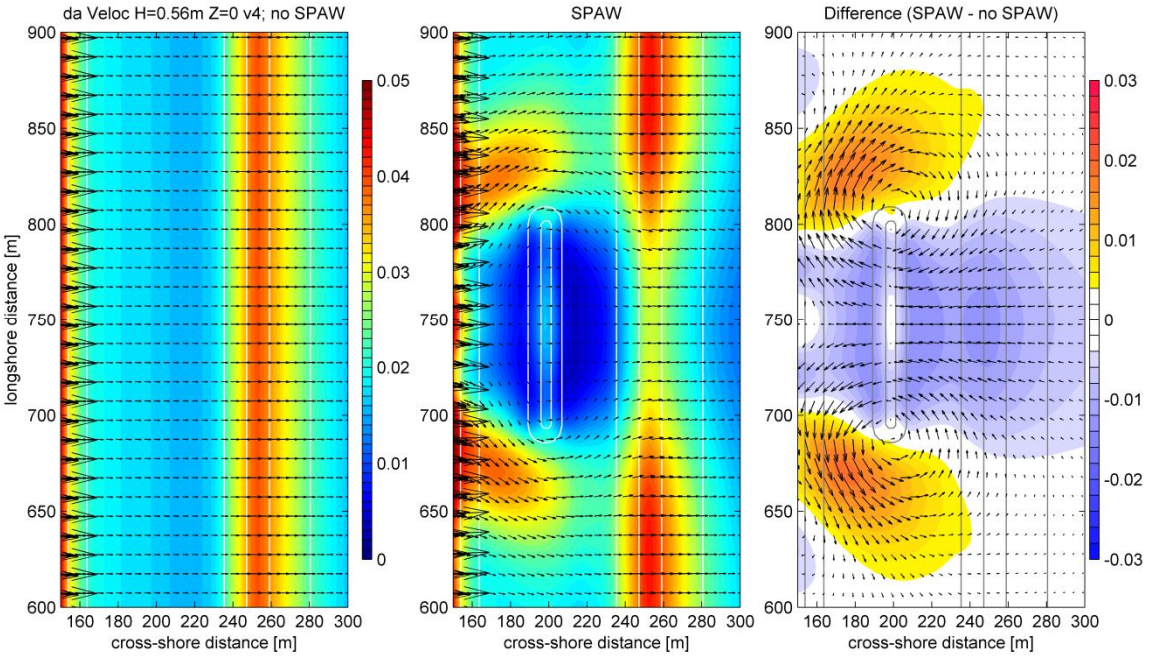

Figure 4.8. Top view of depth-averaged velocity (m/s), showing reference situation (left), situation with a SPAW (middle) and the difference (right). The background colouring represents magnitude, vectors show directions, grey contour lines show bottom contours. Note that the figures are zoomed at the SPAWs location.

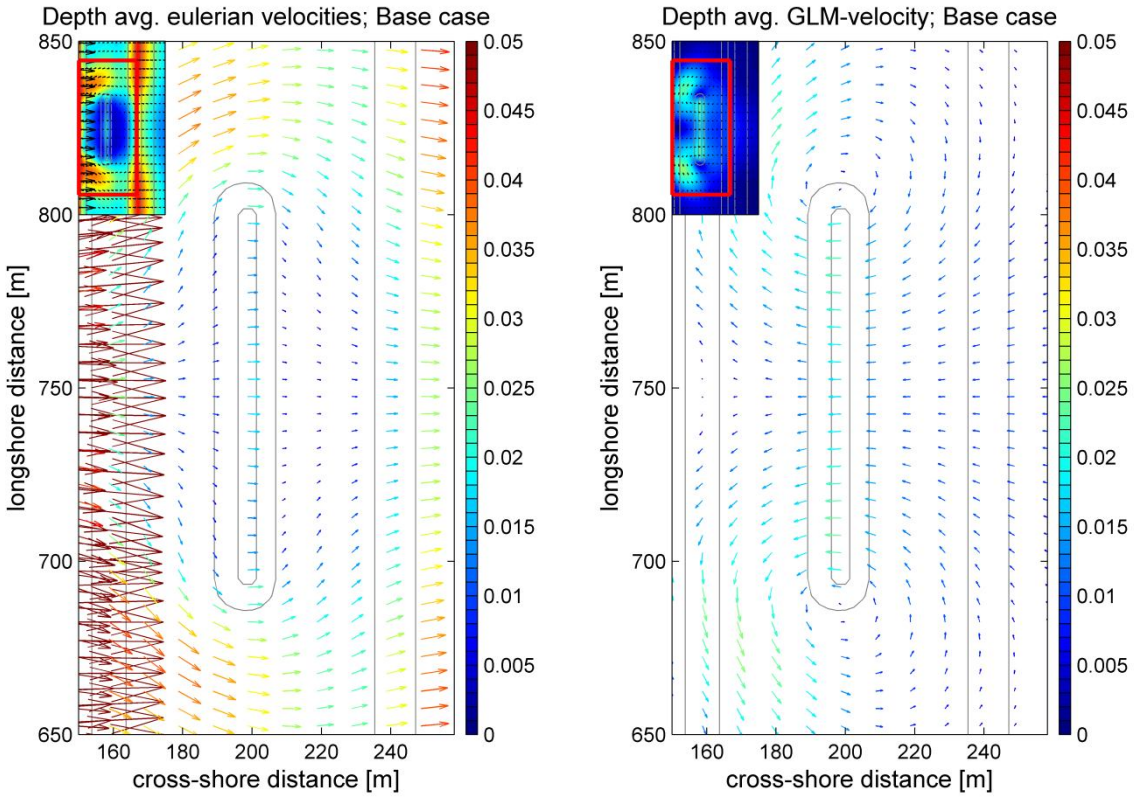

Figure 4.9. Top view of depth-averaged velocities (m/s), Eulerian (left) and GLM (right), zoomed in at the SPAW (red box in top left inset). Vectors show directions and magnitude, contour lines show bottom contours. The inset at the top left shows the velocity pattern around the SPAW for a larger area, is enlarged in Appendix G.

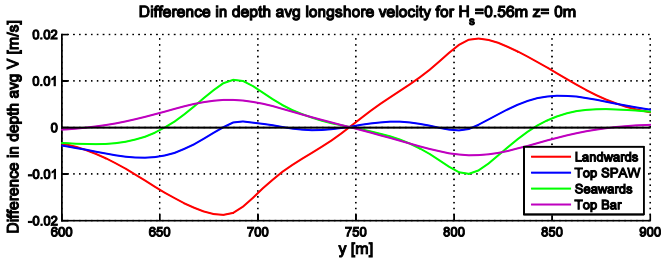

Figure 4.10. Depth averaged longshore velocity over longshore transects. Showing that longshore velocities are present in case of a SPAW; due to the generated horizontal circulation current.

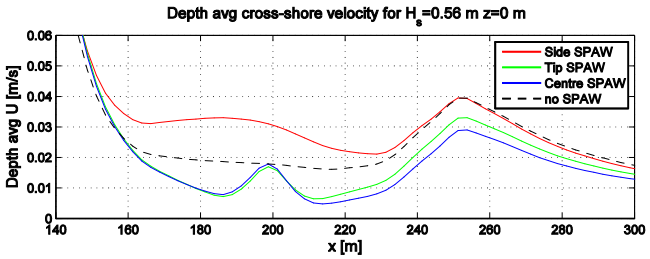

Figure 4.11. Depth averaged cross-shore velocity over cross-shore transects.

Since the model is three-dimensional, also velocity and concentration profiles can be analysed (Figure 4.12). These are especially important for suspended sediment transport. Concerning velocity profiles, the following aspects were observed. GLM velocities are directed more onshore compared to Eulerian velocities, since it includes the onshore Stokes drift. For the SPAW case (full lines), velocities at the SPAW and landwards of it are more onshore directed in the top of the water column because waves break over the feature. In sediment concentration profiles, it was seen that the SPAW presence mainly influenced the profile at the SPAW crest. The reference concentration is much higher and more sediment is entrained in the water column (Figure 4.12 – lower). For the other locations, landwards and seawards of the SPAW, differences in concentration profiles between the reference and the SPAW case are small.

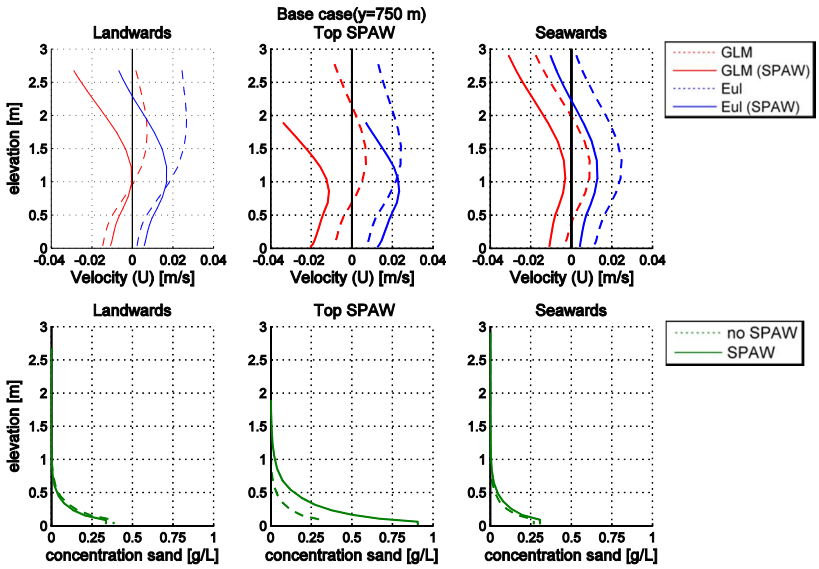

Figure 4.12. Velocity (upper figure) and sediment concentration (lower figure) profiles for the base case at different cross-shore locations around the SPAW. Positive velocities are offshore directed.

4.5 Sediment transport

The presence of a SPAW induces wave-breaking over the feature, higher velocities over it, and the generation of a horizontal circulation current as illustrated in previous paragraphs. These aspects all influence sediment transport, because this is strongly related to local near-bed velocities and vertical mixing of sediment by wave breaking.

There are no data available to calibrate sediment transport calculations, since measuring the flow-field and sediment transports around a SPAW is hard due to its irregular occurrence. In this study Delft3D parameters values are chosen based on current expert knowledge, and are not calibrated to fit any results. In order to give some feeling whether modelling results are valid, they are compared to the hypothesis based on theory and to a rough estimate of the sediment flux based on SPAW observations done by Wijnberg and Holman (2007). The modelling results are in the same order of magnitude of the rough estimate. Therefore they are trusted to give a *qualitative* impression on how sediment transport patterns are expected to be influenced by the presence of a SPAW.

Delft3D considers near-bed and suspended load, adding these two together gives the total sediment load. Near-bed load transport is an order of magnitude larger than suspended load transport (i.e. respectively 10^{-5}[m^3/s/m] and 10^{-6} [m^3/s/m], Figure 4.13) for a low wave height and an average water level.

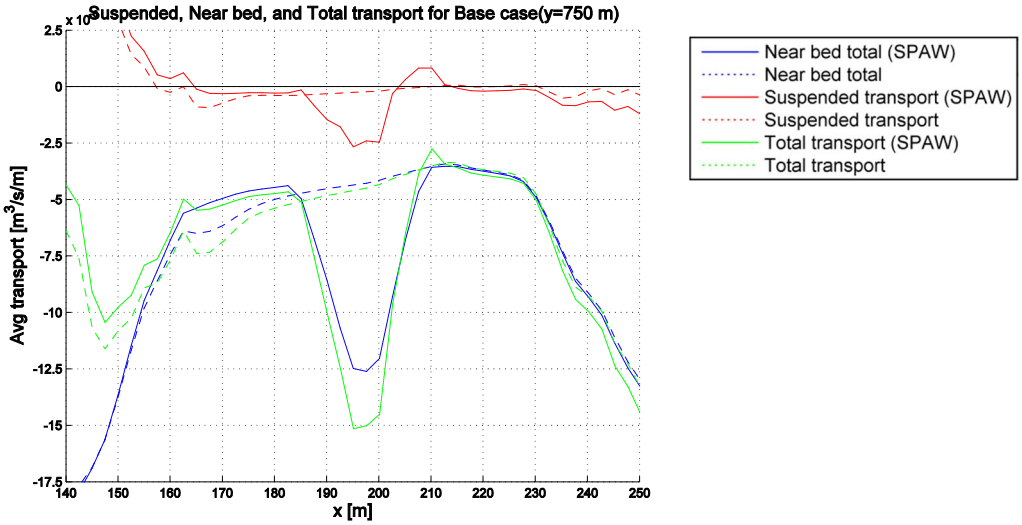

Figure 4.13. Cross-shore sediment transport over the centre of the SPAW. Showing the near-bed, suspended, and total load transport components. Negative values are onshore directed transports. The SPAW crest is located at x=199 m.

4.5.1 Near-bed load transport

In the applied theory of Van Rijn (2007) near-bed load consists of three parts, (i) bed load due to currents, (ii) bed-load due to waves, and (iii) suspended load due to wave asymmetry. In this study bed load refers to bed load due to waves and currents. The overall pattern of near-bed load transport shows the cross-shore component is always directed onshore (i.e. negative values) (Figure 4.13 and 4.14), and an increase is seen at the SPAW crest (order $8x10^{-6}$ m^3/s/m) compared to the reference case.

The onshore directed near-bed transports indicate that components in direction of wave propagation are dominant. Figure 4.14 shows that the suspended load due to wave asymmetry increases over the SPAW in the same order of magnitude as bed load increases.

This implies that wave non-linearity is an important aspect for sediment transport over a SPAW during this low wave conditions.

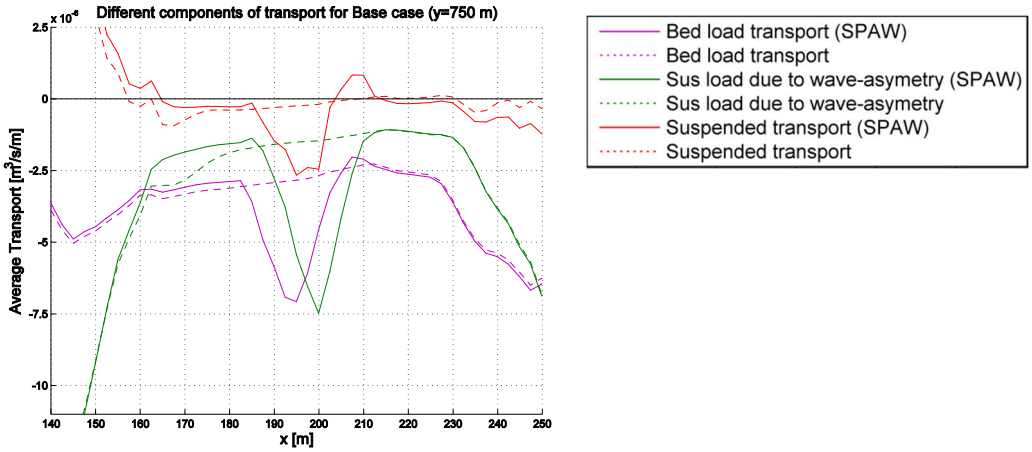

Figure 4.14. Cross-shore sediment transport components over the centre of the SPAW.

Longshore transport rates are an order of magnitude smaller than rates in cross-shore direction (Figure 4.16); this implies that hardly any longshore bed load transport takes place. At the crest and landwards of the SPAW, we see that around the SPAW near-bed load is slightly directed to the middle of the SPAW, which resembles the refraction pattern of the waves (Figure 4.15). This also reinforces the statement that near-bed load transport is mainly dominated by waves and not by the currents induced by the horizontal circulation pattern.

In conclusion, wave skewness and asymmetry are increased over the SPAW due to a modulation of wave field induced by the SPAW presence. This leads to an increase in onshore near-bed load transport in the direction of wave propagation, as was also hypothesized based on literature.

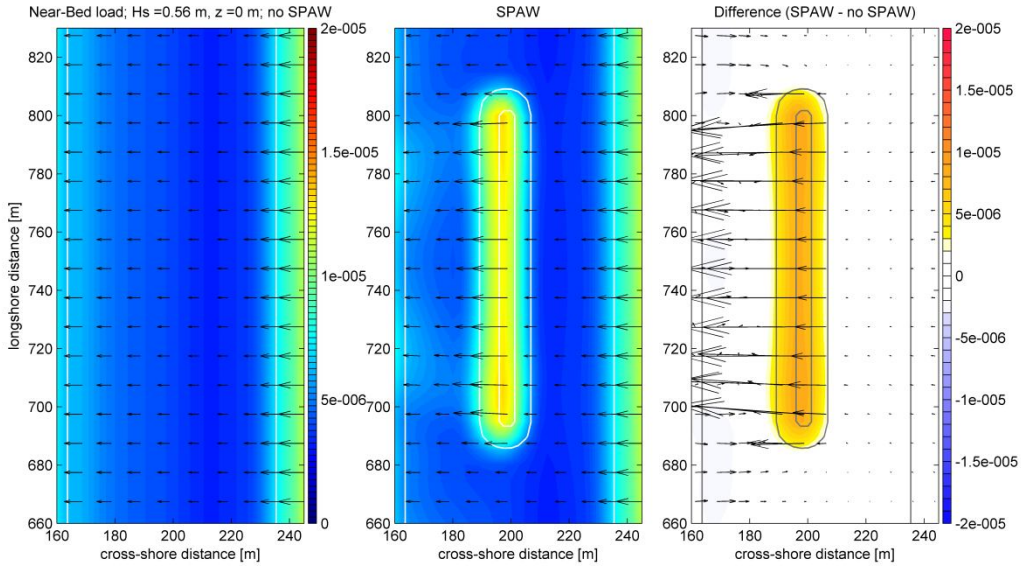

Figure 4.15. Top view of bed load transport (m^3/s/m) showing reference situation (left), situation with a SPAW (middle) and the difference (right). The background colouring represents magnitude, vectors show directions, grey contour lines show bottom contours.

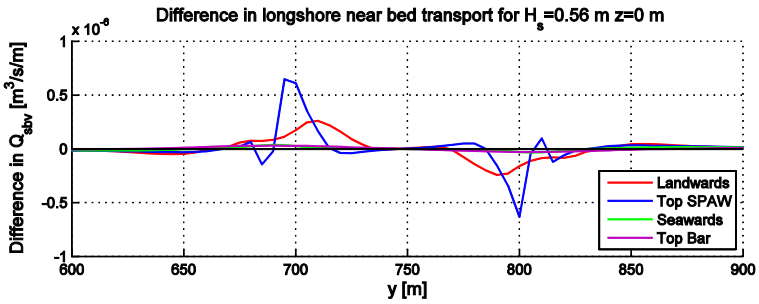

Figure 4.16. Longshore variation in bed-load transport load in y-direction (longshore). Positive values are Northern directed transports.

4.5.2 Suspended transport

The suspended transport for the reference case is very low for the offshore domain, but rapidly increases near the coast and is then offshore directed (Figure 4.13). When depth-induced wave breaking takes place, more sediment is entrained in the water column. This was seen on the SPAW crest (Figure 4.12 – lower figure).

Quantities that are moving with the flow are transported by the GLM velocity. Due to higher onshore GLM-velocities at the SPAW and more entrained sediments in the water column due to wave breaking, suspended sediment transport is increased in magnitude and onshore directed over the SPAW (Figure 4.17).

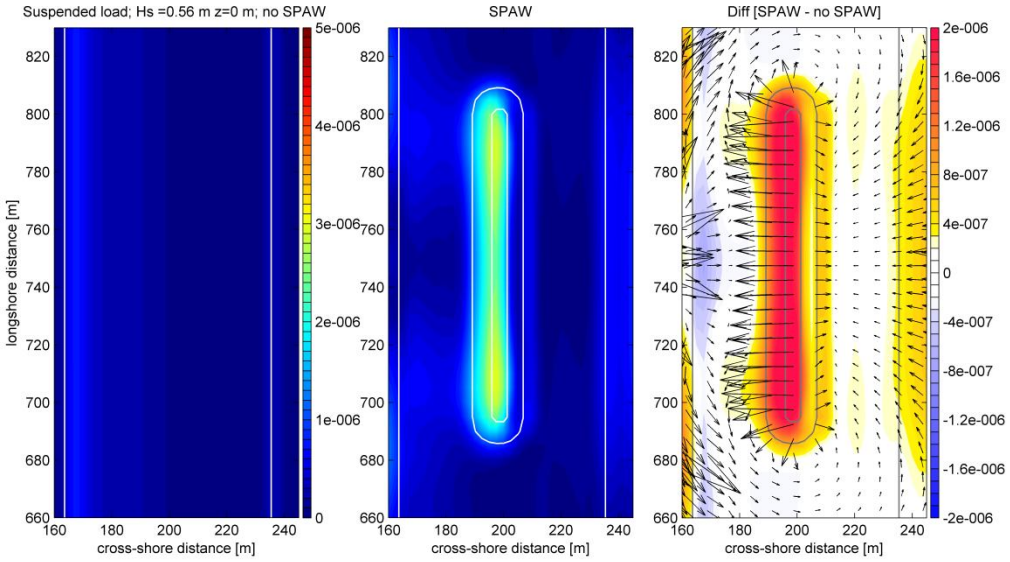

Figure 4.17. Top view of suspended sediment load transport (m^3/s/m). Background colouring represents magnitude, vectors show directions, grey contour lines show bottom contours. No vectors are shown for left and middle, since these plots are then dominated by large vectors directed from the coast as a result of the undertow.

The horizontal circulation current does influence suspended sediment transport, due to the modulation of the wave driven flow-field in the GLM velocities. This can be seen in the top view difference plot (Figure 4.17-right) and in the longshore directed suspended sediment transport load (Figure 4.18). The longshore and cross-shore components of the suspended sediment transport are of the same order of magnitude.

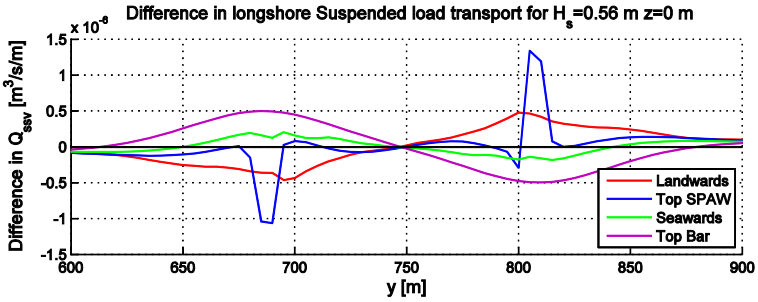

Figure 4.18. Longshore variation in suspended transport load in y-direction (longshore).Positive values are Northern directed transports.

4.5.3 Total load transport

The total load is the sum of the near-bed and suspended transport load. Since for this prevailing wave condition the near-bed load is larger than suspended load, total load is dominated by near-bed-load transport pattern. Figure 4.19 shows the top-view of the total load in which the increasing onshore transport above the SPAW is clearly visible. This is consistent with the formulated hypothesis over sediment transport.

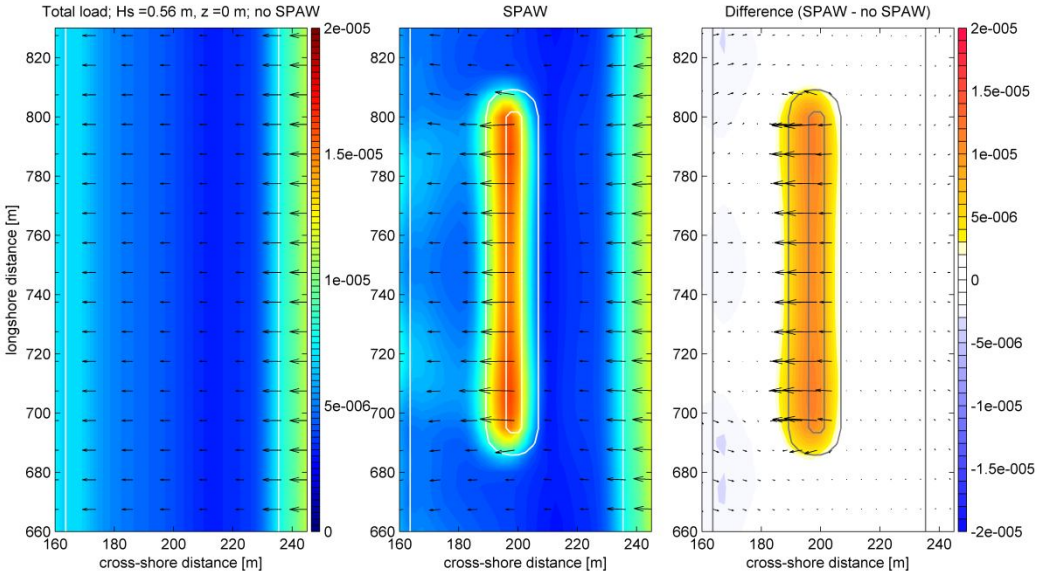

Figure 4.19. Top view of total load transport (m^3/s/m), showing reference situation (left), situation with a SPAW (middle) and the difference (right). The background colouring represents magnitude, vectors show directions, grey contour lines show bottom contours.

The longshore component of sediment transport can induce longshore diffusion of the SPAW. For near-bed load transport the longshore component was negligible and directed towards the middle of the SPAW at the tips; whereas for suspended transport the longshore and cross-shore components had the same order of magnitude and a horizontal circulation pattern was visible. Since for this case near-bed load is dominant, longshore components of transports are negligible. This implies the SPAW is expected to propagate towards the coast maintaining its shape, which is consistent with SPAW observations done by Wijnberg and Holman (2007).

We have confidence in the modelling results, since these are in the same order of the rough estimate based on average shape and migration speed of SPAW observations. Wijnberg and Holman (2007) estimated that with an average onshore propagation speed of 3.1 +/- 0.8

m/day and a height of the SPAW in the order 0.5 m, the average onshore sediment flux related to the SPAW propagation will be about 1 to 2 m^3/m/day. From the simulations the total sediment transport above the SPAW is approximately $1.5x10^{-5}$ m^3/m/s or 1.3 m^3/m/day and is onshore directed.

4.5.4 Initial sedimentation and erosion patterns

The onshore directed transport contributions result in a shoreward displacement of the SPAW. In the initial erosion-sedimentation patterns it can be seen that sedimentation occurs at the landward, and erosion at the seaward side of the SPAW. The onshore propagation of the feature is consistent to all SPAW observations (Wijnberg and Holman, 2007). Also no significant sedimentation or erosion is visible at the sides (north- and southward) of the SPAW. This is a first implication that the feature maintains its shape during shoreward propagation.

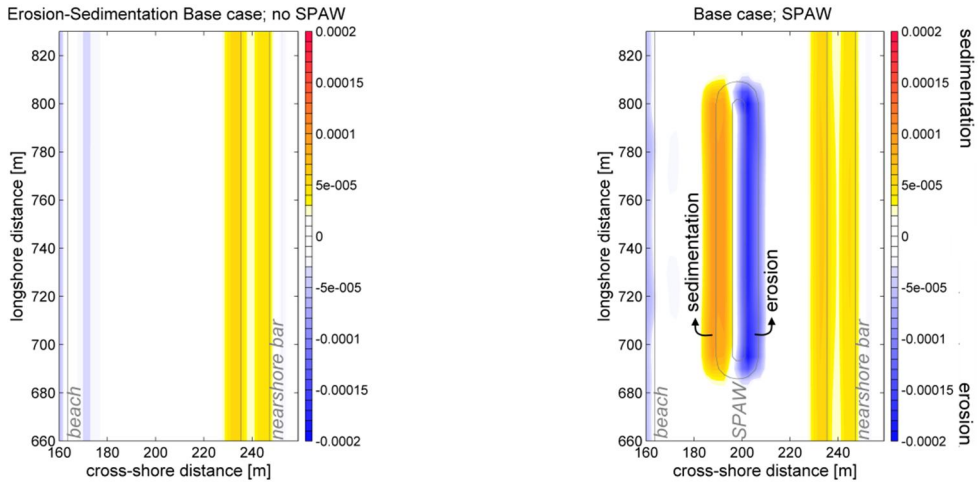

Figure 4.20. Top view of sedimentation and erosion pattern for the reference situation (left) and the SPAW situation (right). Warm colours denote sedimentation, cold colours denote erosion.

4.6 Non-uniformities in the model

Results are expected to be alongshore uniform, because the bathymetry is alongshore uniform for the reference situation (no SPAW). We discovered some minor non-uniformity in velocity profiles in the results which affected the sediment transport. Just seaward of the bar (i.e. around x=280 m) a relatively rapid transition in water level takes place (Figure 4.21 - left). Right at this location non-uniformities are visible for the sediment transports in the reference case. For this specific location no irregular gradients in bathymetry are present, the point lies on the sloping part of the seaward side of the bar. Based on theory and underlying bathymetry, changes at this particular location are not expected, and therefore regarded as numerical flaws in the model (personal communication Roelvink and Walstra). We saw at some grid points just seaward of the bar anomalous eddy viscosity profiles (Figure 4.21 - right). We regarded the cause for these irregularities to fall outside the scope of this study, since available time is limited and the location of these irregularities was outside the area of interest for SPAW dynamics. These anomalous vertical eddy viscosity profiles were also seen at the crest of the SPAW for the case with low wave height and high water level (Appendix I.1).

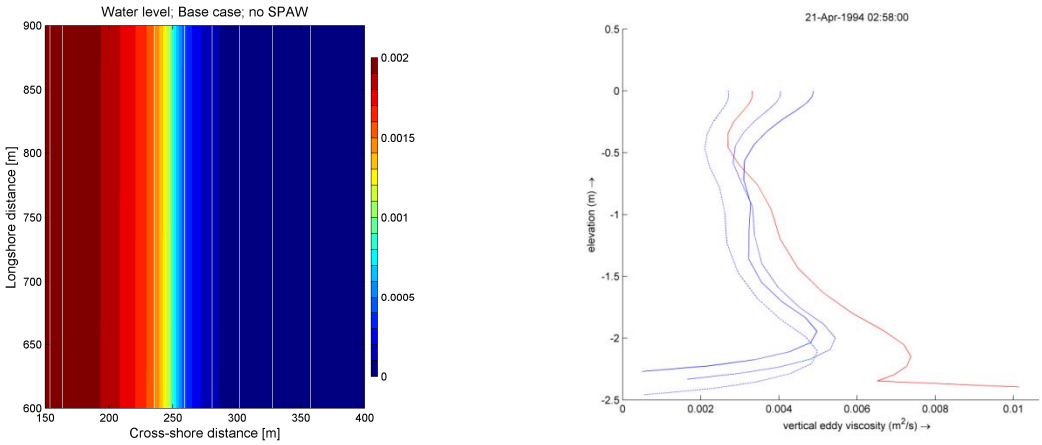

Figure 4.21. Left: Top view of water level variation showing rapid water level variation at x ≈280 m. Right: Vertical eddy viscosity profiles over cross-shore transect over crest of SPAW (y=750m). The blue lines indicate profiles at x=272 m (full), x=275 m (dashed), and x=280 m (dashed-dotted), the red line indicate the anomalous profile for x=277.5 m.

4.7 Summarizing important findings for SPAW dynamics for the base case

Numerical results show consistent results with respect to the hypothesis based on literature (paragraph 2.4), with respect to SPAW observations done by Argus video systems and previous estimates of sediment fluxes (Wijnberg and Holman, 2007). Namely, estimates of Wijnberg and Holman (2007) for average onshore sediment transport flux related to SPAW propagation is about 1 to 2 m^3/m/day, while results from this analysis estimated the flux on 1.3 m^3/m/day. Besides that, results are approximately uniform for the reference case without a SPAW. These above described observations give confidence in obtained model results.

Results for the base case gave insight in SPAW dynamics: by gained knowledge about wave-driven flow-fields and related sediment transport patterns induced by the SPAW presence. It showed that wave height varied locally since waves break over the SPAW, by which energy is dissipated. These variations in wave height induce cross-shore and longshore gradients in radiation stress, due to which local set-up (or relative set-down) is generated. The set-down was not computed since the current version of Delft3D was used. These variations in water level cause pressure gradients, which induce currents. The SPAW induced a modulation of the wave-driven flow field, namely a horizontal circulation current developed around it. Depth averaged Eulerian velocities were dominated by the undertow and offshore directed over the SPAW, but at the sides velocities were higher and directed around the feature. In depth averaged GLM-velocities, important for suspended transport calculations, a clear circulation pattern was visible showing onshore directed velocities at the full SPAW crest.

Sediment transport patterns are related to the flow-field, and are therefore also influenced by the SPAW presence. An onshore sediment transport was seen over the SPAW, which was dominated by near-bed transports in direction of wave propagation (i.e. bed load and suspended load transport due to wave asymmetry). These onshore directed transport contributions result in a shoreward displacement of the SPAW. Initial sedimentation occurred just landwards, whereas erosion occurred seaward of the SPAW. Since longshore velocities are small compared to cross-shore transports, this is a first implication that the SPAW maintains the shape during propagation.

In conclusion, the consistently onshore directed propagation of SPAWs can be explained by the SPAW induced modulation of the wave-driven flow field and related transport patterns. A

remarkable finding from these Delft3D simulations is that, with a low wave height, the generation of a horizontal circulation current is not the driving force for sediment transport. Near-bed sediment transport, mainly due to wave asymmetry, was seen dominant over suspended transport. For higher wave heights suspended transport is expected to be higher (i.e. more wave breaking and thus more suspended material in the vertical), this can effect sediment transport patterns since suspended sediment load is highly influenced by the generated horizontal circulation current. It would be interesting to investigate this in future research.

5 SPAW dynamics for varying water levels, wave height and Delft3D versions

In the former Chapter SPAW dynamics for the base case are analysed, with a low wave height and an average water level (H_s=0.56 m and z=0 m). To investigate how robust the behaviour is as was seen for the base case (Chapter 4), it was analysed how SPAW dynamics are influenced by changing water levels, wave height, inclusion of wave forces, and morphometric characteristics of the SPAW. The first three parameters are discussed in this Chapter, the morphometric characteristics are discussed in Chapter 6. The main driving forces and processes of hydrodynamic flow and sediment transport patterns around a SPAW are already discussed for the base case in the Chapter 4, and are not addressed again.

In Section 5.1 the influence of varying water level is analysed, and subsequently in Section 5.2 we discuss the influence in wave height. Then the results of the Delft3D test-version which includes wave-forces are discussed in Section 5.3. And the Chapter concludes with a summary of important findings in Section 5.4.

5.1 Analysing different water levels

The effect of the vertical tide on SPAW dynamics was investigated by adjusting water levels, doing runs with a water level of z=-0.5 m and z=+0.5 m. During a SPAW occurrence both high and low water levels occur due to the presence of the vertical tide. Water depth is an indicator of whether waves break over a SPAW. For example when water levels are lower, more wave breaking takes place over the bar and SPAW, due to the fact that corresponding water depths are lower. This can influence the wave-driven hydrodynamic flow field and sediment transport patterns around a SPAW. This Section discusses observed differences in cases with other water levels compared to the situation with an average water level (z=0 m).

5.1.1 Significant wave height development for different water levels

Wave breaking mainly depends on water depth in combination with wave height. Figure 5.1 also shows this aspect; with high water level (z=+0.5 m) less dissipation takes place over the bar, and only shoaling/deshoaling takes place over the SPAW. The latter is concluded because wave height is approximately the same landwards of the SPAW; implying that hardly any energy was dissipated. The roller forces (Appendix H) confirm this pattern. For the case with z= 0 m, some waves break over the bar and over the SPAW as discussed earlier. For a lower water level, more waves break over the bar and the SPAW. This was shown in a larger decrease in wave height landwards of both features.

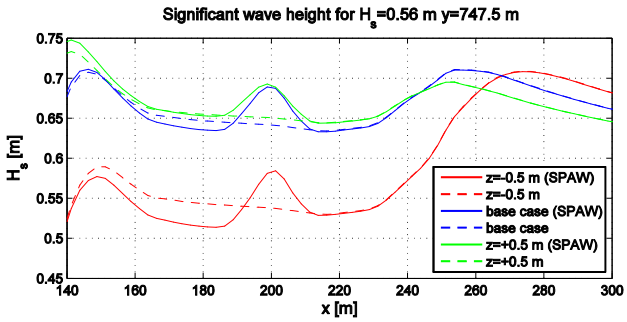

Figure 5.1. Cross-shore variation in significant wave height for different water levels..

An interesting aspect comes forward when looking at the top view of wave height differences between the SPAW and reference situation for the three water levels (Figure 5.2). For all cases wave height decreases north- and southwards of the SPAW due to the directional spreading effect. The wave refraction is also present in all three cases, but interestingly it is dominant for the high water level (i.e. the increase in wave height landward of the SPAW) since in this case hardly any waves break over the SPAW. Wave breaking is dominant for the low water level (i.e. a decrease in water level landwards of the SPAW in which still the refraction pattern is visible).

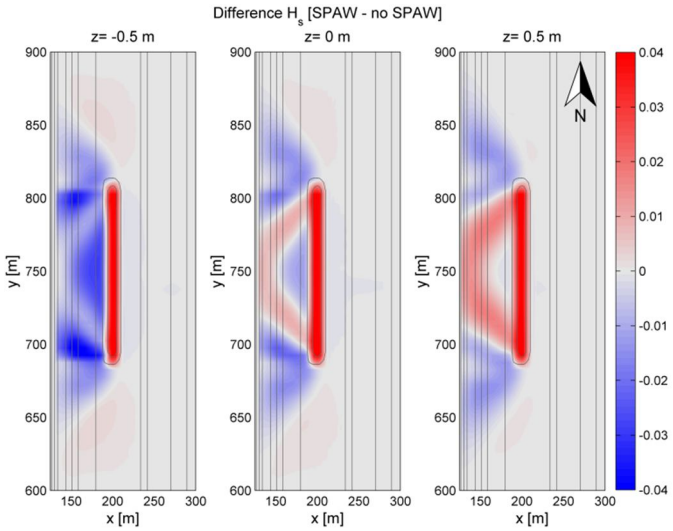

Figure 5.2. Top view of difference plots in significant wave heights (H_s) in meter for different water levels (z) (SPAW – no SPAW).The contour lines show SPAW bathymetry. Background colour shows the difference in H_s.

5.1.2 Water level development for different water levels

In order to compare the three cases with different water levels, the set-up is analyzed. This is the local water level minus the mean water level (Figure 5.3); thus only shows wave set-up and set-down. The latter is not included, since these runs were done with Delft3D-FLOW version 4 (paragraph 3.4.7).

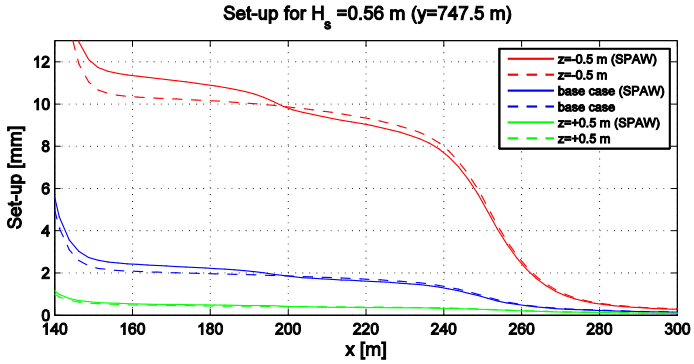

Figure 5.3. Cross-shore variation in set-up (i.e. current water level minus mean water level) over the middle of the SPAW for different water levels. The SPAW crest is located at x=199 m, the bar top is located at x=251 m.

As we expected from the wave breaking pattern, set-up is highest for low water levels, due to induced larger cross-shore and longshore gradients in radiation stresses by wave breaking (which takes place more often by the low water condition). Also additional set-up landwards of the SPAW is highest for the lowest water level. For the high water level set-up is only of the order of 0.1 mm, whereas changes induced by the SPAW are even smaller. From these water

level gradients the horizontal velocity pattern is expected strongest for the lowest water level (z= -0.5 m) and weakest for the highest water level (z= +0.5 m).

5.1.3 Velocity patterns for different water levels

As expected from the above described pressure gradients, hydrodynamic flow patterns around a SPAW are significantly different for different water levels (Figure 5.4), which is explained in this paragraph.

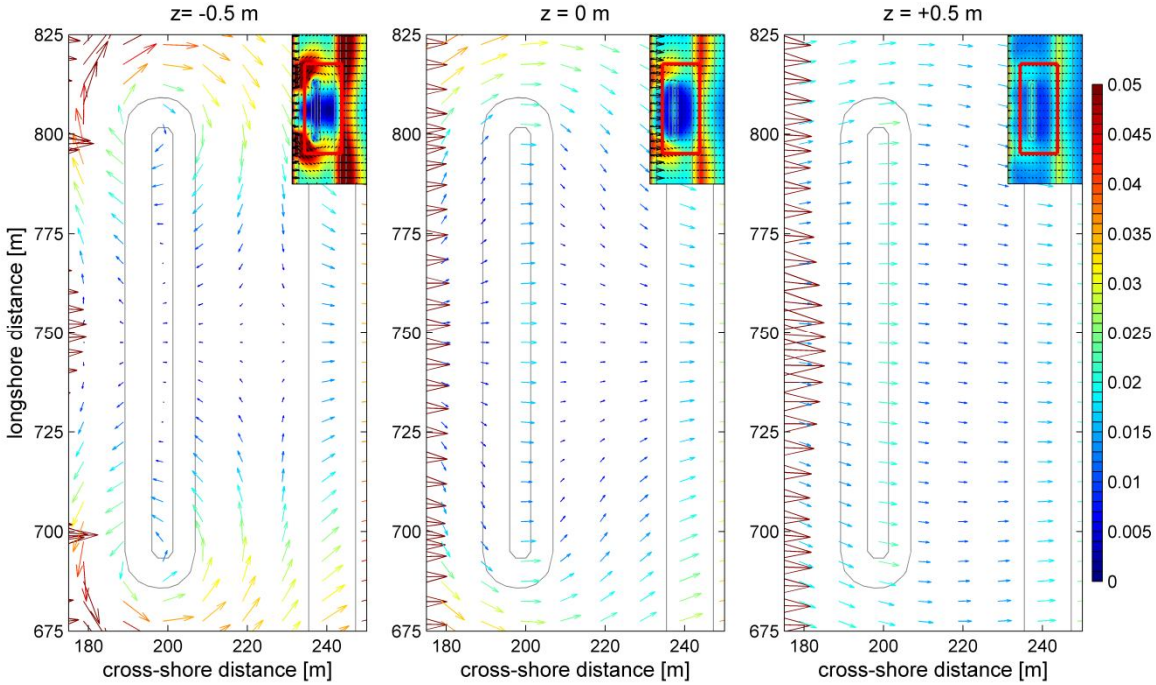

Figure 5.4. Top view of depth-averaged (Eulerian) velocity pattern (in m/s) for different water levels and low wave height, zoomed in at the SPAW (red box in top left inset). The vectors show directions and magnitude, grey contour lines show bottom contours. The inset at the top left shows the velocity pattern around the SPAW for a larger area, this inset is enlarged in Appendix G.

For the low water level (Figure 5.4-left) the horizontal circulation around the SPAW is strong, induced by local wave breaking over the SPAW. Onshore velocities are present over the SPAW, instead of offshore velocities in the reference situation (no SPAW). The colored vectors show that the magnitude of velocities is higher for a lower water level. Also longshore velocities are higher than for the base case, in the order of 0.04 m/s landwards of the SPAW.

For the high water level (Figure 5.4-right) less waves break, resulting in a weak horizontal circulation current that is dominated by the undertow and therefore not visible in Eulerian depth-averaged velocities. Since the horizontal circulation is weaker, velocities over the SPAW are higher and offshore directed than for the base case. Longshore velocities are negligible landwards of the SPAW.

5.1.4 Sediment transport for different water levels

The wave-driven flow field is approximately symmetrical around the SPAW for all water level cases. From these patterns we expect an approximately symmetric transport pattern around the SPAW. For the high water level however, transport at the SPAW crest varies significantly from North to South. Therefore, we consider sediment transport results for the high water

level not realistic due to numerical issues when running the model (i.e. anomalous vertical eddy viscosity profiles occur). Appendix I.1 shows results for this case.

The sediment transport patterns for the low water level case qualitatively show similar results to the case with an average water level (Figure 5.5and 4.24). For both cases near-bed, suspended and total load show an increasing onshore transport at the crest and just landwards of the SPAW. Sediment transport is a result of many processes (e.g. wave asymmetry, water depth, wave breaking, bottom shear stress, etc.) interacting with each other. Therefore it is difficult to isolate one particular parameter or process that induces observed small differences in transport between the low and average water level cases.

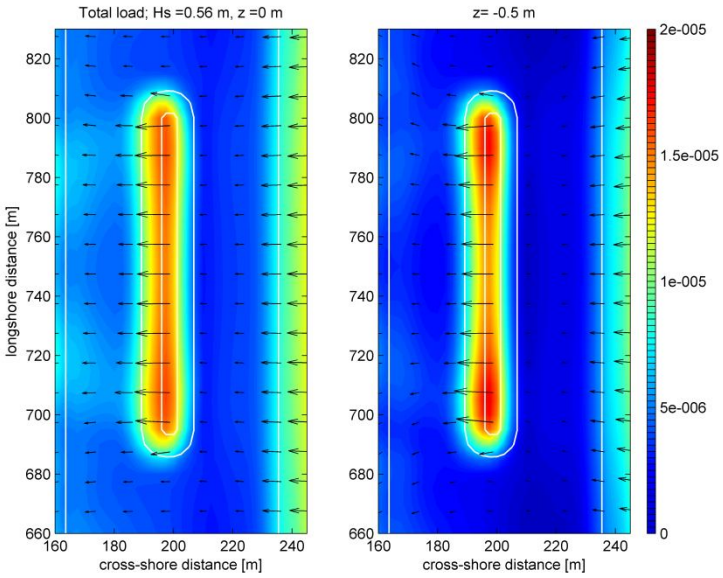

Figure 5.5. Top view of total load transport ($m^3/s/m$), showing average water level case (left) and low water level case (right). The background colouring represents magnitude, vectors show directions, grey contour lines show bottom contours.

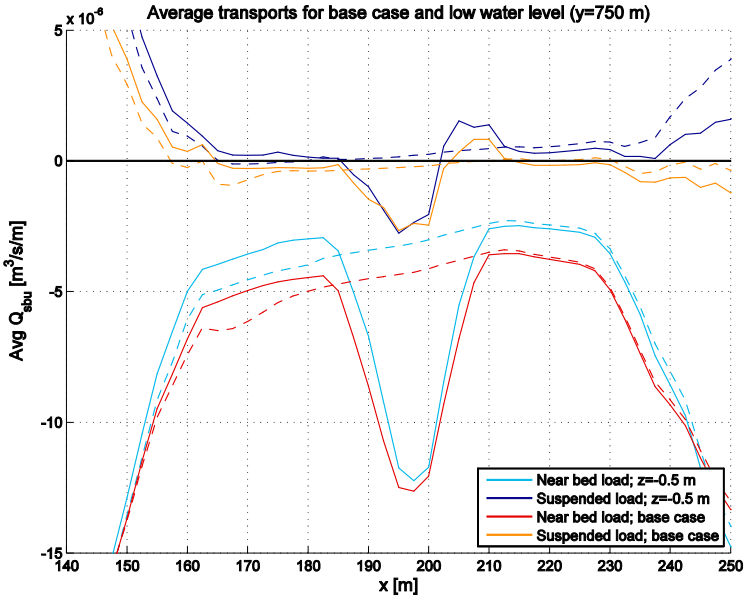

Figure 5.6. Comparison of near-bed and suspended transports in x-direction, for low (blue tints) and average water levels (red tints).

For the bed-load transport (current and wave related) the bed shear stress near the bottom is an important parameter. It is influenced by for example water depth and wave height; bed shear stress increases with higher wave heights but also with lower water depth. Compared to the low water case wave heights are higher near the SPAW for an average water level case, because less wave energy is dissipated over the bar. This will result in a higher bed shear stress. But for an average water level case water depth is higher compared to the low water case, resulting in a lower bed shear stress. This example shows that many processes (e.g. water depth and wave height development) influence resulting sediment transports. Since bed-load transport is similar for both water level cases, it shows that processes counteract each other. For suspended load transport due to wave asymmetry (included in the near-bed load transport), wave asymmetry is an important factor. This depends on local wave height and water depth as well.

The concentration of sediment over the vertical is important for suspended transport, for the suspended transport due to currents and due to wave asymmetry (which is defined as a component of the near-bed load). When wave breaking takes place more sediment is entrained over the water column, which can induce higher sediment concentrations in the water column. For both low and average water level cases the concentration profiles around the SPAW are very similar in shape and magnitude (Figure 5.7). The differences observed between SPAW case and reference cases are much larger than differences between different water level cases. In the SPAW case it can be observed that the reference concentration and the concentration in the water column is higher, implying that more sediment is entrained by wave breaking over the SPAW.

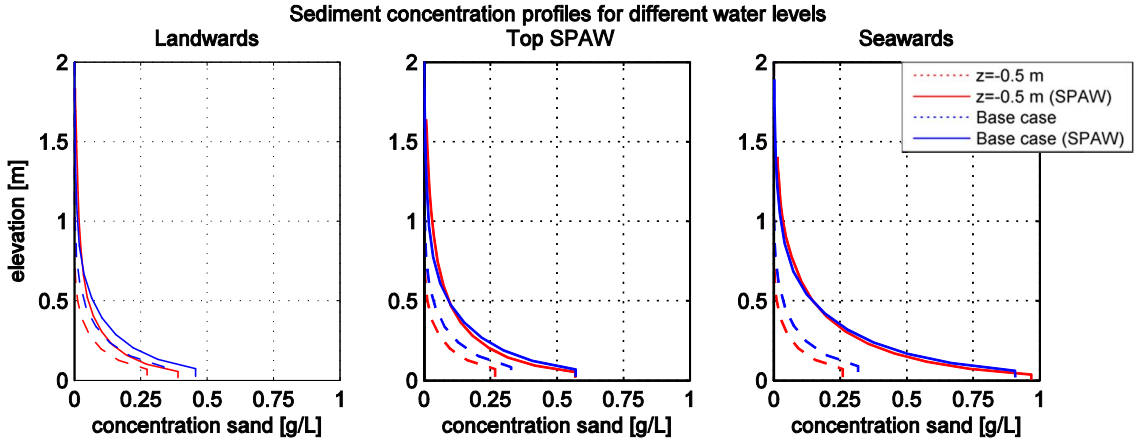

Figure 5.7. Sediment concentration profiles for different cross-shore locations onshore of the SPAW location (in middle of domain).

Based on the analysis we can conclude that although water level influences how strongly the flow-field is modulated by the SPAW presence, effects on sediment transport patterns are small. Simulated sediment transport patterns are a result of many different processes (i.e. non-linear wave transformation, concentration profiles, and velocity patterns) interacting with each other. Since observed differences between water level cases are small, the processes probably counteract each other.

5.1.5 Initial sedimentation and erosion

The sediment transport patterns for both water levels were similar, which results in similar erosion - sedimentation patterns. For the low water level we see that erosion and sedimentation values are slightly higher than for the average water level. Nevertheless,

results for both water levels show a shoreward displacement of the SPAW. This is consistent with the observation of Wijnberg and Holman (2007) that water depth above the SPAW does not influence general SPAW behavior.

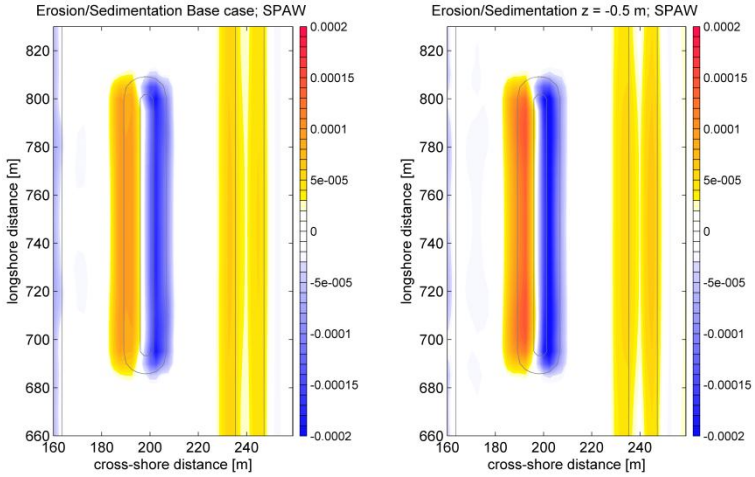

Figure 5.8. Initial sedimentation and erosion rates (m) for average water level (left) and low water level (right).

5.2 Analysing different wave height

In order to simulate the effect of higher waves on wave-driven flow field and sediment transport patterns, we did a run with a higher wave height. The chosen wave height was H_s = 2.23 meter, which was also observed at the end of the SPAW period of 1994. Although the SPAW merely transits the trough during low wave conditions, it is interesting to see what would happen if a period of high waves occur during a SPAW event. Also it can be used as a check whether simulation results endorse the observation of Wijnberg and Holman (2007) that no relationship was found between mean offshore wave conditions and average onshore propagation speed over the life time of a SPAW.

Figure 5.9 shows that for the high wave height case an unrealistic high longshore current directed to the North is generated near the coast for the reference as well as the SPAW case.

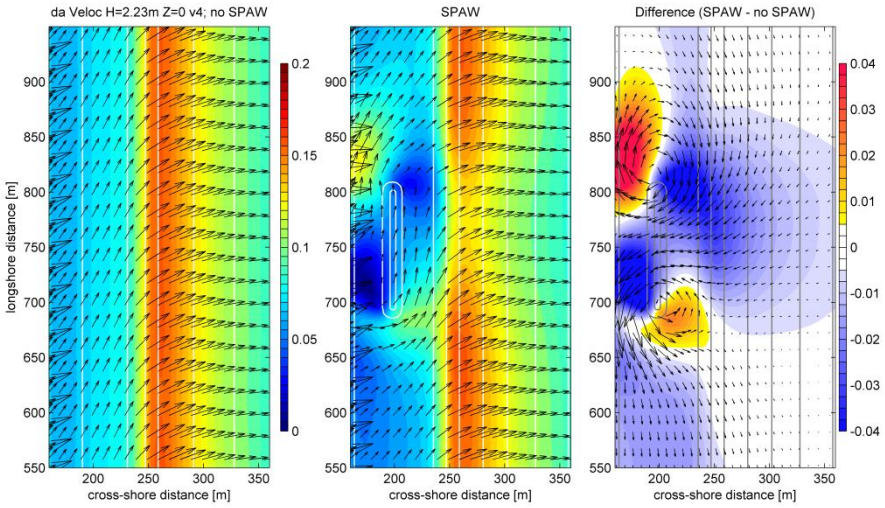

Figure 5.9. Top view of depth-averaged velocity (m/s), showing reference situation (left), situation with a SPAW (middle) and the difference (right). The background colouring represents magnitude, vectors show directions, contour lines show bottom contours.

Although the general wave field is not as we expected, relative differences show a horizontal circulation cell as was seen for other cases (Figure 5.9 - right). This indicates that the processes for a high wave height will be similar to a case with a low wave height. Unfortunately, no more time was available to investigate why this longshore current was generated in the simulation. It is worth to look into the influence of wave height on the wave-driven flow field and sediment transport patterns in more detail in future research.

5.3 Analysing results for test-version Delft3D

During the analysis it turned out that the current version of Delft3D (v4) does not compute organized wave forces, when applying the roller model. We run a test-version of Delft3D (v5) to investigate the influence of including wave forces, and thereby set-down. The implementation of the roller model in Delft3D and the test-version is discussed in paragraph 3.4.7. Due to numerical issues when running the test-version results were unstable for the average and high water level case, therefore only the low water level case was analysed.

5.3.1 Hydrodynamics

For wave heights, no significant differences are present between simulations of both Delft3D versions (Figure 5.10). The main differences are present in water level variations over the domain, resulting in a slightly different flow pattern around the SPAW as will be discussed in this Section.

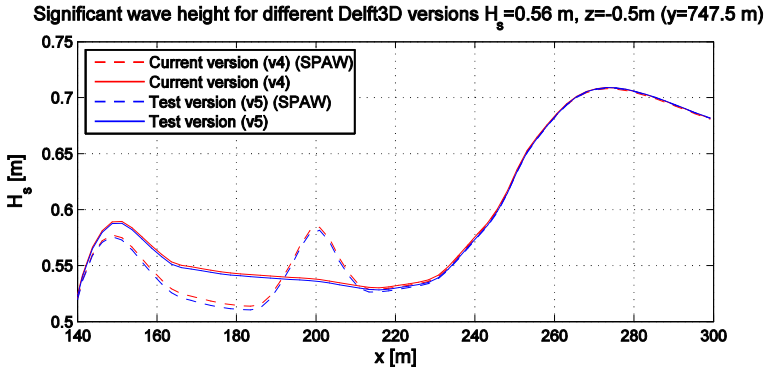

Figure 5.10. Cross-shore variation in wave height over the middle of the SPAW for different Delft3D-versions.

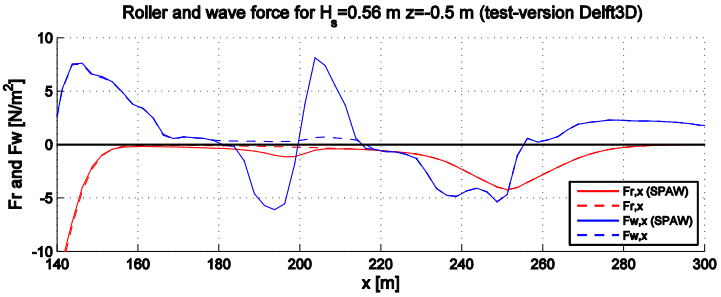

Figure 5.11. Cross-shore variations in roller (Fr =red lines) and wave forces (Fw =blue line) for Delft3D test-version over the middle of the SPAW (y=747.5 m). Negative forces are forces directed onshore.

Figure 5.11 shows roller and organized wave forces computed by the test-version. The computed roller forces are the same for both versions. Seaward of the bar and SPAW the wave force is directed offshore, whereas it is directed onshore just shoreward of the bar and SPAW (location of bar and SPAW tops are respectively x = 251 m and x= 198 m). This is in line with wave theory, since waves shoal over a bar leading to positive gradients in radiation

stress in the direction of wave propagation. This gradient in radiation stress induces wave forces directed offshore.

This local wave forces around the SPAW generate significant local set-up/set-down (Figure 5.12). For the test version (blue lines) a set-down is seen seaward of the bar and a set-up shoreward of the bar. Then going shoreward a set-down is generated seaward of the SPAW again and a set-up shoreward of the SPAW, due to which the water level becomes slightly higher than seaward of the SPAW. At the coast a set-down is generated again, by shoaling of waves to the coast. These areas of set-down are not present in the current version where no organized wave forces are calculated (red line). Despite these differences, for both cases without a SPAW (dashed lines) generated set-up and water levels are very similar for the area in which the SPAW is located (i.e. between x = 170 m and x = 230 m).

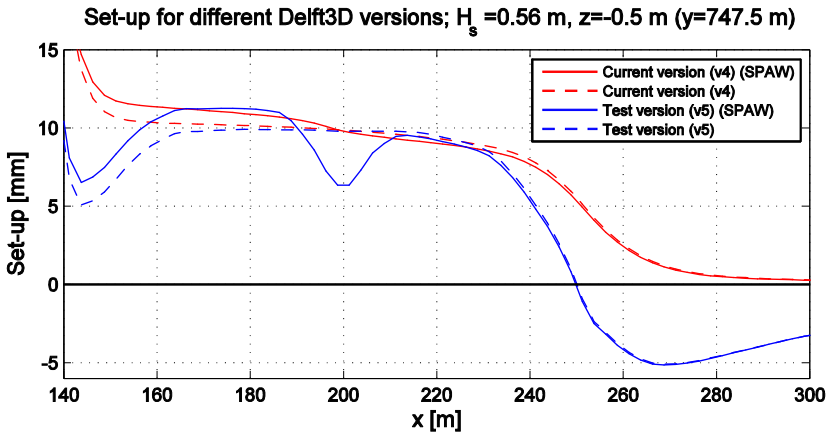

Figure 5.12. Cross-shore variation in set-up (i.e. current water level minus mean water level) over the middle of the SPAW for different Delft3D-versions for situation with SPAW and without a SPAW.

The different water level gradients for the test-version case generate a slightly different flow-field than for the current Delft3D version. The general pattern of water level development is similar: namely there is less set-up seaward of the SPAW. In contrary, landward of the SPAW an increase in set up is visible, since waves break over the feature. The main difference between the two Delft3D versions is that there is a local set-down region over the SPAW.

The depth averaged velocity pattern shows a similar horizontal circulation pattern for both Delft3D versions (Figure 5.13), thus inclusion of organized wave forces in the simulation only show second order effects. Second order effects can be seen in the two aspects; (i)) the flow-field computed by the test-version shows that velocities just landwards of the SPAW are more directed towards the side than onshore as is the case for the results of the current version. And (ii) the centers of the circulations cells are shifted a bit landwards and towards the side of the SPAW for the test-version case.

The main differences in cross-shore velocity between both Delft3D-versions are present over the SPAW and at the SPAW tips (Figure 5.14). In the middle of the SPAW (top figure blue line) velocities are more onshore directed for version 5 than for version 4. Furthermore the shift of location of circulation cell centre is visible in the cross-shore velocities, since at the tips of the SPAW (Figure 5.14 – top figure green line) velocities are directed onshore landward of the SPAW and offshore directed at the seaward side.

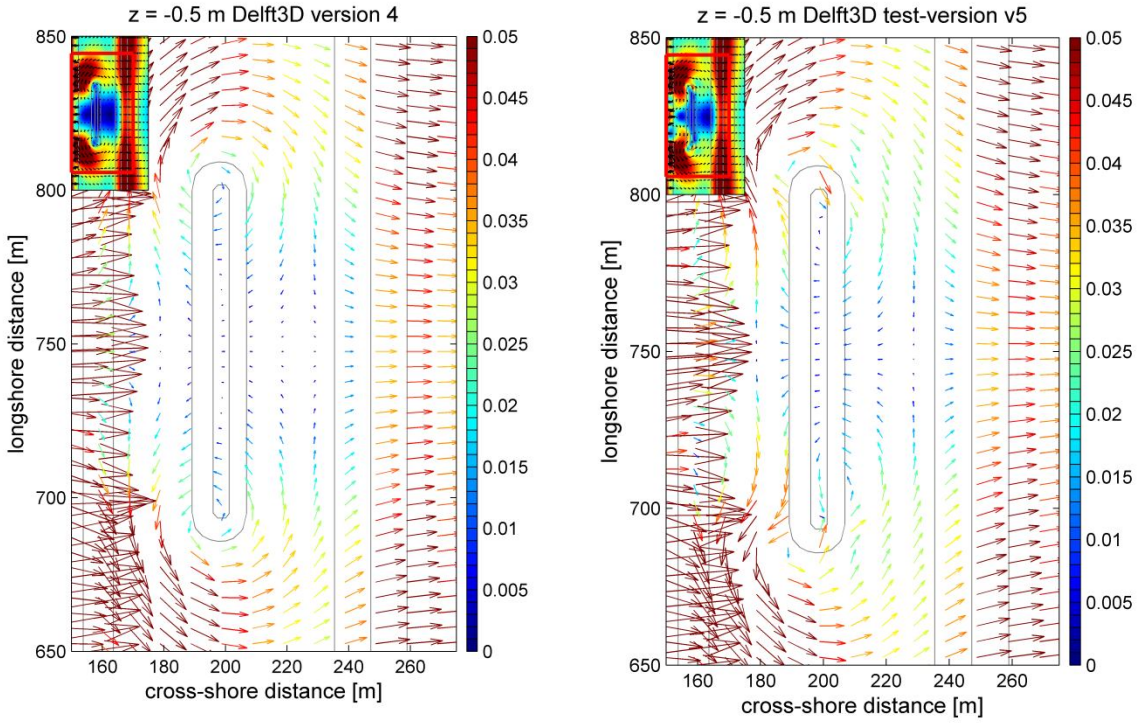

Figure 5.13. Top view of depth-averaged Eulerian velocities (m/s) zoomed in at the SPAW (red box in top left inset). The vectors show directions and magnitude, grey contour lines show bottom contours. The inset at the top left shows the velocity pattern around the SPAW for a larger area, this inset is enlarged in Appendix G.

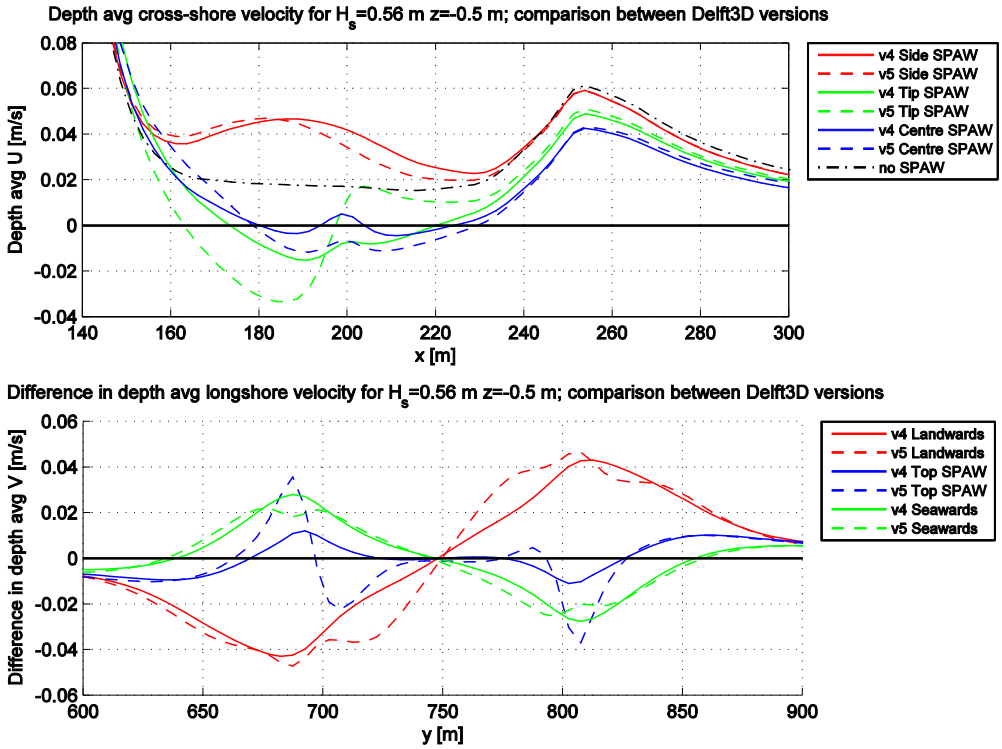

Figure 5.14. Depth averaged velocities over different transects. Upper figure: cross-shore variation in cross-shore velocity (negative values are onshore directed). Lower figure: Longshore variation in longshore velocity (negative values are southwards directed).

The longshore velocities show that differences between both versions shoreward and landward of the SPAW are small, whereas over the SPAW crest they are different for both versions (Figure 5.14 – bottom figure, blue line). This can also be explained by the shift of the centre of the horizontal circulation cell. The magnitudes of longshore velocities are stronger for Delft3D version 5, which indicates that the horizontal cell circulation is stronger.

5.3.2 Sediment transport

Figure 5.15 shows suspended, near-bed, and total load sediment transport patterns for runs with the current version of Delft3D (v4) and test-version of Delft3D (v5). Results show similar sediment transport patterns for both model versions (Figure 5.15).

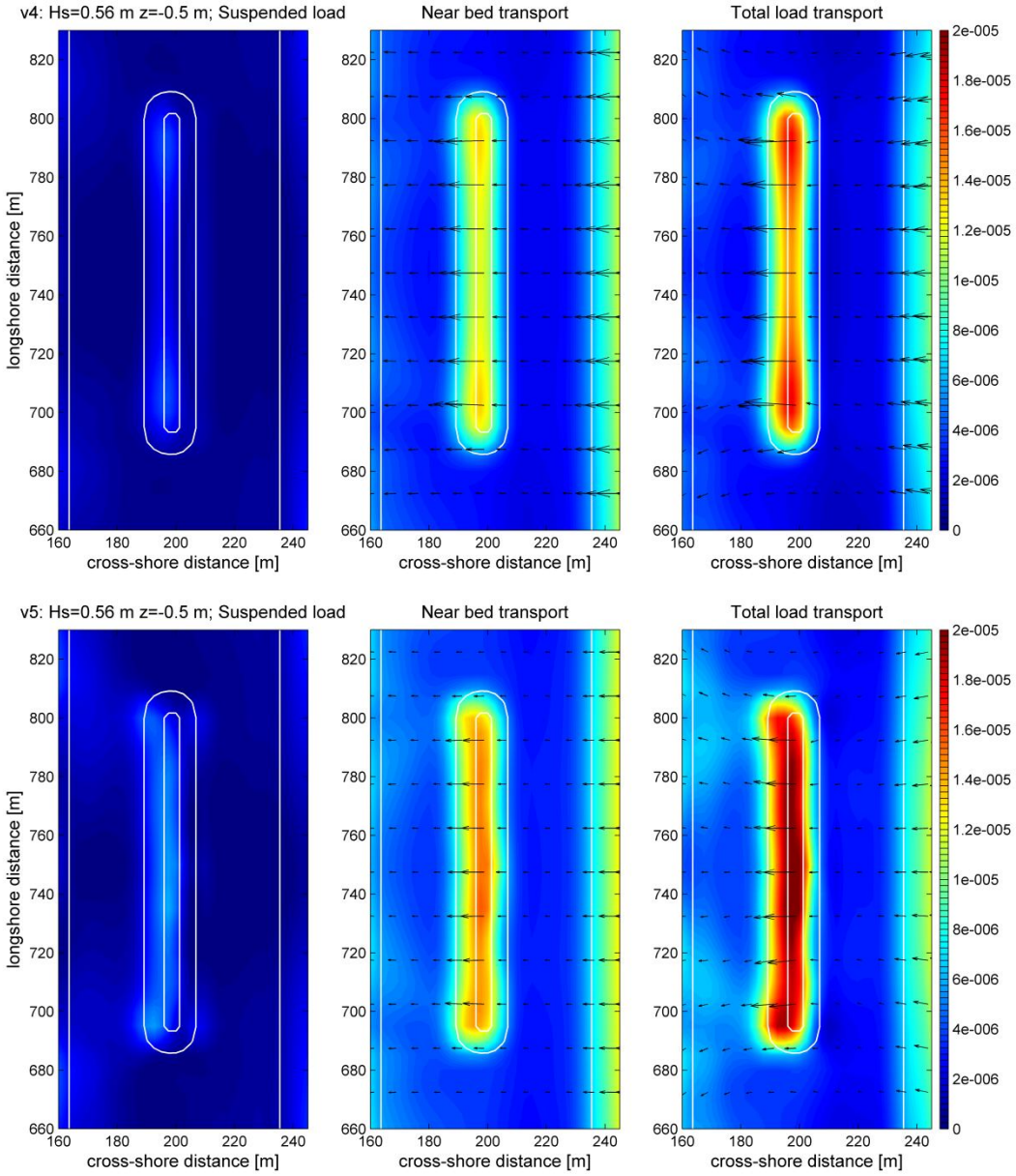

Figure 5.15. Top view of sediment transport ($m^3/s/m$) over the SPAW. Upper figure shows results for the current version of Delft3D (v4 - only roller forces) and the lower figure for the test version of Delft3D (v5 - with wave and roller forces). Colours indicate magnitude (scaling is the same for all plots), vectors show direction and white contour lines indicate SPAW bathymetry.

The sediment transport over the SPAW increases locally and is directed onshore, similar to other cases. The near-bed load (due to wave asymmetry) is again dominant. This explains why differences seen in the wave-driven flow fields for both Delft3D versions are hardly visible in results for near-bed transport. Sediment transport rates are slightly higher for test version; this is probably due to the fact that the generated horizontal flow circulation induced by the SPAW was stronger for this version. This resulted in higher onshore velocities over the SPAW, and consequently higher (particularly suspended) onshore transports.

5.3.3 Initial sedimentation and erosion patterns

The inclusion of organized wave forces in the model only has second order effects on wave-field and sediment transport patterns. This results in a similar erosion and sedimentation pattern for both the version including organized wave forces (the test version – v5) and the version which only takes roller forces into account (the current version - v4); showing an initial shoreward displacement of the SPAW (Figure 5.16).

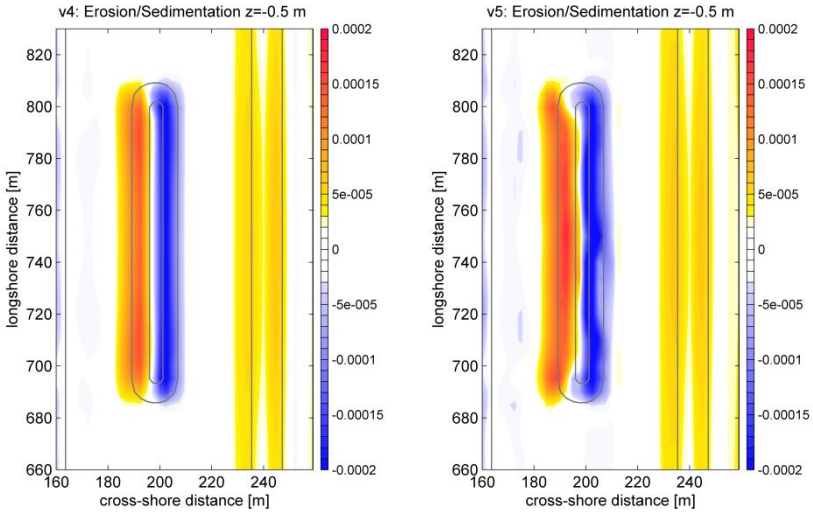

Figure 5.16. Initial sedimentation and erosion rates (m) for current Delft3D version (left) and test-version (right).

5.4 Summarizing important findings for SPAW dynamics for varying water levels, wave height and Delft3D version

To investigate the robustness of the behaviour seen for the base case (Chapter 4), we analysed how SPAW dynamics are influenced by changing (1) water levels, (2) wave height, and (3) inclusion of organized wave forces. Important findings are summarized below.

Firstly, results show that for different water levels the wave breaking pattern over the bar and SPAW differs. More waves break over both features if water level is lower, which results in a higher wave set-up shoreward of the SPAW. Consequently, longshore pressure gradients are larger for the low water level case, which results in the development of a stronger horizontal circulation current for this case. Sediment transport is a result of many different processes that can counter act each other (for example wave height and water depth both influence bed shear stress). Sediment transport patterns for the low and average water level case were very similar, which implies that indeed processes influencing sediment transport counteract with each other. As a result of the sediment transports, also erosion-sedimentation patterns showed very similar results for a low as well as for an average water level.

Also a simulation was done for a higher wave height. Unfortunately an unrealistic high longshore current developed for the reference case and for the SPAW case. It would be worth to investigate in future research what the wave-driven flow field and initial sediment transport patterns would be for higher wave heights and why this particular wave height gives such unrealistic results.

The third parameter that was varied was the Delft3D version. The simulation was also done with a version that includes organized wave forces in the roller model as well. Due to numerical issues only the wave height for z = -0.5 m was stable and analysed in this Chapter. Local organized wave forces generated local set-down at the crest of the SPAW. For the case with the Delft3D test-version a slightly different wave-driven flow field was generated, because of differences in longshore pressure gradients. Since near-bed transport was dominant for both Delft3D versions, differences in wave-driven flow field were not reflected strongly in sediment transport patterns, resulting in similar sediment transport patterns for both versions. Onshore transport over the SPAW was higher for the test-version, because for that case a stronger horizontal circulation current developed. As a consequence the SPAW showed an initial shoreward displacement, similar to results of the current Delft3D version. Thus inclusion of organized wave forces in the Delft3D computation only induces second order effects. Therefore we are confident that other results obtained with the current Delft3D version do also approximately represent reality. Nevertheless, it is advisable to critically review the implementation of the roller model in Delft3D, and investigate why numerical issues appear for different water levels.

In conclusion, this Chapter shows that compared to the base case, qualitative wave-driven flow-fields and initial sediment transport patterns induced by the SPAW presence are similar for cases with varying water levels and cases including organized wave forces in the computation. As a result of the modulated flow-field by the SPAW presence, all cases show an initial shoreward displacement of the SPAW.

6 SPAW dynamics by morphometric changes of the SPAW

SPAW dynamics for the base case are addressed in Chapter 4. Then in Chapter 5 the influence of water level, wave height and inclusion of wave forces on SPAW dynamics are discussed. These cases all show that a horizontal circular current develops around the SPAW and sediment transports over the SPAW are larger and onshore directed, dominated by near-bed transport. The earlier analysed cases are all based on a chosen representative SPAW event. This Chapter investigates SPAW dynamics for cases with different morphometric SPAW characteristics (paragraph 3.4.3.3), Appendix F shows applied bathymetries.

It should be noted that analysis focus on erosion and sedimentation patterns. Causes for differences in flow-field and sediment transport patterns among cases were not assessed in detail. The aim of this Chapters analysis is to check whether shoreward displacement of a SPAW persists for features at different locations, with different sizes and different nearshore bar topography. Results for different SPAW locations give an indication of the morphodynamic SPAW behaviour. Also results from this Chapter are used to compare modelling results with the observation in nature that regardless size or location of the SPAW it always propagates onshore.

Section 6.1 shows results for different SPAW locations. Then Section 6.2 discusses a case with a wider and longer SPAW, since the features observed in nature has different sizes. Subsequently Section 6.3 presents results for a SPAW with a local bathymetric change of the bar. Finally, Section 6.4 shows a summary of insights obtained from analysis of morphometric changes of the SPAW.

6.1 Varying SPAW location

For the base case the SPAW is located at x=198.75 m. To investigate how hydrodynamics and sediment transport develop for different SPAW locations, also a run was done with the feature closer to the bar (i.e. x=225 m) and closer to shore (i.e. x=175 m).

6.1.1 Hydrodynamics for different SPAW locations

For all runs with different SPAW locations, the pattern of refraction and directional spreading effect is visible when investigating differences in significant wave heights (Figure 6.1).

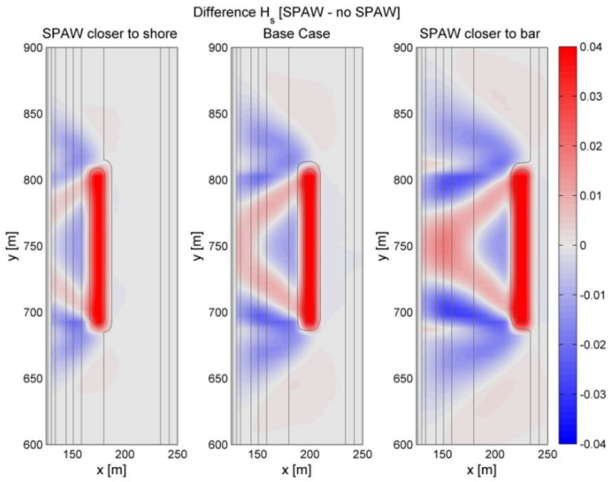

Figure 6.1. Top view of difference plots in significant wave heights (H_s)(m) for different SPAW locations. The contour lines show bottom contour lines for a SPAW case. Background colour shows the difference in H_s.

For a SPAW located further from shore, refracted waves reinforce each other landwards of the feature. Figure 6.2 - left also shows that the shoaling of the waves is very similar for all cases on cross-shore transects, only the effect landwards of the feature differ. Extra wave set-up as a result of the SPAW presence is in the same order of magnitude for all locations, only the relative set-down seawards of the SPAW is larger for a SPAW located further from shore (Figure 6.2- right). Thus, if the SPAW is located close to the shore, hardly any longshore pressure gradient develops seawards of it.

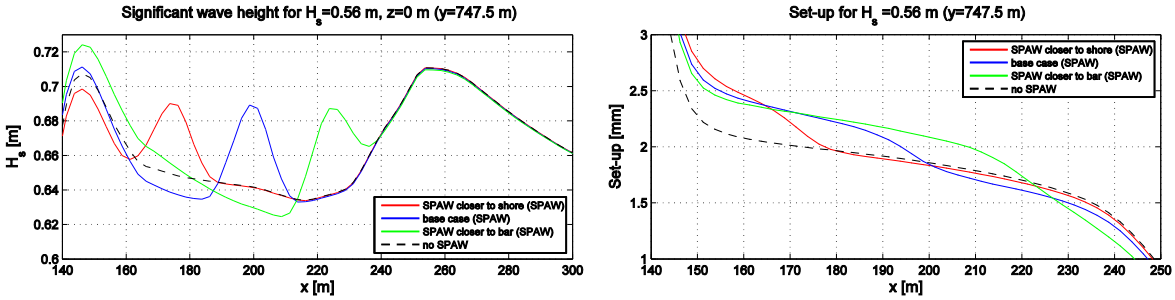

Figure 6.2. Cross-shore variation for different SPAW locations in significant wave height (left figure) and set-up (i.e. current water level minus mean water level) (right figure) over the middle of the SPAW.

Variations in wave height induced by the SPAW presence generate pressure gradients which drive a horizontal circulation flow. Figure 6.3 shows depth-averaged GLM velocities, which are used for calculating suspended sediment transport. It can be seen that the circulation pattern is strongest if the SPAW is located closest to the bar and extends over the full length of the SPAW crest (i.e. Figure 6.3 - right). If the SPAW is located close to the shore a horizontal circulation current only develops at the SPAW tips; velocities are directed towards the sides landwards of the feature whereas seawards velocities are only slightly directed towards the SPAW centre. This is probably due to the small longshore pressure gradient seaward of the SPAW for this case. It results in a weak horizontal circulation pattern around the tips (Figure 6.3-left).

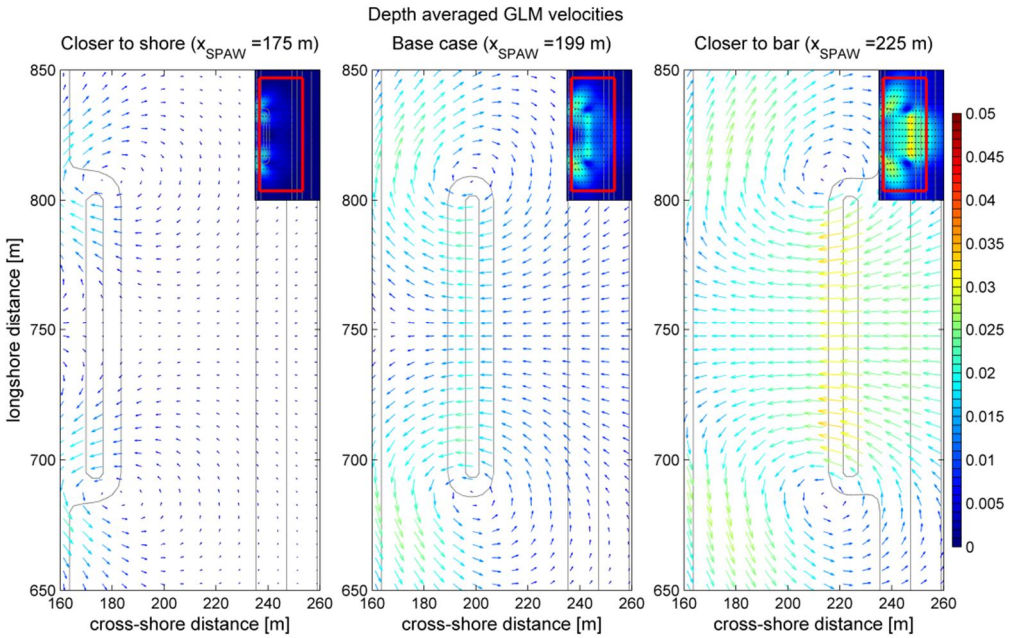

Figure 6.3. Top view of depth averaged GLM velocities (m/s) for different SPAW locations, zoomed in at the SPAW (red box in top right inset). The colour vectors show directions and magnitude, grey contour lines show bottom contours. The inset at the top right shows GLM velocity pattern for a larger area

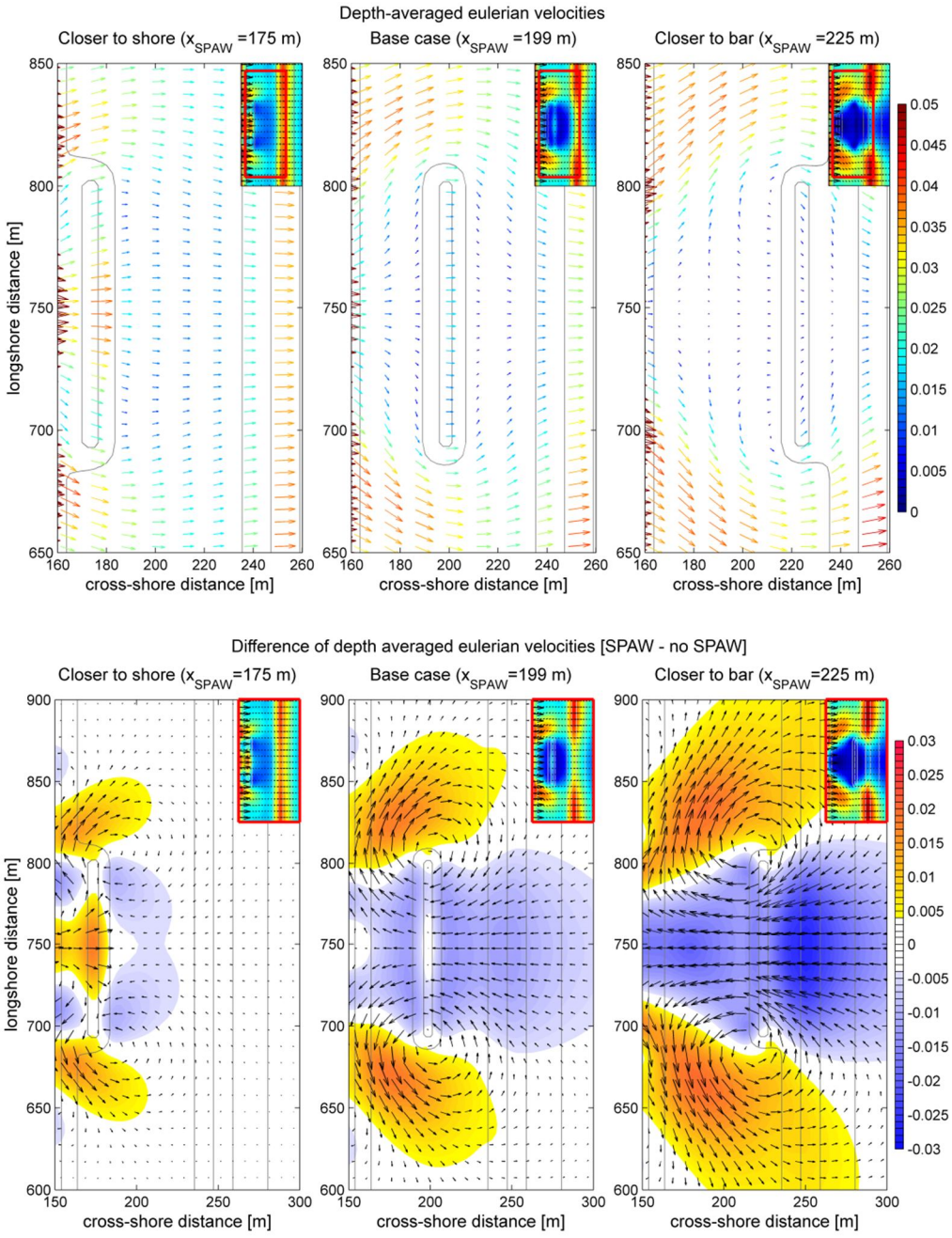

Figure 6.4. Top view of depth averaged Eulerian velocities (m/s) (top figure) and difference plots (SPAW minus no SPAW) for depth averaged Eulerian velocities (bottom figure). Coloured vectors show directions and magnitude, black vectors show directions, background colouring shows magnitude. Contour lines show bottom contours. The inset at the top left shows the velocity pattern around the SPAW for a larger area, the red rectangle shows the area at which the figure zooms in. The inset is enlarged in Appendix H.

Depth averaged Eulerian flow velocity patterns and corresponding difference plots confirm that the generated horizontal circulation pattern is strongest for a SPAW located further from shore, and weakest for a SPAW located closer to shore (Figure 6.4). For a SPAW located closer to shore, offshore directed velocities at the SPAW crest increase. This is because water depth is decreased above the SPAW, due to which velocities should be higher in order to satisfy the mass balance. This is similar to results for the low wave height and high water level (paragraph 5.1.3).

6.1.2 Sediment transports for different SPAW locations

Sediment transports for all SPAW locations (close to shore, in between shore and bar, and closer to bar) show similar patterns. Namely, the near-bed transport (i.e. bed load transport plus suspended transport due to wave-asymmetry) is dominant in both cases and is larger and onshore directed at the SPAW crest. The observed horizontal circulation currents are reflected in the sediment transport patterns. Figure 6.5 shows that if the SPAW is located closer to shore suspended sediment contribution mainly concentrate at the tips similar to depth-averaged GLM velocities. For a SPAW closer to the bar suspended load is onshore over the full length of the SPAW crest.

Furthermore, a local increase in sediment transport is visible landwards of the SPAW for a SPAW located further from shore. This can be due to modulations of the wave-driven flow field (for example the reinforcement of waves due to refraction at that location might cause additional shear) or to inadequacies of Delft3D. It is worth to investigate the cause of this local increase in future research.

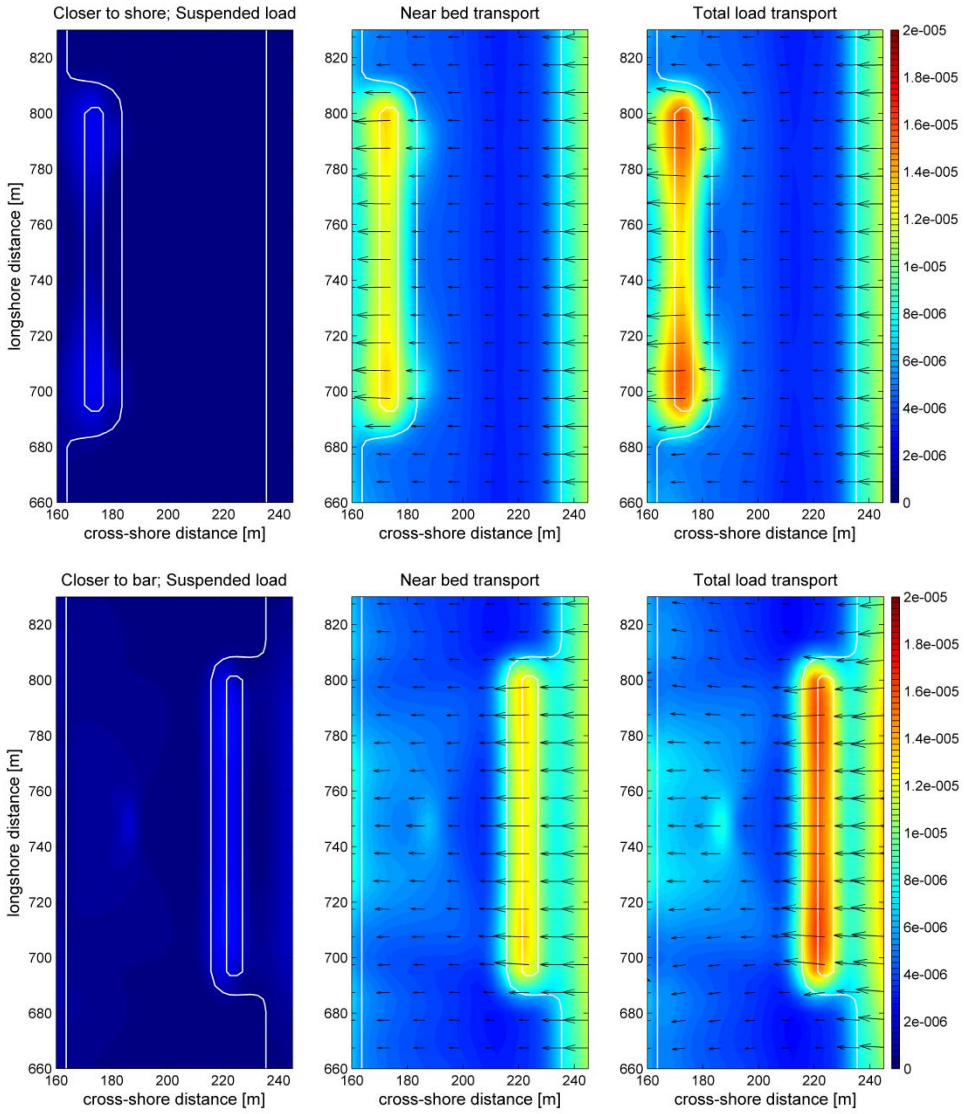

Figure 6.5. Top view of sediment transport patterns over the SPAW. Upper figure shows results for SPAW located closer to the shore, lower figure for the SPAW closer to the bar. Colours indicate magnitude (scaling is the same for all plots), vectors show direction and white contour lines indicate SPAW bathymetry.

Although sediment transport over the SPAW crest is either concentrated at the tips (closer to shore) or over the full length of the SPAW crest (closer to bar), the observation of onshore transport over the SPAW persists for all locations. Consequently, erosion and sedimentation patterns show qualitatively similar patterns for all locations. Sedimentation occurs landwards, whereas erosion occurs seaward of the feature. These results are in agreement with SPAW observations at Argus cameras (Wijnberg and Holman, 2007), which show that SPAWs transit the trough between bar and shore and propagate onshore.

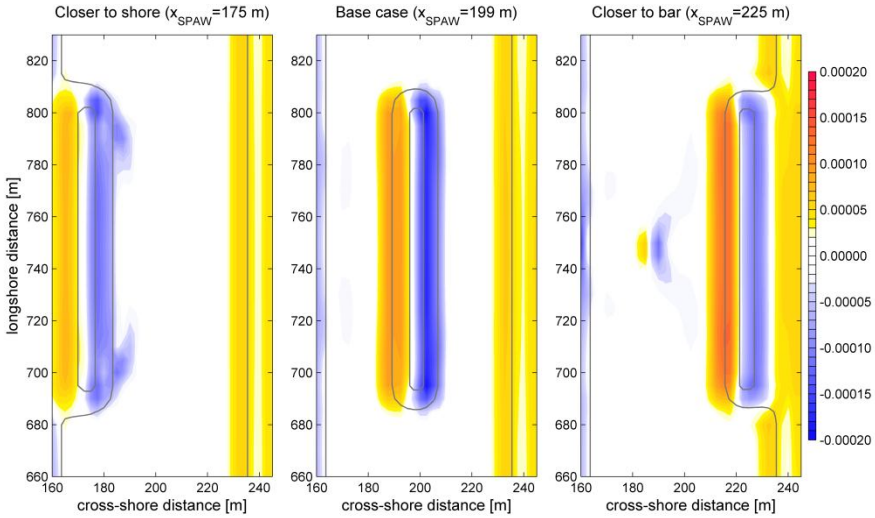

Figure 6.6. Initial sedimentation and erosion rates (m) for SPAW at different x-locations. Contour lines show SPAW bathymetry, colouring shows erosion or sedimentation rate in meters.

6.2 Varying length and width of the SPAW

For the base case the SPAW length is 130 m and width is 25 m (based on the chosen representative SPAW event). To investigate how SPAW dynamics are influenced by SPAW dimensions, runs were done with a longer (L=400 m) and wider feature (W=60 m).

6.2.1 Hydrodynamics for different SPAW dimensions

Differences in significant wave height show the refraction and directional spreading effect for the tested SPAW dimensions (Figure 6.7).

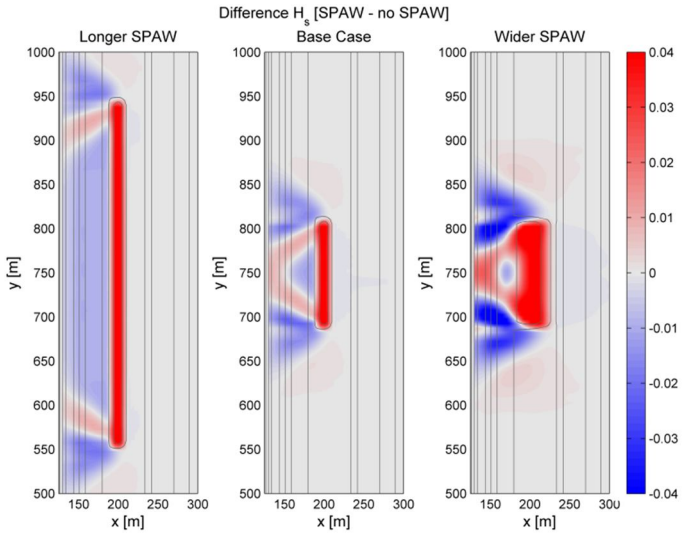

Figure 6.7. Top view of difference plots in significant wave heights for different SPAW locations. The contour lines show bottom contour lines for a SPAW case. The background colour shows the difference in Hs.

For a longer SPAW effects are local at the tips. For the wider SPAW refraction effects are stronger. This is due to the fact waves over the SPAW are for a longer distance (width of the SPAW) in lower depth than for the base case. More wave refraction is generated since waves at the sides of the SPAW travel faster for a longer distance (width of the SPAW).

Depth averaged velocity overviews show that for the longer SPAW the generated circulation pattern concentrates around the tips (Figure 6.8 - left). At the features centre Eulerian velocity is more offshore due to a decreased water depth over the SPAW. For the wider SPAW depth averaged Eulerian as well as GLM velocities show a horizontal circulation pattern induced by the SPAW (Figure 6.8– right). Onshore GLM velocities over the SPAW are relatively large, compared to the base case.

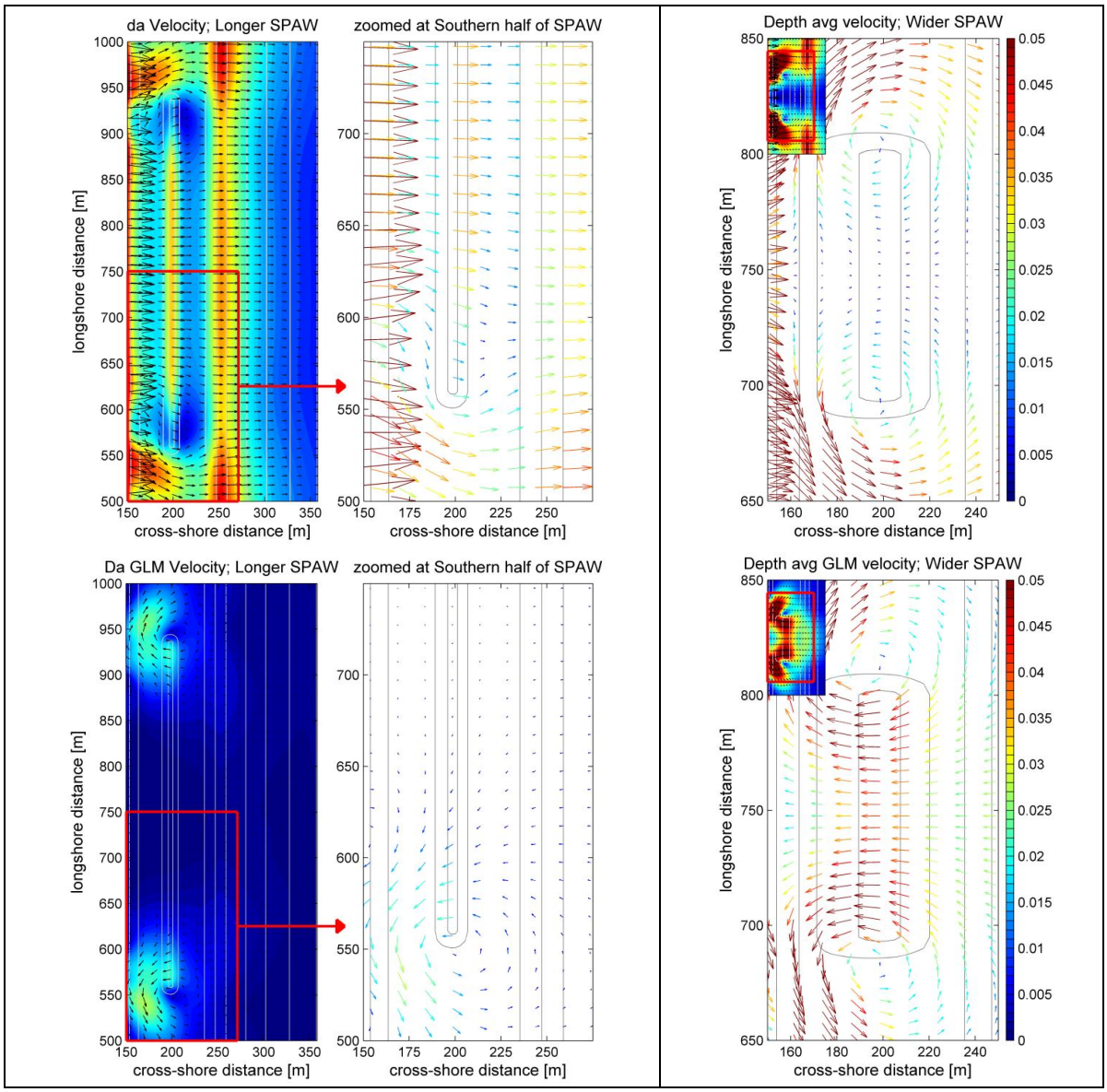

Figure 6.8. Top view of depth averaged Eulerian (top figures) and GLM (lower figures) velocities for the longer SPAW (left) and wider SPAW (right). Coloured Vectors show directions and magnitude, black vectors show directions, background colouring shows magnitude, contour lines show SPAW bathymetry. Overviews of Eulerian velocity patterns are enlarged in Appendix H.

The GLM velocities, by which suspended sediment transport is computed, also show horizontal circulation patterns (Figure 6.8 - bottom). The depth averaged pattern should be interpreted with care, because also the velocity profiles should be taken into account. In the top of the water column GLM velocities are highest, where the sediment concentration is lowest. Nevertheless this gives a qualitative view on how GLM velocities have developed.

6.2.2 Sediment transport for different SPAW dimensions

A wider or a longer SPAW show similar qualitative sediment transport patterns as the base case. Namely, the near-bed transport in direction of wave propagation is dominant in both cases and is larger and onshore directed at the SPAW crest. The horizontal circulation currents as observed in the flow-fields are reflected in the related sediment transport patterns (Figure 6.9).

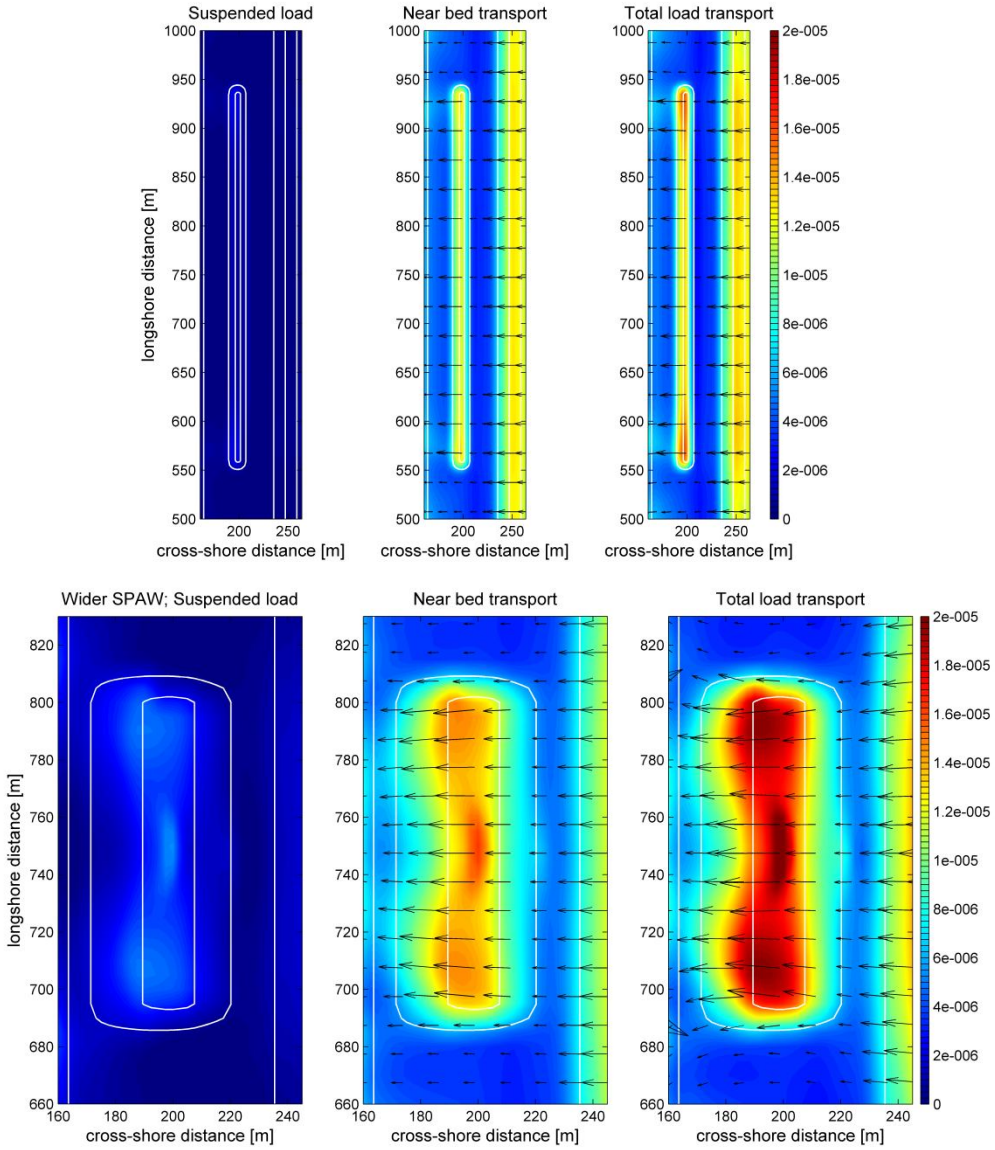

Figure 6.9.Top view of sediment transports (m^3/s/m) over the SPAW. Upper figure shows results for a longer SPAW, lower figures for a wider SPAW. Colours indicate magnitude (scaling is the same for all plots), vectors show direction and white contour lines indicate SPAW bathymetry.

For a longer SPAW (upper Figure 6.9) near-bed transport is increased over the full features length. Suspended load concentrates at the SPAW tips, since at this point onshore GLM velocities are higher than at the centre. For a wider SPAW (lower Figure 6.9) sediment transport is also dominated by near-bed load. Suspended load and near-bed load concentrates at the SPAW tips and centre. The latter can be due to suspended load due to wave-asymmetry, but this was not analysed. The responsible processes for these local increases should be investigated in further detail in future research.

The onshore directed transport contributions over the SPAW results in a shoreward displacement of the SPAW. All show erosion-sedimentation patterns show sedimentation landwards and erosion seawards of the SPAW (Figure 6.10). An interesting aspect is the fact that the erosion/sedimentation at the wider SPAW is spread out over a larger width and is smaller in magnitude, while the total load is slightly higher in magnitude. Furthermore, at the SPAW crest for a larger width the sedimentation-erosion rates are zero compared to the base case. Also the (unexplained) local increase of sediment transport at the SPAW centre is reflected in the pattern. An aspect for a longer SPAW, worth to look into further, is that although total load is higher at the tips hardly any effect of this local increase is visible in the initial erosion and sedimentation pattern.

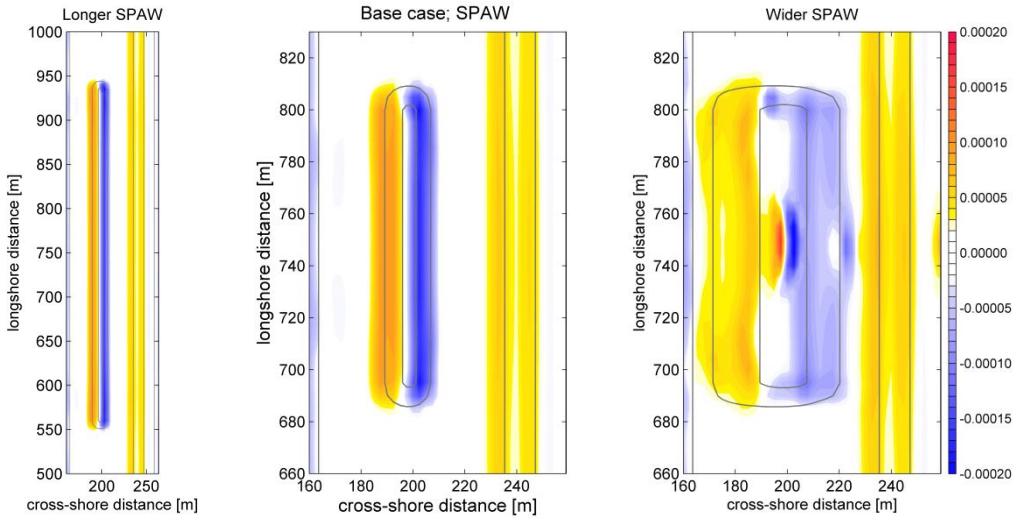

Figure 6.10. Initial sedimentation and erosion rates (m) for different SPAW dimensions. Contour lines show SPAW bathymetry, colouring shows erosion or sedimentation rate in meters.

6.3 Varying local bathymetry of the nearshore bar

For the base case a SPAW is superimposed on the reference bathymetry. Nevertheless, in one measured SPAW bathymetry it was seen that the bar was lowered locally seaward of the feature. To investigate whether described qualitative behaviour of a SPAW would be affected by a local decrease of the nearshore bar, we also run the model with a bathymetry where the bar was locally lowered seawards of the SPAW.

6.3.1 Hydrodynamics for a local bathymetry change of the nearshore bar

Since the bathymetry of the bar is changed, also the development of wave height and water level is different (Figure 6.11 and 6.12). These patterns are not discussed any further. The resulting modulated flow-field differs from the base case; it shows that for a case with a locally lowered nearshore bar no clear horizontal circulation current is generated and visible in neither the depth-averaged Eulerian nor the GLM velocities (Figure 6.13). Depth-averaged velocities (Eulerian as well as GLM) are directed to the location where the bar is lowered. Velocities coming from the SPAW tips and sides are highest.

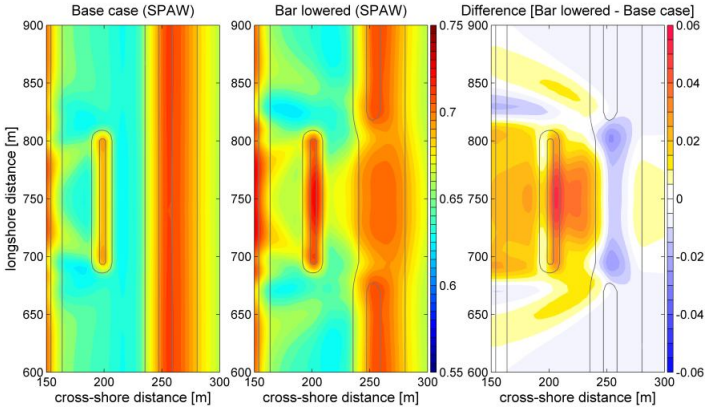

Figure 6.11. Top view of significant wave height (m). Background colour show magnitude, contour lines bathymetry.

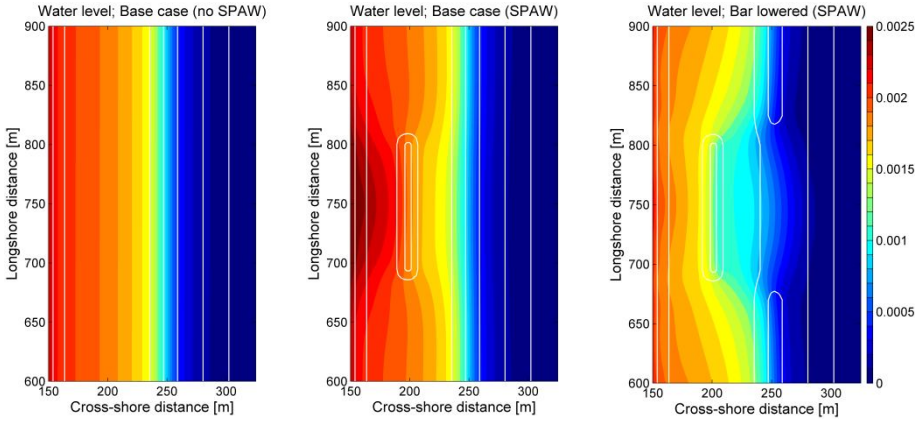

Figure 6.12. Top view of water level (m). Background colouring show magnitude, contour lines show bathymetry.

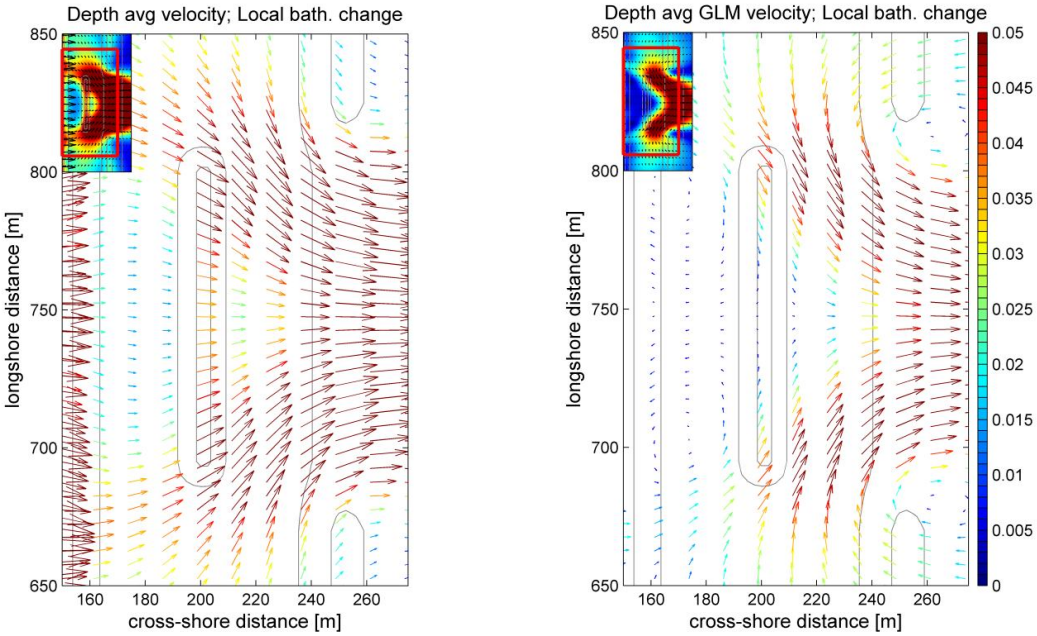

Figure 6.13. Top view of depth-averaged velocity pattern for the case with a local bathymetry change zoomed in at the SPAW (red box in top left inset), Eulerian velocities (left) and GLM velocities (right). Vectors show directions and magnitude, grey contour lines show bathymetry. The inset at the top left shows velocity patterns around the SPAW for a larger area, Eulerian velocity patterns are enlarged in Appendix H.

6.3.2 Sediment transport for a local bathymetry change

Due to modulations in the flow-field by the presence of a SPAW, sediment transport over the feature is locally increased and onshore directed, similar to the previous discussed cases. Three main topics interest can be identified. Firstly, when focussing at the bar it can be seen that at the place where the bar is lowered, onshore near-bed transport is decreased and the suspended load is offshore directed. This results in less onshore transport at this part of the bar. Secondly, the suspended and near-bed transports of the bar side at original height are both onshore directed, and therefore total load is onshore directed and relatively large at the sides of the inner bar. Thirdly, at the SPAW sediment transport is increased and directed onshore. The transport at the tips is directed slightly to the middle of the SPAW, which can be a contribution for the SPAW maintaining its shape during its propagation to the coast. For the base case the total load is mainly directed straight onshore (Figure 4.19). It is interesting to investigate during further research whether the lowering of the bar is essential for the SPAW maintaining its shape.

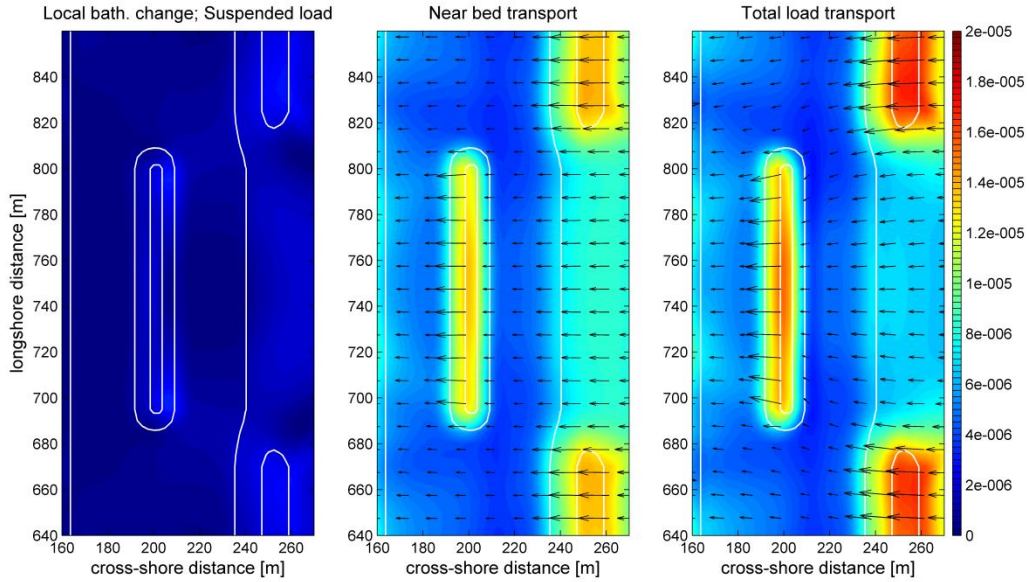

Figure 6.14. Top view of sediment transport patterns over the SPAW for the case with a local bathymetry change. Colours indicate magnitude (scaling is the same for all plots), vectors show direction and contour lines indicate bathymetry.

The initial sedimentation/erosion pattern at the SPAW is again similar to all previous cases (Figure 6.15); showing a shoreward displacement of the SPAW. The main difference with the base case is that no sedimentation occurs at the bar where it is lowered. This is, inter alia, due to the changed flow velocity field.

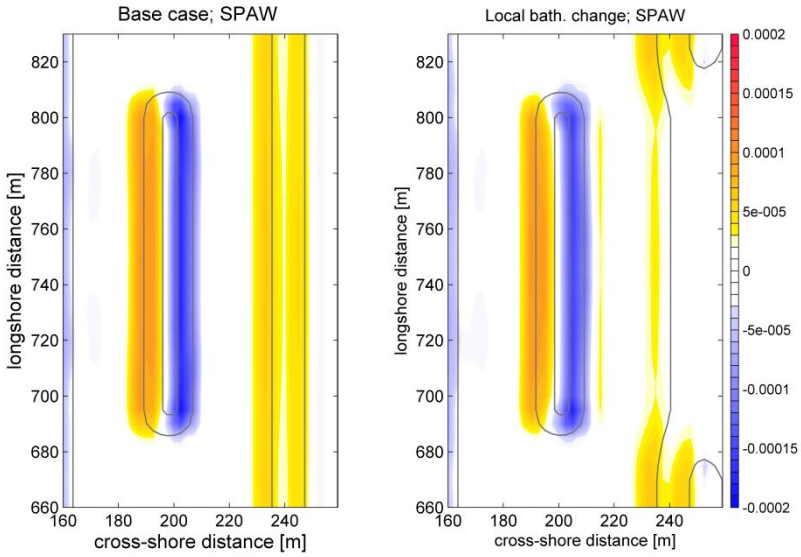

Figure 6.15. Initial sedimentation and erosion rates (m) for base case (left) and a case with a local bathymetry change (right). Contour lines show bathymetry, colouring shows erosion or sedimentation rate in meters.

6.4 Summary of influence of morphometric changes in SPAW characteristics

This Chapter presents results for Delft3D simulations for runs with varying morphometric changes in SPAW characteristics. The following parameters were varied: SPAW location, width, length and local bathymetry of the bar. In general, although depth-averaged wave-driven flow fields differed between cases resulting sediment transport patterns were qualitatively similar. For all cases it was shown that for a low wave height sediment transport is dominated by near-bed load (bed load due to waves and suspended load due to wave-asymmetry). The onshore directed transport components resulted in a shoreward displacement of the SPAW for all SPAW cases. Specific observations for all cases are summarized below.

In nature, SPAWs are observed to propagate onshore across the trough as an intact form. This implies that SPAW dynamics at different cross-shore locations should be similar, in order let the feature propagate shoreward. Results for different SPAW locations show that sediment transports are indeed qualitatively similar. For a SPAW located closer to shore suspended sediment transport is concentrated at the tips, because the generated horizontal circulation in velocity is intense at the tips. If the SPAW is located closer to the bar the horizontal circulation extends to the full length of the SPAW centre, due to which suspended transport is increased and onshore directed over the full length of the SPAW crest. Local increases in sediment transports for the case with a SPAW closer to the bar were not explained, this is an interesting aspect to further investigate.

Furthermore, Argus observations show that SPAWs occur in nature with varying length and width. These are, regardless of their dimensions, observed to transit the trough and approximately maintain their shape. The modelling results are in agreement with this observation; namely in situations with low wave height SPAW length and width do not considerably change sediment transport patterns and related initial erosion/sedimentation rates. For the case with a wider SPAW, a stronger horizontal circulation cell developed compared to the base case, which resulted in onshore directed depth averaged Eulerian velocities over the SPAW. Also local hotspots of sediment transports were present at the SPAW tips and centre which were not explained and should be investigated in more detail. For the longer SPAW total load was higher at the tips, but hardly any effect is visible in initial

erosion and sedimentation pattern. It is interesting to study the cause for this result, since it is expected that for elongated bars the tips of the bar propagate faster onshore.

Also a run was done with a local lowering of the nearshore bar. This case showed that the flow-field was significantly different from the base case. Velocities and related suspended sediment transports are offshore directed at the location where the bar was lowered, resulting in less onshore directed transport at this part of the bar. Transports increased at the place where the nearshore bar has its original height, since both suspended and near bed transports are onshore directed and relatively large at the sides of the inner bar. A remarkable result was that the onshore directed sediment transports at the tips of the SPAW were directed slightly to the middle of the SPAW, because the suspended sediment transport component is directed from the sides to the middle of the feature. This is due to a generated horizontal circulation current slightly landward of the SPAW. This can be a contribution for the SPAW maintaining its shape during its propagation to the coast. It is worth to investigate this in further detail.

7 Discussion, Conclusion and Recommendations

This report provides insights in SPAW dynamics in the nearshore. During the study several assumptions and choices were made. The implications of these are discussed in Section 7.1. In Section 7.2 the conclusion is presented, reflecting on the research questions and hypothesis about SPAW dynamics. Recommendations for further research related to SPAW dynamics and Delft3D modelling are presented in Section 7.3.

7.1 Discussion

7.1.1 Choices and assumptions made during this study

The three-dimensional Delft3D model with a large domain and a high spatial and temporal resolution, as used in this study, is rather unique. Most Delft3D studies use 2DV-models or a coarser grid (e.g. Hsu et al., 2006 and 2008; Van der Werf, 2009; Koster, 2006).The high resolution was necessary in order to model SPAWs, which are a relatively small-scale morphological feature. Following a 3-dimensional approach vertical velocity and concentration profiles are computed, by which suspended transport is better simulated than by following a 2DV approach; particularly within the surfzone with strong undertow. The analysis showed that with a low wave height, near-bed transport is dominant for all SPAW cases. Therefore this study shows that a 2DV model would probably give comparable results for this specific situation. However, when suspended sediments become more important a 3D approach can be necessary. Before this study was done it was not known whether a 3D-model would give similar results to a 2DV model. It is a useful insight to know a 2DV approach would also be sufficient, since applying a 2DV model will reduce computation time.

We have modelled a representative SPAW event on Duck Beach (USA, North Carolina), since most SPAW observations were done here. Duck is a swell-dominated beach (i.e. waves with long waves periods – peak periods are around 8-12 s) with one nearshore bar. The results for this study are therefore specifically applicable for Duck. However, Koster (2006) studied small-scale nourishments on Egmond aan Zee. This beach is wave dominated, which implies that waves are wind generated and have shorter periods. Kosters analysis showed similar flow-fields and sediment transport patterns around the nourishments compared to results for SPAW cases in this study. Furthermore, SPAW observations done by Wijnberg and Holman (2007) at other beaches also display onshore migration. Based on these two reasons it is expected that processes important for SPAW development, are similar for beaches with different hydrodynamics and bathymetries.

The model schematization is based on a hydrodynamically validated Delft3D-model for Duck that was made by Hsu et al. (2006 and 2008), Van der Werf (2008), and Treffers (2009). No field measurements of the flow-field and sediment transports during a SPAW event are available for calibration, because it is hard to measure a SPAW due to its irregular and unpredictable occurrence. We have chosen Delft3D parameters based on expert knowledge, and simulated results are not calibrated to fit any results. Nevertheless, qualitative modelling results are trusted since these are in line with the formulated hypothesis based on theory. Also the reference situation (i.e. situation without a SPAW) showed approximately longshore uniform results. Furthermore, results are compared to observations done by Wijnberg and Holman (2007) and the rough estimate they made of the sediment flux. Their rough estimate (1 to 2 m^3/m/day) was in the same order of magnitude for the sediment flux induced by the SPAW for the base case (1.3 m^3/m/day). It should be noted that particularly sediment transport results should be interpreted with care, because Delft3D parameters for sediment

transports are normally calibrated on measurements. A parameter which was seen to influence sediment transports as well was the horizontal diffusion coefficient.

It is important to realize that this study is based on a highly schematized Delft3D model of a SPAW. This was done to study the autonomous effects of a SPAW, i.e. isolated from other processes that are expected to be less importance. The following schematizations were done. Firstly, the bathymetry was assumed alongshore uniform based on bathymetry measurements. Secondly, a constant wave height and water level was assumed instead of a time series. Simulating a time series is of particular interest for morphodynamic modelling, since then the SPAW could move onshore/offshore depending on the wave conditions. Thirdly, a JONSWAP spectrum was applied which is based on North Sea characteristics. Nevertheless, since for the input in a JONSWAP spectrum specific wave conditions for Duck are used the JONSWAP also gave a good representation of the wave field. Furthermore, winds and horizontal tide were excluded, and the angle of wave incidence is assumed to be coast normal. Due to the latter schematizations, longshore currents are strongly reduced and even absent for the reference case without SPAW. This makes the analysis of SPAW dynamics easier since it is determined by fewer factors. However, in reality a longshore current will be present most of the time. It will tend to advect and diffuse sand in alongshore direction. Nevertheless, SPAW development is observed by Wijnberg and Holman (2007) to be essentially a cross-shore process, and therefore it was worthwhile to first study dynamics excluding longshore currents. Also it should be noted that it was chosen to carry out morphostatic instead of morphodynamic simulations, since sediment transports are uncertain and the available time for this study was limited. However, because we also modelled SPAWs at several locations (near the shore, between the bar and shore, and closer to the bar) an indication of the morphodynamic development of a SPAW was given. A shoreward displacement of the SPAW was visible for all locations. However, we could not estimate how long it takes a SPAW to transit the trough and compare the estimate with SPAW observations in nature; a morphodynamic run is needed to make such estimation.

Using a highly schematized model has large advantages. Mainly because modelling results are not disturbed by other factors, such as local longshore variations in bathymetry. Furthermore, it facilitates to investigate solely the SPAW influence on hydrodynamics and sediment transport.

7.1.2 Delft3D modelling issues

The highly schematized approach had as additional advantage that it becomes easier to detect model inadequacies and irregularities in the results. Consequently, this study revealed a few Delft3D model inadequacies. Namely, anomalous eddy viscosity profiles for the reference base case were detected at specific grid cells near the point where water levels rapidly increases. Also they were found at the SPAW crest for the high water level case. These anomalous profiles induce irregular and unrealistic results for sediment transports. Within this study these aspects are regarded as numerical flaws in the model. Since they were located outside the area of interest for the base case, the cause of these flaws were regarded outside the scope of this study. However, to improve robustness of Delft3D, it is worth to investigate what the cause is for these irregularities.

Furthermore, it turned out that the stationary roller model as implemented in the current Delft3D version did not compute organized wave forces, but only roller forces, by which the model could not simulate wave set down. A Delft3D test-version was made in which the stationary roller model was adjusted. This test-version indeed improved prediction of set-down, but also numerical issues arose leading to instable results for the average and high

water level case. For the low water level, it showed that inclusion of organized wave forces had second order effects on the flow-field and related sediment transports. Nevertheless, it is a fact that the current implementation of the stationary roller model in Delft3D does not include organized wave forces, inducing set-down, which is a natural phenomenon. Therefore, it is advisable to critically review the implementation of the roller model.

Finally, it was not possible to use the model a high wave event, because unrealistic high longshore currents near the coast were predicted for such case. For the low wave height near-bed sediment transport was dominant, while for a high wave height suspended transport can become more important. Therefore a higher wave height might lead to more diffusion and advection of sediment in the longshore direction by the generated horizontal circulation current. It is worth to look into the influence of wave height in more detail in future research.

Although it was a challenge to resolve numerical issues which came by during the modelling process, obtained results show that Delft3D can be applied in a detailed way and generates results that are consistent with theory.

7.1.3 Relevance for nearshore nourishment strategies

A specific study on humplike nourishments for the shoreface was done by Koster (2006). He set-up a 2DV Delft3D model to investigate whether humplike nourishments would be more effective than elongated bar nourishments. Likewise to humplike nourishments, SPAWs can be regarded as natural small-scale nourishments. Nevertheless, this study and Koster's differ. For example, Koster studied Egmond aan Zee with a 2DV model instead of a 3D model. Furthermore, his bathymetry did not include an alongshore bar. He placed nourishments further offshore, and they were higher and thus contained a larger volume of sand. In his computation the waves approached the shore obliquely, so he included longshore currents. Besides that, wave heights he imposed at the boundaries were larger (i.e. 1 to 3 meter compared to a wave height of 0.56 m in this study). Also his study was about three small scale nourishments next to each other. Nevertheless, his study also showed that a horizontal circulation current developed around the humps, sediment transports were onshore directed at the nourishment, and consequently onshore migrations of the humps occurred.

However, he did not particularly zoom in at the processes important for the onshore transports over a nourishment and consequently onshore propagation of nourishments. And he did not distinguish the contribution of suspended and near-bed transport, whereas this study does. An important finding from this analysis is that near-bed load is dominant, and mainly driven by wave asymmetry.

For nourishment strategies specifically, this study contributes to the idea that small scale nourishments can be an interesting alternative way of nourishing the shoreface. SPAWs are located very close to the shore and therefore the construction costs are expected to be higher. However, it is very well possible that these more nearshore nourishments are more effective (i.e. more sand eventually reaches the beach), making it an attractive way of nourishments. Future research can be done to investigate what the cost-efficiency will be for small-scale nourishments at different locations and shapes in the nearshore.

7.2 Conclusions

The objective of this study was to assess which nearshore processes control shoreward propagation of the SPAW phenomenon after it was initiated. This was fulfilled by formulating a hypothesis based on theory of nearshore processes and literature, and subsequently simulating several schematized SPAW cases with a 3-dimensional Delft3D model. Water

levels, wave heights, and SPAW dimensions were varied to understand SPAW behaviour. The wave-driven flow field and related sand transport patterns around the SPAW were analysed. By means of these insights the research questions could be answered.

7.2.1 Answers on research questions

1) What is the effect of a SPAW on the wave-driven flow field and related initial sediment transport pattern, and what is the resulting SPAWs initial morphologic development?

Delft3D simulations for the base case gave insight in the wave-driven flow field and related sediment transports, particularly in comparison to the case without SPAW. The base case uses a schematized bathymetry based on the representative SPAW event and a low wave height (H_s=0.56 m and T_p=8.2 s) and an average water level (z=0 m). It showed that wave height varied locally since waves break over the feature, by which energy is dissipated. These variations induce cross-shore and longshore gradients in radiation stress, due to which local set-up (or relative set-down) is generated. These variations in water level cause longshore pressure gradients, which induce currents. As a result, a horizontal circulation current develops around the SPAW tips, which is onshore directed over the crest and offshore directed around the SPAW. The Eulerian flow pattern was dominated by the undertow, induced by wave breaking at the coast.

Due to changes in the wave-driven flow-field, the SPAW presence also influences sediment transport. Waves shoal over the SPAW, leading to wave deformation in which waves become more asymmetric and skewed. An onshore sediment transport was seen over the SPAW, which was dominated by near-bed transports in direction of wave propagation (i.e. bed load and suspended load transport due to wave asymmetry). These onshore directed transport contributions result in a shoreward displacement of a SPAW, i.e. initial sedimentation occurred just landwards, and erosion just seawards of the SPAW. A remarkable result is that, with a low wave height, the generation of a horizontal circulation current around the SPAW is not the driving force for increased onshore sediment transport. Instead, the driving force is the wave deformation over the SPAW, influencing near-bed transport.

The obtained results are consistent with the hypothesis based on literature. A horizontal cell-circulation current indeed develops around the SPAW, and sediment transport is onshore directed over the SPAW. Interestingly, also another aspect became clear from the Delft3D modelling study; namely due the modulation of the flow-field the depth-averaged velocities over the bar at the location of the SPAW were lower if a SPAW was present. This stimulates crescentic bar pattern as observed after long periods of calmer weather conditions (Wright and Short, 1984). Additionally, results are consistent with SPAW observations done by Argus video systems and previous estimates of sediment fluxes (Wijnberg and Holman, 2007). The average onshore sediment transport flux related to SPAW propagation was roughly estimated about 1 to 2 m^3/m/day based on SPAW observations, whereas results from this analysis estimated the flux on 1.3 m^3/m/day.

2) How are the wave-driven flow field and related initial sediment transport over a SPAW, and the resulting initial morphologic development, affected by changing water levels, wave height, and morphometric characteristics of the SPAW?

To begin with, for all cases the qualitative patterns of initial sedimentation and erosion patterns were similar to the base case. This implies that these are not strongly influenced by water levels, or morphometric changes of the SPAW (i.e. SPAW width, length, location or bar bathymetry).

For different water levels the analysis showed that the wave breaking pattern over the bar and SPAW differs. More waves break over both features if the water level is lower, which results in a higher wave set-up shoreward of the SPAW. Consequently, longshore pressure gradients are larger for the low wave height, which results in the development of a stronger horizontal circulation cell for a low water level. Nevertheless, no extreme differences in sediment transport could be seen between a case with a low and an average water level. This is due to the fact that sediment transport is a result of many processes counteracting each other (e.g. wave asymmetry, concentration in the vertical due to wave-breaking, velocity patterns etc). But also due to the fact that near-bed transport due to wave asymmetry is dominant. When suspended transport would be more important, differences between different water levels could become bigger because this type of transport is influenced more by the flow-field. Since the generated horizontal circulation current is stronger for the low water level case, sediment transport patterns are then expected to be different for both cases.

The effect of SPAW locations was investigated to see whether the SPAW is expected to show similar behaviour regardless its cross-shore locations (between bar and shore). The developed flow-field around a SPAW was different for all SPAW locations. For a SPAW located further from the shore, the generated horizontal circulation current was stronger than for a feature located closer to shore. It extended over the full length of the SPAW crest, whereas for the latter it was only concentrated at the tips. This was because longshore water level gradients seaward of the SPAW were small when it was located closer to the shore, inducing a weaker current. Consequently, related sediment transport patterns were also different. For a case with a SPAW located closer to shore (suspended) sediment transports were higher at the SPAW tips, whereas for a feature located further from shore they were higher over the full length of the SPAW crest. Initial erosion-sedimentation patterns confirm SPAW observations and show a shoreward displacement of the SPAW for all cases. This is mainly due to the fact that near-bed sediment transport due to wave asymmetry is dominant.

For a wider or longer wave-driven flow fields and related initial sediment transport patterns are again similar to the base case. For a wider SPAW a stronger horizontal circulation cell developed around the SPAW. For the longer SPAW horizontal circulation currents concentrated at the SPAW tips, which resulted in higher onshore directed sediment transports at the tips than in the centre. However, hardly any effect of the sediment transport being larger at the tips for a longer SPAW was seen for the initial morphodynamic results.

Finally, the bathymetry of the nearshore bar was lowered seaward of the SPAW, since this was seen in the one bathymetric measurement of a SPAW. For this case the depth averaged flow field differed from the base case, since velocities were mainly directed through the location of the lowered bar. Velocities and related suspended sediment transport are offshore directed at the location where the bar was lowered, resulting in less onshore directed transport at this part of the bar. Transports increased at the place where the nearshore bar has its original height, since both suspended and near bed transports are onshore directed and relatively large at the sides of the inner bar. A remarkable result was that the onshore directed sediment transports at the tips of the SPAW were directed slightly to the middle of the SPAW, because the suspended sediment transport component is directed from the sides to the middle of the feature. This is due to a generated horizontal circulation current slightly landward of the SPAW. This can be a contribution for the SPAW maintaining its shape during its propagation to the coast.

7.2.2 Synthesis on objective

To come back to the objective, the process of wave transformation (i.e. increasing wave skewness and asymmetry) over the SPAW is important to generate onshore sediment transports over the feature. Near-bed transport in the direction of wave propagation due to wave asymmetry was dominant in all cases.

Furthermore, the process of local wave breaking (i.e. energy dissipation), generates a horizontal circulation current around the SPAW. This current is especially important for suspended sediment transports, which are transported by the GLM-velocities. When suspended transport becomes higher, this can be for sediments with a smaller grain size, or higher wave heights. We expect the horizontal circulation current to become more important for the sediment transport patterns. Since near bed load is dominant for our cases with a low wave height, it was shown that the generated circulation pattern did hardly influence sediment transport patterns over the SPAW.

7.3 Recommendations

7.3.1 Further investigating SPAW dynamics

We recommend carrying out morphodynamic simulations to investigate further whether a SPAW maintains its shape during propagating to the shore which is observed in nature, or that it will diffuse along the coast while propagating onshore. Also with a morphodynamic run it can be simulated how long it takes the SPAW to transit the trough. For nourishing practices the time scale in which a SPAW is expected to transit the trough is important to know.

It would also be interesting to investigate why in the case of a longer SPAW the higher sediment transport concentrations at the tips are hardly reflected in related initial sedimentation-erosion patterns. Based on the sediment transport patterns, we expect the tips to propagate faster, but this is not confirmed by the simulation results. It is important to investigate this aspect, since it will give insight in the different morphodynamic behaviour of features with different lengths, which is important for nourishing strategies.

The analysis of morphometric changes of SPAWs focused on initial erosion-sedimentation patterns. However, several interesting aspects in the flow-fields and sediment transport patterns came forward which are worth to investigate further. Firstly, for the SPAW located further from the shore sediment transport was increased around x=180 m. Secondly, for the wider SPAW an increase in sediment transport was seen at the tips and in the middle of the SPAW. Knowing what cause these patterns will give insight in whether sediment transport patterns for these cases are indeed realistic.

Also the influence of wave height should be investigated in more detail, since this can influence sediment transport patterns and suspended transports are expected to become more important. Besides that, it is interesting to test what a longshore current would do for SPAW dynamics. This can for example be tested by varying the wave angle and inclusions of a horizontal tide.

Finally, these results are particularly applicable for the study site of Duck. Although similar behaviour and important processes are expected for other beaches, it is good to check this by doing a comparable study for another beach at which SPAWs are observed. Also with respect to nourishment strategies, it is worth to investigate the expected cost-efficiency for small-scale nourishments with different shapes and at different locations in the nearshore.

7.3.2 Recommendations regarding Delft3D modelling

It is important to critically review the current roller model implementation in Delft3D. The current version does not take organized wave force into account and therefore does not include wave set-down and additional wave set-up. A Delft3D test-version was made which includes roller forces as well as wave forces. Modelling results for both versions for this specific study were similar and only showed second order effects. Nevertheless, it should be investigated whether this holds for other cases/situations (i.e. not only SPAW cases, but also cases for bars more offshore etc.). Another aspect is that some numerical problems arose when using the test-version including organized wave forces for higher water levels; it should be investigated where these numerical instabilities come from.

Additionally, the model schematization is an interesting case to investigate numerical Delft3D problems in more detail; because it is three-dimensional for a large domain, has a very fine grid, and is highly schematized. It is advisable to use it as a test case to investigate several modelling aspects in more detail. Such as the anomalous vertical eddy viscosity profiles which induced gradients for the sediment transports.

The model was not calibrated on sediment transport data, but parameters were chosen based on experts' opinion. Modelling results were trusted by the circumstantial evidence that they were similar to the hypothesis based on literature, and to SPAW observations in nature, and sediment transports were in the same order of magnitude as the rough estimate of Wijnberg and Holman (2007). Nevertheless, it is important to check the sensitivity of results for parameters that can influence sediment transport patterns; such as sediment grain size, free parameters in the roller model (now default values are used), factors determining the importance of sediment transport components, and the background horizontal diffusion/viscosity parameters. In the best case we would like to calibrate the model using measured data of the flow-field and sediment transport patterns for a SPAW case. But unfortunately, it is probably not feasible to obtain these data due to the irregular occurrence of a SPAW.

References

Almar, R., B. Castelle, B.G. Reussink, N. Sénéchal, P. Bonneton, V. Marieu (2010). Two- and three-dimensional double-sandbar system behaviour under intense wave forcing and a meso-macro tidal range. Continental Shelf Research, 30, 781-792.

Bosboom, J. and Stive, M.J.F. (2011). Coastal dynamics I. Delft University of Technology.
Bowen, A.J., D.L. Inman (1968). Wave set-down and set-up. Journal of Geophysical Research, 73 (8), 2569 – 2577.

Capo, S., J.P. Parisot, S. Bujan, and N. Senechal (2009). Short time morphodynamics response of the TrucVert Beach to storm conditions. Journal of Coastal Research, ICS Proceedings, SI 56, 1741 – 1745.

Dean, R. G. and R. A. Dalrymple, 1991. Water wave mechanics for engineers and scientists, vol. 2 of Advanced series on ocean engineering. World Scientific Publishing Company. 242

Deltares (2011). Delft3D – Flow. User manual. Deltares, Delft.

Deltares (2011b). Delft3D – Wave. User manual. Deltares, Delft.

Deltares(2011a). Delft3D – RGFGRID. User manual. Deltares, Delft.

De Vriend, H.J. and M.J.F. Stive (1987). Quasi-3D Modelling of Nearshore Currents. Coastal Engineering, 11, 565 – 601.

Haas, K.A., Svendsen, I.A. and Haller, M., 1998. Numerical modelling of nearshore circulation on a barred beach with rip channels. In Proceedings 26th Coastal Engineering Conference, ASCE, 1: 801814, Copenhagen.

Hasselmann, K., T. P. Barnett, E. Bouws, H. Carlson, D. E. Cartwright, K. Enke, J. Ewing, H. Gienapp, D. E. Hasselmann, P. Kruseman, A. Meerburg, P. Muller, D. J. Olbers, K. Richter, W. Sell and H. Walden (1973). Measurements of wind wave growth and swell decay during the Joint North Sea Wave Project (JONSWAP)." Deutsche HydrographischeZeitschrift 8 (12).

Holthuijsen, L.H., Booij, N. andHerbers, T.H.C. (1989). A prediction model for stationary, short-crested waves in shallow water with ambient currents. Coastal Engineering, 13: 23-54.

Holthuijsen, L.H., Booij, N. and Ris, R.C.(1993). A spectral wave model for the coastal zone. Proceedings of the 2nd International Symposium on Ocean Wave Measurement and Analysis, New Orleans, pp. 630–641.

Hsu, Y.L., Dykes, J.D., Allard, R.A. and Wang, D.W. (2008). Validation Test Report for Delft3D, Naval Research Laboratory, Texas.

Hsu, Y.L., Kaihatu, J.M., Dykes, J.D. and Allard, R.A. (2006). Evaluation of Delft3D performance in nearshore flows, Naval Research Laboratory, Texas.

Komar, P.D. (1998). Beach Processes and sedimentation. New Jersey, Prentice Hall, Inc.
Koster, L. (2006). Humplike nourishing of the shoreface, Deltares, Delft.

Larson, M. and N.C. Kraus (1993). Dynamics of longshore bars. Coastal Engineering, Proceedings of the 23rd International Conference, ASCE, New York, 2,219 – 2,232.

Leffler, M.W., and C.F. Baron, B.L. Scarborough, K.H. Hathaway, and R.T. Hayes (1992). Annual Data Summary for 1990 CERC Field Research Facility, Vol. 1, Technical Report ERC-92-3, Coastal Engineering Research Center, US Army Engineer Waterways Experiment Station, Vicksburg, MS., 69 pp + Appendices.

Lesser, G.R., J.A. Roelvink, J.A.T.M. van Kester, and G.S. Stelling (2004). Development and validation of a three-dimensional morphological model. Coastal Engineering, 51, 883 – 915.

Lippmann, T.C. and R.A. Holman (1990). The spatial and Temporal Variability of Sand Bar Morphology. *Journal of Geophysical Research*, 95, C7, 11,575-11,590.

Longuet-Higgins, M.S. and R.W. Stewart (1964). Radiation stresses in water waves; a physical discussion, with applications. Deep Sea Research and Oceanographic Abstract, 11 (4), 529 - 562.

Masselink, G., and Hughes, M.G. (2003). Introduction to coastal processes and geomorphology. London, UK, Hodder Arnold.

Nairn, R.B., Roelvink, J.A. and Southgate, H.N., 1990. Transition Zone Width and Implications for Modelling Surf zone Hydrodynamics. Coastal Engineering, 1: 68 -81.
Ojeda, E., B.G. Reussink, J. Guillen (2008). Morphodynamic response of a two-barred beach to a shoreface nourishment. Coastal Engineering, 55, 1185 – 1196.

Park, D. (1999). Waves, tides and shallow-water processes. Oxford, UK, Butterworth-Heinemann.

Ronde, J.G. (2008). Toekomstige langjarige suppletiebehoefte. Deltares report Z4582.24, september 2008.

Ruessink, B.G., D.J.R. Walstra and H.N. Southgate, 2003. Calibration and verification of a parametric wave model on barred beaches. Coastal Engineering, 48, 139-149.

Svendsen, I.A. (1984). Wave heights and set-up in a surf zone. Coastal Engineering, 8, 303 – 329.

Treffers, R. (2009). Wave-Driven Longshore Currents in the Surf Zone. Deltares, Delft.

Van der Werf, J.J. (2009). Hydrodynamic Validation of Delft3D using Data from the SandyDuck97 Experiments, Deltares, Delft.

Van Duin, M.J.P. and Wiersma, N.R., Walstra, D.J.R., van Rijn, L.C., Stive, M.J.F. (2004). Nourishing the shoreface: observations and hindcasting of the Egmond case. The Netherlands. *Coastal Engineering*, 51, 813 – 837.

Van Rijn, L.C. (1993). Principles of Sediment Transport in Rivers, Estuaries and Coastal Seas. Aqua Publications, The Netherlands. 82, 86, 336, 337, 338, 339, 340, 345, 346, 349, 350, 352, 354, 355, 556, 557.

Van Rijn, L.C. (2007). Unified View of Sediment Transport by Currents and Waves. I: Initiation of Motion, Bed Roughness, and Bed-Load Transport. Journal of Hydraulic Engineering, 133. 649 – 667.

Van Rijn, L.C. (2007a). Unified View of Sediment Transport by Currents and Waves. II: Suspended Transport. Journal of Hydraulic Engineering, 133. 668 – 689.

Van Rijn, L.C., and D.J.R. Walstra (2004). Analysis and modeling of shoreface nourishments. WL|Delft Hydraulics report, Augustus 2004.

Walstra, D.J.R., J.A. Roelvink, and J. Groeneweg (2000). Calculation of Wave Driven Currents in a 3D Mean Flow Model. In Proceedings 27th International Conference on Coastal Engineering (ICCE), Sydney, Australia, pp. 1050-1063, 331.

Wijnberg, K.M. and R.A. Holman(2007). Video-observations of shoreward propagating accretionary waves. *Proceedings of RCEM*2007, 737-743.

Wijnberg, K.M. and R.A. Holman, not published. Shoreward propagating accretionary waves in the nearshore (personal communication).

Wright, L.D. and A.D. Short (1984). Morphodynamic variability of surf zones and beaches: a synthesis. Marine Geology, 56, 93-118.

A Concept of Radiation stress and wave set-up/set-down

This appendix explains the concept of radiation stress in more detail than in the main text. It firstly describes the phenomenon of radiation stress followed by the concept of wave set-up and set-down.

A.1 Radiation stress and wave force

Radiation stress in water waves plays an important role in a variety of oceanographic phenomena, such as additional water mean sea level variation known as wave "set up" and "set down" and to wave-driven mean flows. It is also especially important for the nearshore zone, and is therefore particularly interesting for this research. Longuet-Higgins and Stewart (1964) define radiation stress as "*the excess flow of momentum due to the presence of waves"*. In the direction of the wave propagating the momentum flux consists of two components: one with the horizontal water velocity (i.e. ρu^2), and a component associated with water pressure (i.e. p). When considering only an excess of momentum flux the hydrostatic pressure should be subtracted.

Longuet-Higgins and Stewart (1964) assumed that linear wave theory could be applied to describe expressions for the velocity and pressure, in order to develop relations to describe radiation stress. Thus to calculate radiation stress in the direction of the flow the following equations can be applied:

$$S_{xx} = \overline{\int_{-h}^{\zeta} (p - \rho u^2) dz} - \int_{-h}^{0} p_0 dz \qquad \text{(A.1)}$$

$$S_{xx} = \left(\frac{2kh}{\sinh 2kh} + \frac{1}{2}\right) E = \left(2n - \frac{1}{2}\right) E \qquad \text{(A. 2)}$$

In which S_{xx} is the radiation stress, h the waterdepth [m], ζ the surface elevation [m], p the pressure [N/m^2], ρ the density of the water [kg/m^3], u the velocity in x-direction [m/s], p_0 the hydrostatic pressure [N/m^2], k the wavenumber [rad/m], E the wave energy [J/m^2]. A situation with the x-direction in the direction of propagation direction of the waves is considered. The n value for deep and shallow conditions are known, respectively n=1/2 and n=1. This implies:

$$S_{xx,deep} = \tfrac{1}{2}E \qquad S_{xx,shallow} = \tfrac{3}{2}E \qquad \text{(A. 3)}$$

For the transverse components of the radiation stress, normal to the direction of wave propagation, only the pressure contributes to the total mean momentum flux. Since for gravity waves the transverse velocity component vanishes everywhere (i.e.v = 0).
Thus:

$$S_{yy} = \overline{\int_{-h}^{\zeta} p\, dz} - \int_{-h}^{0} p_0 dz \qquad \text{(A. 4)}$$

$$S_{yy} = \left(\frac{kh}{\sinh 2kh}\right) E = \left(n - \frac{1}{2}\right) E \qquad \text{(A. 5)}$$

Considering the deep and shallow conditions again, gives:

$$S_{yy,deep} = 0 \qquad S_{yy,shallow} = \tfrac{1}{2}E \qquad \text{(A. 6)}$$

It should be noted that for a more general situation with a horizontal x-y coordinate system and waves propagating in an arbitrary direction (angle θ with the x-axis), additional radiation

stresses are present due to momentum in x-direction transported in y-direction and vice versa (S_{xy} and S_{yx}):

$$S_{xx} = \left(n - \frac{1}{2} + n\cos^2\theta\right)E \quad \text{(A. 7)}$$

$$S_{xy} = S_{yx} = (n\sin\theta\cos\theta)E \quad \text{(A. 8)}$$

$$S_{yy} = \left(n - \frac{1}{2} + n\sin^2\theta\right)E \quad \text{(A. 9)}$$

Only in a spatially non-uniform situation with varying wave characteristics and/or water depth a resulting net wave force is present due to gradients in radiation stress. The wave force vector, $\vec{R}$ in the direction of wave propagation can be calculated by:

$$R_x = -\frac{\partial S_{xx}}{\partial x} - \frac{\partial S_{xy}}{\partial y} \qquad R_y = -\frac{\partial S_{yx}}{\partial x} - \frac{\partial S_{yy}}{\partial y} \quad \text{(A. 10)}$$

This wave force can be considered an external force, which induces the process of wave set-up and set-down as discussed in paragraph 4.2.4. Radiation stresses also play a part in the generation of infragravity waves, but next to that they are responsible for the generation of longshore currents.

A.2 Wave set-up and set-down

Radiation stress can modify motions on a scale larger than the waves themselves. One of the most important wave driven effects occurs when waves encounter a sloping beach. Changes in bottom topography influence wave forms and result in changes in radiation stress, which subsequently lead to changes in the mean surface level, referred to as wave set-up and set-down (Longuet-Higgins and Stewart 1964). These two phenomena are discussed below.

When assuming the following described aspects the equation of motion reduces to equation A.11. Assuming a uniform coast, with the coastline as well as the depth contour lines of sea bed are schematized as parallel straight lines. Assuming wave-dominance, i.e. tidal flow can be neglected in the near-shore zone. And assuming a steady flow and that bed-shear stress can be neglected when considering merely flow and not sediment transport.

$$g\frac{\partial\bar{\xi}}{\partial x} = -\frac{1}{\rho h}\frac{\partial S_{xx}}{\partial x} \quad \text{(A. 11)}$$

Wave energy approaching a shore may either be reflected or dissipated to heat (Longuet-Higgins and Stewart, 1964). Considering slopes sufficiently gentle that reflection is often of negligible importance, which is generally the case for beaches addressed in this research, two distinctive regions can be identified. The nearshore zone seawards of the breaker line (wave set-down) and landwards of the breaking zone (wave set-up).

A.2.1 Wave set-down

When waves encounter a sloping beach just outside the surf zone, shoaling processes are present. Shoaling leads to increasing wave heights and thus increasing wave energy. This leads to a positive gradient in radiation stress in flow direction, from which it follows that the total right term of equation A.11 is negative. Thus the slope in mean water level is negative; implying a lowering of the mean water level defined as set-down. When integrating equation A.11 a general expression for the mean water level can be found, which can also be specified for shallow water conditions (i.e. $\sinh 2kh \approx 2kh$):

$$\bar{\xi} = -\frac{1}{8}\frac{kH^2}{\sinh 2kh} \qquad \bar{\xi}_{shallow} = -\frac{1}{16}\frac{H^2}{h} \quad \text{(A. 12)}$$

A.2.2 Wave set-up

Inside the breaker lines wave energy decreases shoreward, due to strongly decreasing wave heights by energy dissipation due to wave breaking and friction. This leads to a negative gradient in radiation stress, from which it follows that the total right term of equation 11 is positive. Thus the slope in mean water level is positive.

Although Longuet-Higgins and Stewart (1964) remark that it is probably not valid to apply linear wave theory, they state that assuming $S_{xx} = \frac{3}{2}E$ for shallow water conditions still remains approximately valid. Also $H_{br} = \gamma h_{br}$ is the relation for the decreasing wave height in the surf zone. Then the expression for the slope in mean water level becomes:

$$\frac{\partial \xi}{\partial x} = -\frac{3}{8}\gamma^2 \frac{\partial h}{\partial x} \qquad \text{(A. 13)}$$

Since water depth decreases approaching the shore, the right-hand side of the above equation becomes positive. This indicates that breaking waves lead to increasing water-level in the onshore direction, defined as wave set-up.

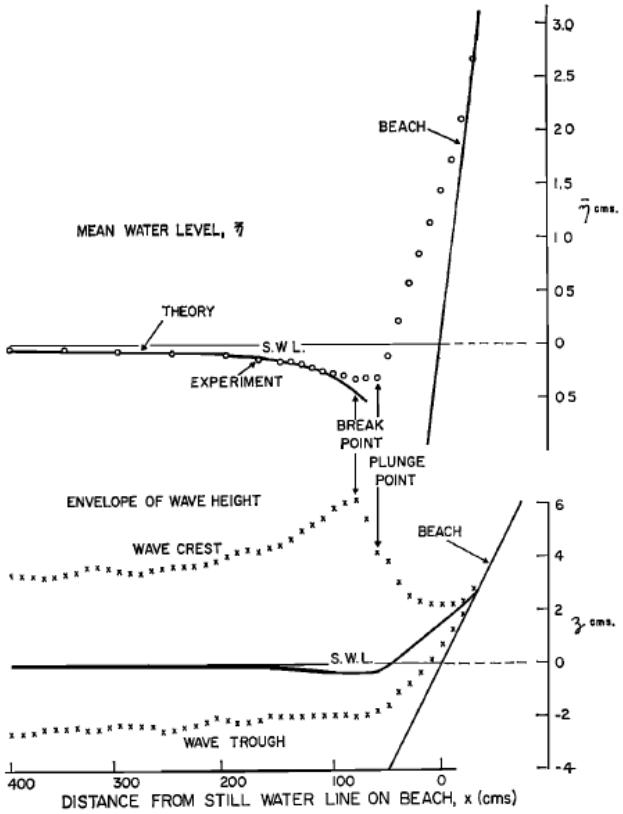

Figure 0.1. Profile of the mean water level and the envelope of the wave height showing wave set-up and wave set-down (adopted by Bowen and Inman, 1968).

It should be noted that wave set-up is much larger than the set-down and it takes place on a shorter distance. Experiments from Bowen, Inman et al.(1968) showed the theory of Longuet-Higgins and Stewart (1964) describe the phenomenon wave set-up and set-down reasonably well (Figure 0.1). However, it can be seen that just outside the break point measured values of 'set-down' are consistently less than the theory would predict, since the assumptions of Linear wave theory are no longer justified.

B Delft3D software

This appendix explains the basics of the Delft3D software (Version 4.00.01) which was used in this study to simulate SPAW dynamics. The Delft3D software is developed by WL | DelftHydraulics, at present Deltares. Look for more detailed information (such as model equations etc.) in the references (Lessers et al., 2004; Deltares, 2011 and 2011a). This appendix firstly gives general information about the software, then the modules FLOW and WAVE are described, followed by the SWAN and roller model which are applied in this study, and finally sediment transport calculations within Delft3D are explained.

B.1 Delft3D in general

Delft3D is a process-based morphodynamic model developed to simulate phenomena occurring in water environments. It can simulate flows, sediment transports, waves, water quality, morphological developments and ecology. Process-based implies that relevant processes such as tide, currents, waves, sediment transport, and bed updating are implemented using detailed descriptions. The software is widely used and proven reliable regarding sediment transport and morphological evolutions. It is possible to make 1D, 2D horizontal averaged, 2D depth-averaged and 3D calculations; especially the ability to calculate three-dimensionally is important for this research, since SPAWs are local and relatively small features. To investigate the hydrodynamic field, also the 3D flow pattern is of interest.

The WAVE and FLOW modules are used. Delft3D-FLOW calculates the flow-field, sediment transport field and evolution of the morphology; Whereas Delft3D-WAVE calculates the short wave field. These two modules are coupled in an online morphodynamic way (Figure 0.2), which implies Delft3D-FLOW makes several computations before the wave field is updated again.

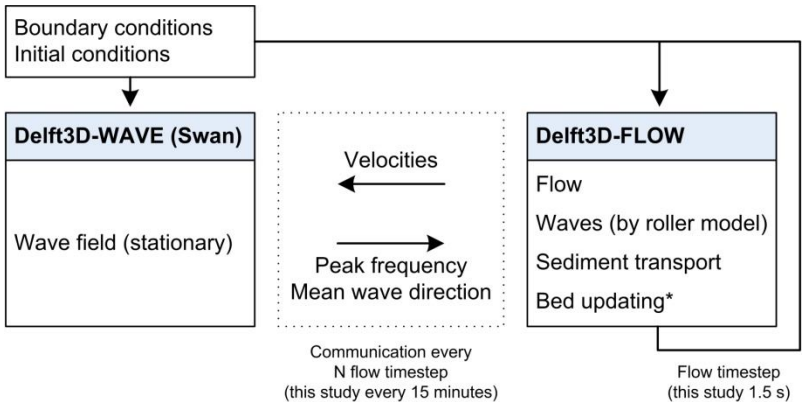

Figure 0.2. Structure of Delft3D in stationary mode.

B.2 Delft3D horizontal and vertical grid

Delft3D is a numerical model based on finite differences. It uses a rectangular (applied in this study), curvilinear or spherical grid, which should be orthogonal and well structured. Well-structured in the sense that it should comply with some requirements. For example: Delft3D requires an aspect ratio in m/n direction between 1 and 2, unless the flow is predominantly along one gridline; also m-(n-) smoothness (i.e. the ratio between adjacent grid cell lengths in m-(n-)direction) should preferably be less than 1.2 (Deltares, 2011a). Variables in the model are arranged in a staggered grid, meaning that not all variables are quantified at the same

location in the grid (Figure 0.3, right). The water level points are in the centre of a (continuity) cell, whereas the velocity components are calculated perpendicular to the grid cell faces.

For 3D computations, a so called boundary fitted (σ-coordinate) approach is used for the vertical grid direction (Figure 0.3, left). The sigma layer approach implies that each layer is a percentage of the total water depth, instead of a fixed value. Due to this the individual depth layers follow the contour of the water depth. For vertical layers the number of layers and thickness of each layer can be adjusted. In paragraph 3.4.2 the vertical grid settings of this model are described in further detail.

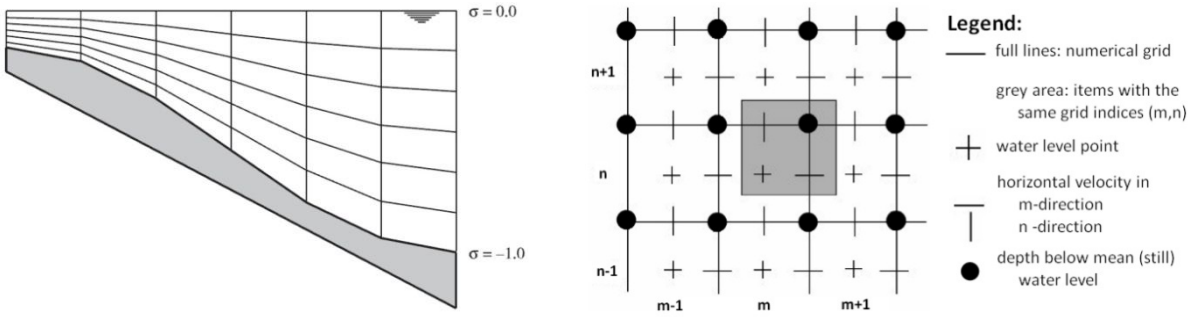

Figure 0.3. Vertical grid schematization showing σ-coordinate system (left) and horizontal grid showing staggered grid (right) Deltares (2011).

B.3 Delft3D-FLOW

Delft3D-FLOW solves the unsteady shallow-water equations in two (depth-averaged) or three dimensions. The system of equations which is solved by the FLOW module consists of 4 equations: horizontal momentum equation, continuity equation, transport equation, and a turbulence closure model. The vertical momentum equation is reduced to the hydrostatic pressure relation as vertical accelerations are assumed to be small compared to gravitational acceleration and therefore are not taken into account. The module takes phenomena as tide, wind and wave-driven flows into account.

Also three-dimensional wave effects can be taken into account by Delft3D-FLOW (Walstra and Roelvink, 2000) such as; (i) wave forcing due to breaking, (ii) wave induced mass flux, (iii) streaming, and (iv) additional turbulence production due to dissipation in the wave boundary layer and due to wave white capping and breaking at the surface.

B.4 Delft3D-WAVE

A separate module Delft3D-WAVE can be used to simulate the evolution of wind-generated waves in coastal waters. It computes root mean square wave height, peak spectral period, wave direction, and mass fluxes. The wave simulations can be done in two ways; with the HISWA wave model (**HI**ndcasting **S**hallow water **Wa**ves, Holthuijsen et al., 1989) or the third generation SWAN model (**S**imulating **Wa**ves **N**earshore, Holthuijsen et al., 1993). In this study the latter is used, which is explained in more detail below.

B.4.1 SWAN Wave model

The SWAN wave model, standing for Simulating Waves Nearshore (Holthuijsen et al., 1993), is used in Delft3D-WAVE to simulate waves. SWAN describes waves with a two-dimensional wave action density spectrum N(σ, θ); in which σ is the relative frequency and θ is the wave direction. The action density is used rather than the energy density spectrum E(σ, θ) since in presence of currents, action density is conserved whereas energy density is not. The action density equals the energy density divided by relative frequency. The following processes are

accounted for in SWAN; (i) generation of wind, (ii) dissipation by white capping, bottom friction and depth-induced breaking, and (iii) non-linear wave-wave interaction. For Cartesian coordinates the spectral action balance equation, which is the basis for wave evolution of the wave spectrum in SWAN, reads (e.g. Hasselman et al., 1973):

$$\underbrace{\frac{\partial}{\partial t}N}_{1} + \underbrace{\frac{\partial}{\partial x}c_x N}_{2} + \underbrace{\frac{\partial}{\partial y}c_y N}_{3} + \underbrace{\frac{\partial}{\partial \sigma}c_\sigma N}_{4} + \underbrace{\frac{\partial}{\partial \theta}c_\theta N}_{5} = \underbrace{\frac{S}{\sigma}}_{6} \qquad (14)$$

In which N is action density, c is propagation velocity, t is time, x and y denotes geographical space, σ is relative frequency, θ is wave direction, and S is the source term. The terms in the equation represent:

1. The local rate of change of action density in time
2. The propagation of action in geographical space (x-direction)
3. The propagation of action in geographical space (y-direction)
4. Shifting of relative frequency due to variations in depth and currents
5. Depth-induced and current-induced refraction.
6. Source term in terms of energy density representing the effects of generation of wind, dissipation (white capping, bottom friction and depth-induced breaking) and non-linear wave-wave interactions. For each of these source terms, different equations are used.

B.5 Roller model

The transition zone is the zone where rapid transitions of wave shapes are observed (i.e. wave decay), however no associated increase in energy dissipation is observed. This implies that wave energy dissipation should occur further to the shore. Svendsen (1984) suggested that the large amount of potential energy lost in the transition zone is converted to forward momentum flux, especially in the surface roller. Thus organized wave energy is not dissipated immediately, but first converted to roller energy (storage of kinetic energy inside the roller). The surface roller is defined as a recirculation part of the flow above the dividing streamline, it is a volume of water carried shoreward with the breaker (Figure 0.4). Therefore the roller is carried with the propagation speed of the wave. This paragraph broadly summarizes the implications of using the roller model. For theoretical background look in Svendsen (1984) and Nairn (1990), for equations and implementation in Delft3D look in Deltares (2011).

The roller model as applied in Delft3D-FLOW has been introduced to delay transfer of wave energy to the current. When using the roller equations, the wave set-up and longshore and cross-shore flow are shifted shoreward. The roller model allows modelling the effect of short-wave groups on long waves. Long waves travel along with groups of short waves (called carrier waves) and are referred to as bound long waves or locked waves. Wave breaking causes the carrier waves to vanish and hereby releasing the locked waves, and causes variations in radiation stresses. The roller model can only be applied in cases with a narrow-banded wave spectrum, both in direction and frequency. The SWAN wave model is used to supply a dominant frequency (peak frequency) and mean wave direction field, which indicates the direction of propagation of the carrier waves.

The roller model applies the balance of short wave energy (Deltares, 2011). Through the process of wave breaking the wave energy is reduced and transformed into roller energy. This energy is located in down-wave region after wave breaking. The propagation of roller energy is modelled by transporting it with twice the local celerity of the carrier wave. The energy that is lost from the organized wave motion is converted to roller energy through a roller energy balance. The time- and space varying wave energy and roller energy cause a variation in radiation stresses. The roller model can be turned on in the FLOW-module by using the keywords: Cstbnd = #yes# and Roller = #yes#.

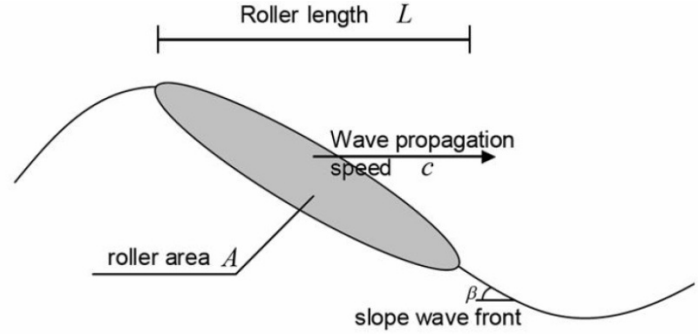

Figure 0.4. The concept of a roller travelling on top of a wave (Treffers, 2009).

B.6 Sediment calculations

In this model the sediment online version is used, which continuously updates transport of sediments in the FLOW module. Therefore it is possible to update the bed level and give feedback to hydrodynamics. Different sediment fractions and mixtures can be used; however in this study only uniform non-cohesive sediment fraction is used (i.e. sediment sand). Delft3D computes two types of sediment transport, suspended and bed load transport, as described in this paragraph. The transport formulation TRANSPOR2004 of Van Rijn (2007) was used. This is an updated version of TRANSPOR1993 (Van Rijn, 1993). In TRANSPOR2004 the bed-shear stress is based on a new bed roughness predictor. Also the reference concentration function has been recalibrated using laboratory and field data for combined steady and oscillatory flow (Van Rijn, 2007a). In Deltares (2011) a detailed description of the equations and methodology is given. In this paragraph the main topics are discussed.

B.6.1 Reference height and kmx-layer

In this calculation the definition kmx-layer is used. This refers to the layer that is entirely above Van Rijn's reference height (Figure 0.5), which is calculated based on bed roughness. The sediment concentrations in the layer below the kmx-layer are assumed to rapidly adjust to the same concentration as the kmx-layer.

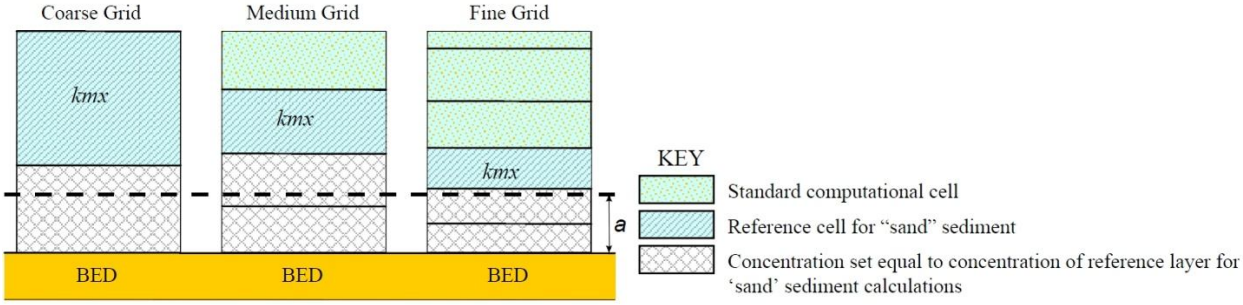

Figure 0.5. Selection of the kmx layer; where a is Van Rijn's reference height (Deltares, 2011).

B.6.2 Suspended sediment transport (non-cohesive)

The suspended sediment is calculated over the whole vertical of the water column. The Van Rijn (2000) approach is followed by default. Firstly the settling velocity of material calculated following method of Van Rijn (2007). Then the output of the turbulence closure model (the eddy viscosity at each layer interface) is used to calculate the vertical sediment mixing coefficient. The k-ε turbulence closure model (as applied in this study) has been extended to include three-dimensional effects of waves. Finally, the transfer of sediment between the bed and flow is modelled using sink and source term acting on the near-bottom layer that is entirely above Van Rijn's reference height (kmx, layer). Sediment is entrained in the water

column by imposing a reference concentration at the reference height. For this modelling the approach of Van Rijn (2007) is followed as well.

B.6.3 Near-bed load sediment transport (non-cohesive sediment)

For simulations including waves (this study) the magnitude and direction of the near-bed load transport on a horizontal bed are calculated using the selected transport formula (in this study TRANSPOR2004; Van Rijn 2007), assuming sufficient sediment and are adjusted for bed-slope effects. Bed composition is ignored except for e.g. hiding and exposure effects on critical shear stresses. Van Rijn regards sediment transported below the reference height as belonging to 'bed-load sediment transport'. This study refers to this as the near-bed load transport, since also a suspended load component is included. This responds almost instantaneously to changing flow conditions and feels the effects of bed slopes.

For simulations including waves, TRANSPOR2004 formula distinguishes three transport components all treated as bed or total load, i.e. without relaxation effects of an advection diffusion equation:

1. Bed-load due to currents (Sbc), acting in the direction of the (Eulerian) near-bed current.
2. Bed-load due to waves (Sbw), acting in the direction of wave propagation.
3. Suspended load due to wave asymmetry effects (Ssw), acting in the direction of wave propagation.

The third component represents effects of asymmetric wave orbital velocities on the transport of suspended material within approximately 0.5 m of the bed. It also accounts for the bulk of the suspended transport affected by high-frequency wave oscillations.

Bed load transport is affected by bed level gradients, in terms of magnitude and direction. Two bed slope corrections are distinguished: the slope in the initial direction of the transport (i.e. longitudinal bed slope) and the slope in the direction perpendicular to that (referred to as the transverse bed slope). Corrections for the bed slope are included by default in Delft3D.

B.6.4 Sediment correction vector

Some transport can be double counted since the suspended sediment transport is computed over the entire water column, and the bed-load is regarded the load below the reference height. To prevent for double counting, a sediment correction vector is applied, which is estimated by the load of the suspended load in the reference layer.

B.6.5 Sediment initial and boundary conditions

The initial conditions for non-cohesive sediment concentrations can be set to a uniform zero concentration, since the concentrations for non-cohesive sediments adapt very rapidly to equilibrium conditions. For the boundary conditions, the vertical diffusive flux through the free surface is set to zero. The bed boundary condition exists of the exchange of material in suspension and the bed. This is modelled by calculating the sediment fluxes from the bottom computational layer to the bed, and vice versa. At open boundaries the flow should enter carrying all sand sediment fractions at their equilibrium concentration profiles.

B.6.6 Morphological updating

It is possible to also calculate the morphological development of the bathymetry during a simulation. For this model the morphological updating is only started in the last minute of the simulation in order to simulate the initial sedimentation and erosion patterns. These patterns are only qualitative, since no data are available to calibrate anything.

C Representative transect for bathymetry

For this research, bathymetric measurements on the 6th of April 1994 were analyzed and a representative transect was chosen and extended uniformly along the coast. This appendix explains the choice for a specific transect.

Bathymetric surveys at the FRF are conducted monthly over a series of 26 shore perpendicular transects (profile lines) from the dunes to approximately 950 m offshore. They are conducted using a Coastal Research Amphibious Buggy (CRAB).

Since the Argus camera is installed at the top of a 40 m high tower, looking north. The area of interest in the field of view of the camera starts about 200 m north of the pier and extends 1 km alongshore (Wijnberg and Holman, n.p.). Figure 0.6 (left) shows transects at which the bathymetry was measured. Transect 58 to 95 are within the visualized area of the Argus camera, therefore it is preferred to take one of these as representative. Transects between 64 and 95 have a longshore bar at approximately the same location and height, although transect 67 has a trough much deeper than the other transects in this section. It could be seen from the data that between transect 160 and 171 the bathymetry is largely influenced by the pier.

A representative profile (dashed bold line in Figure 0.6) could be transects 85, since it approximately represents the cross-sections within the area of interest of the Argus camera. However, the measurement does not extend far offshore, and is not very detailed compared to other available cross-sectional measurements. Therefore transect 176 is chosen to be representative for the area instead. The shape of the bar is approximately the same as transects between 64 and 95 (Figure 0.6), only the measurement extends further offshore and more depths are measured per distance. Thus, transect 176 was taken for representing the bathymetry in September 1994.

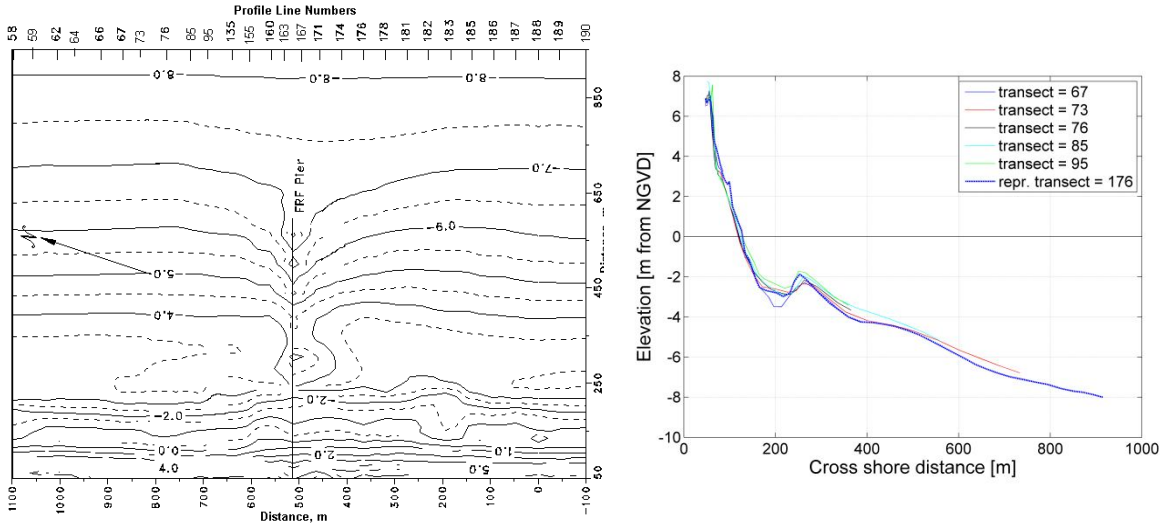

Figure 0.6. Choice for representative transect for bathymetry. Left: Transects over which bathymetry is measured (from http://www.frf.usace.army.mil/). Right: representative transect compared to others.

D Time step analysis

The computational time largely depends on the time step; a larger time step decreases the total computation time. Nevertheless, when having a very high grid resolution (as is the case in this study) the time step should become smaller as well in order to get accurate and stable results. The time step can be chosen on accuracy arguments, since stability is in most cases not an issue (Deltares, 2011).

The Courant (Friedrichs-Lewy) number [CFL] is an important parameter to check the accuracy of a model and gives a guideline for choosing a good timestep:

$$CFL = 2\Delta t\sqrt{gh}\sqrt{\frac{1}{\Delta x^2}+\frac{1}{\Delta y^2}} < 10 \qquad (15)$$

In which Δt is the time step (s), g is the acceleration of gravity, h is the waterdepth, and $\Delta x, \Delta y$ is a characteristic value (in many cases the minimal value) of the grid spacing in either direction. CFL should in general not be larger than 10 for an implicit numerical scheme such as Delft3D, in order to secure accuracy (Deltares, 2011). From Delft3D it could be obtained that the maximum allowed time step for accurate computation of wave propagation is 2.0 seconds. However this is a rough estimate and the timestep should be checked by executing a sensitivity test.

To investigate the influence of the time step to the model results, we did trial runs with different time steps (a time step of 1.5, 3, and 6 seconds).The results of these trial runs show that for time step 6 the results in the water level become instable when looking at the last timestep (Figure 0.7). Note that the magnitude of water level values is very small (10^{-4}).

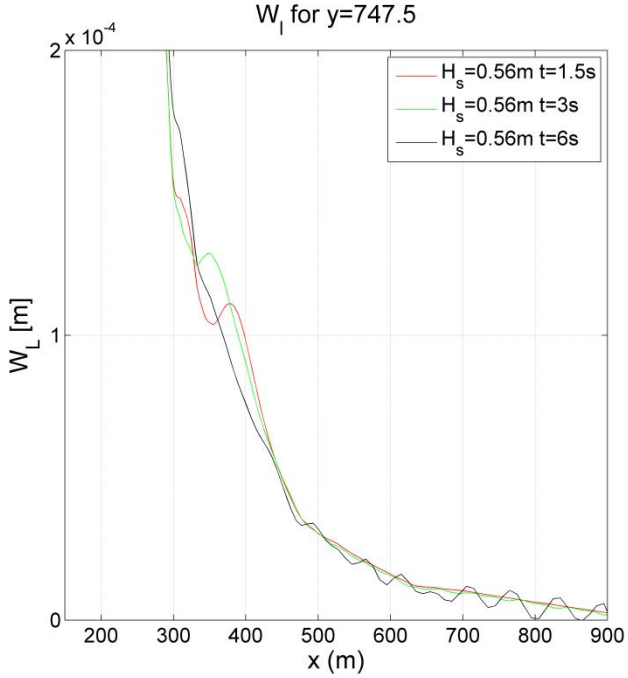

Figure 0.7. Water level after 2 hrs over the whole cross-section for different time steps.

If looking at the water level over time at an observation point located at the top in the middle of the SPAW(Figure 0.8), it shows that both time steps 6 and 3 seconds show irregularities.

These irregularities are once every 15 minutes, so they could be caused by the communication with the WAVE module which takes place at that interval. For the depth averaged velocity the cross-shore component (Figure 0.9, left) all timestep converge to an equilibrium value. For a step of 6 seconds, some irregularities can be seen. For the longshore velocity the results seem to differ a lot (Figure 0.9, right), however when looking at the magnitude of these velocities differences are not that big. After 120 minutes all timestep seem to be converged to an equilibrium value.

From this sensitivity analysis a time step of 1.5 second is chosen, since this seemed to give the most accurate results. Also, this value is lower than the suitable time step as given by Delft3D.

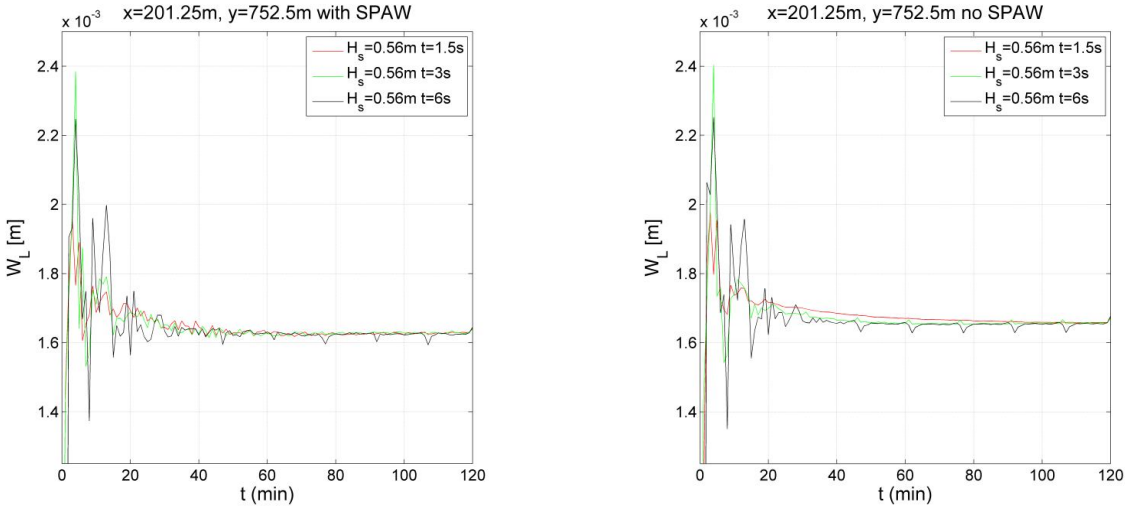

Figure 0.8. Water levels in time for the observation point on top of the middle of the SPAW for different timesteps; with SPAW (left), without SPAW (right).

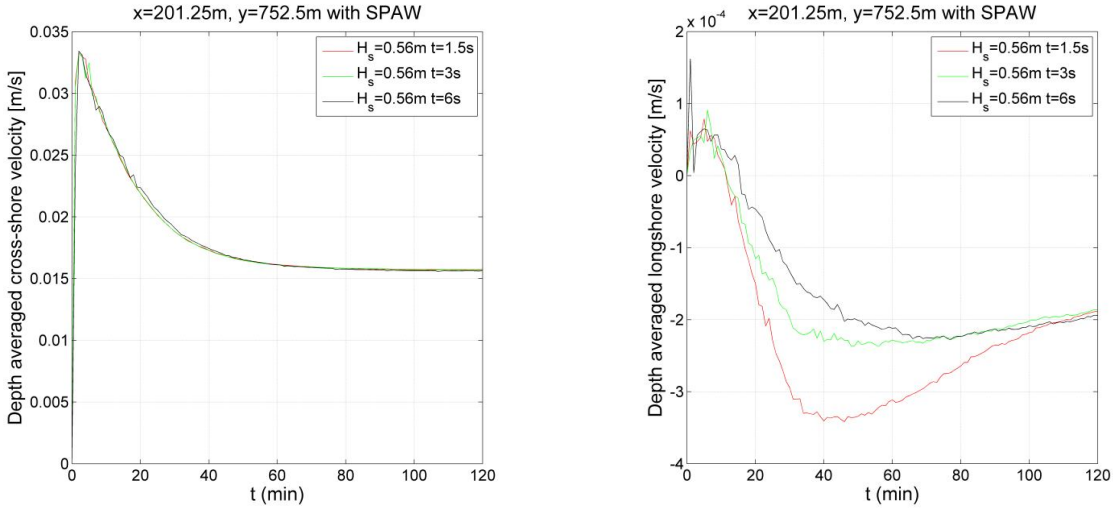

Figure 0.9. Depth averaged velocity in time for the observation point on top of the middle of the SPAW for different time steps; cross-shore velocity [U] (left), longshore velocity [V] (right).

E Conditions SandyDuck97

The conditions during the SandyDuck97 experiments as Van der Werf (2009) used are shown in this Appendix. The figures below show the water level, wind speed, wind direction, significant wave height, spectral peak period, and peak wave direction from 27th of September to 21st of October 1997. The wind direction is defined nautically (same as in Figure 3.3), the wave direction is different than in Figure 3.4, and represents the angle in degrees counter-clockwise from normal to the array, i.e. 0˚ represent coming from East and +90˚ represents coming from the North.

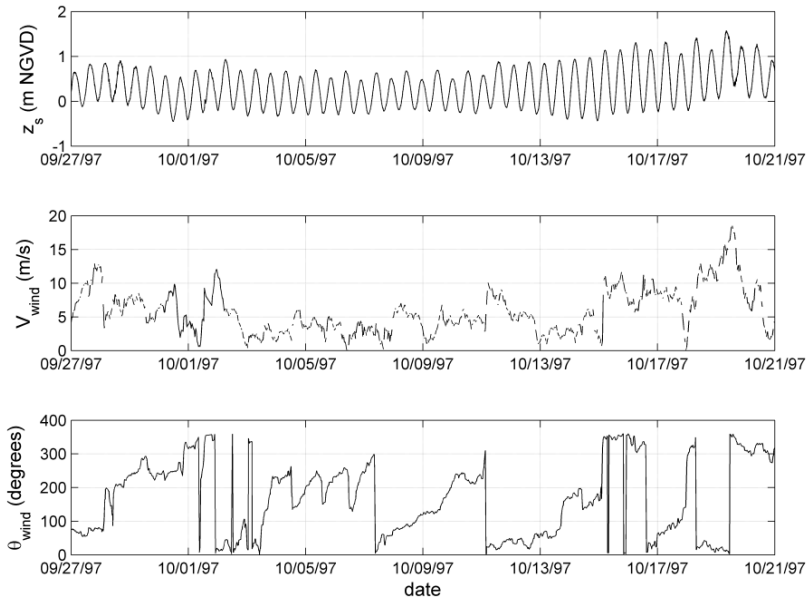

Figure 0.10. Water elevation, wind speed, and wind direction during SandyDuck97 field campaign. The wind direction is defined nautically and positive in clockwise direction (Van der Werf, 2009).

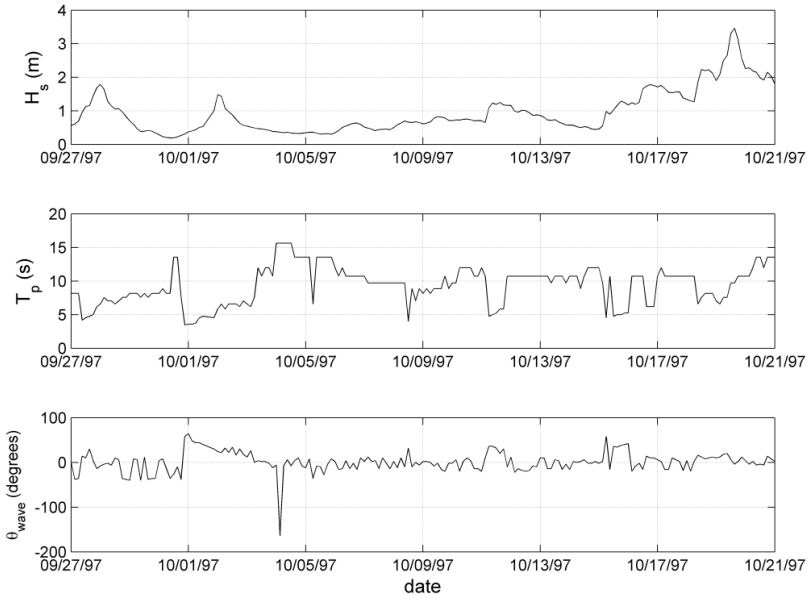

Figure 0.11. Significant wave height, spectral peak period, and wave direction during SandyDuck97 field campaign. The wave direction represents the angle in degrees counter clockwise from shore normal (Van der Werf, 2009).

F Bathymetries for SPAW scenarios

This appendix shows bathymetries as applied in the different scenarios. The specifications for SPAW configurations in different scenarios are summarized in Table 5. Note that the axis and colouring of bathymetry and top view figures do not have the same scaling.

Table 5. SPAW configurations for different scenarios

	Hs [m]	Z [m]	Width [m]	Length [m]	Location [m]	Remarks
S1: longer SPAW	0.56	0	25	400	198.75	
S2: wider SPAW	0.56	0	60	130	198.75	
S3: closer to shore	0.56	0	25	130	175	
S4: closer to bar	0.56	0	25	130	225	
S5: local bathymetry change	0.56	0	25	130	198.75	Bar lowered

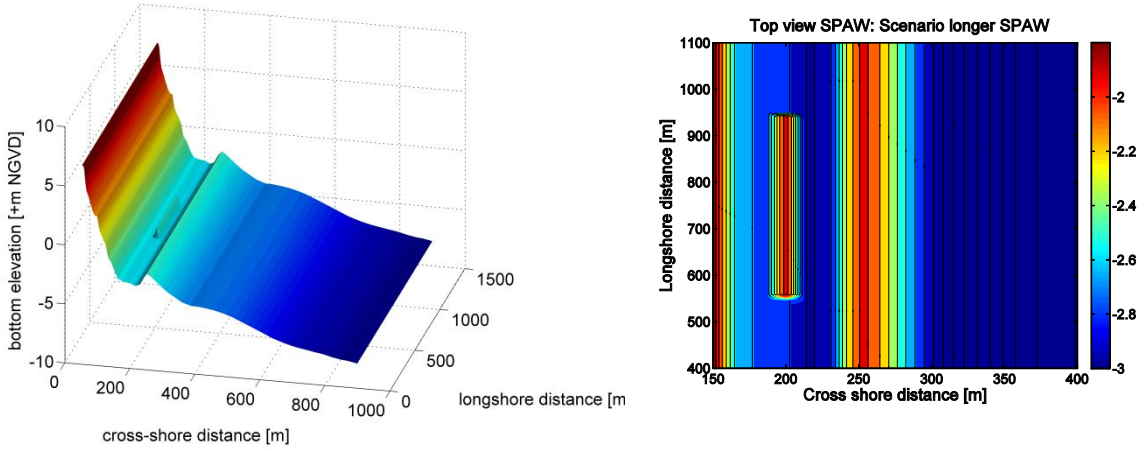

Figure 0.12. ***Scenario with a longer SPAW****: Schematic alongshore uniform bathymetry including a SPAW (left), and top view of SPAW configuration zoomed in at SPAW location (right).*

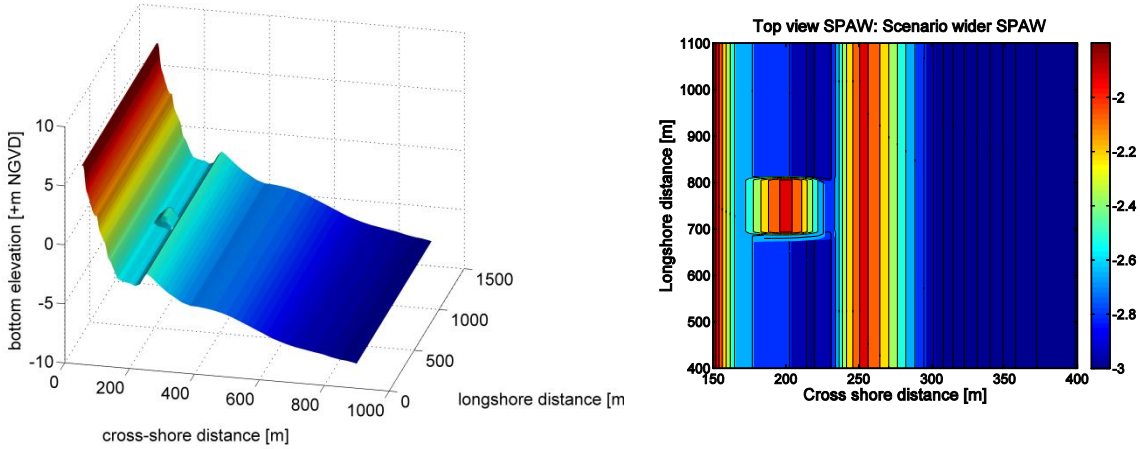

Figure 0.13. ***Scenario with a wider SPAW:*** *Schematic alongshore uniform bathymetry including a SPAW (left), and top view of SPAW configuration zoomed in at SPAW location (right).*

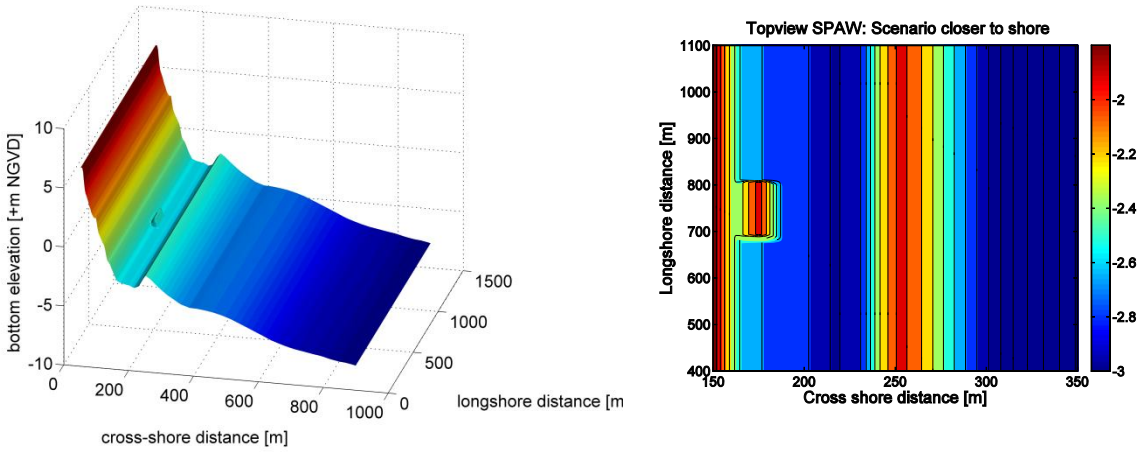

Figure 0.14. ***Scenario with SPAW closer to shore:*** *Schematic alongshore uniform bathymetry including a SPAW (left), and top view of SPAW configuration zoomed in at SPAW location (right).*

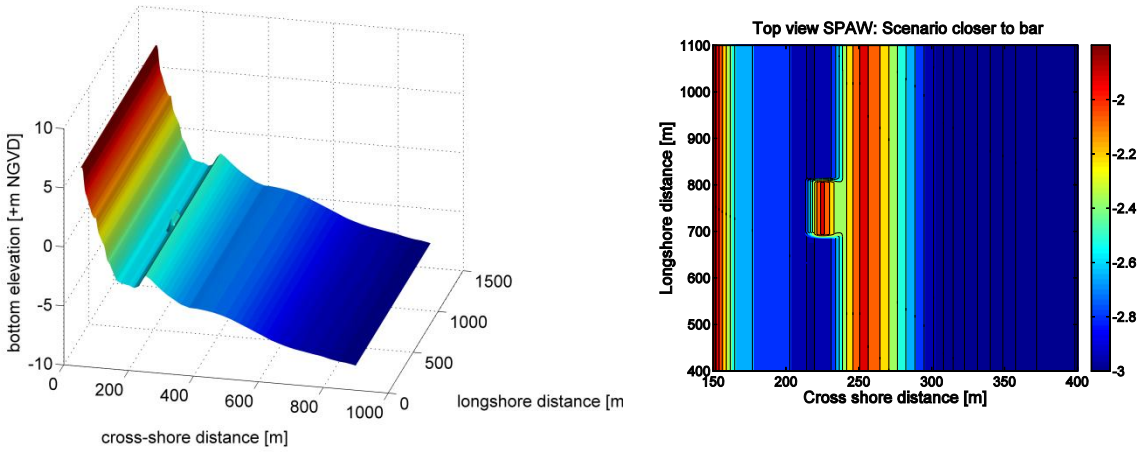

Figure 0.15. ***Scenario with SPAW closer to bar:*** *Schematic alongshore uniform bathymetry including a SPAW (left), and top view of SPAW configuration zoomed in at SPAW location (right).*

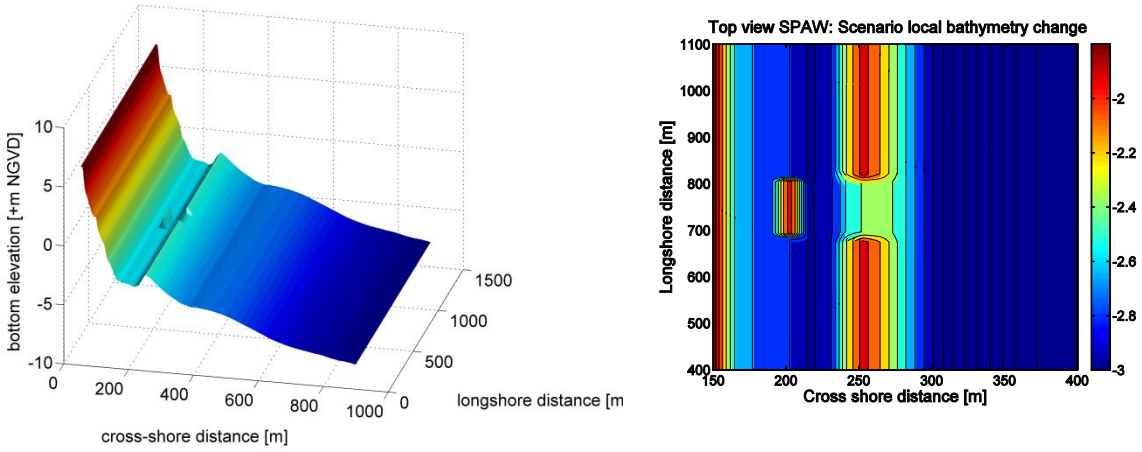

Figure 0.16. ***Scenario with local bathymetry change:*** *Schematic alongshore uniform bathymetry including a SPAW (left), and top view of SPAW configuration zoomed in at SPAW location (right).*

G Wave-driven depth averaged flow fields – initial bathymetry

This Appendix shows the depth-averaged velocity patterns around a SPAW for cases with the initial bathymetry and different water levels.

Depth-averaged Eulerian velocity, SPAW, Base case.

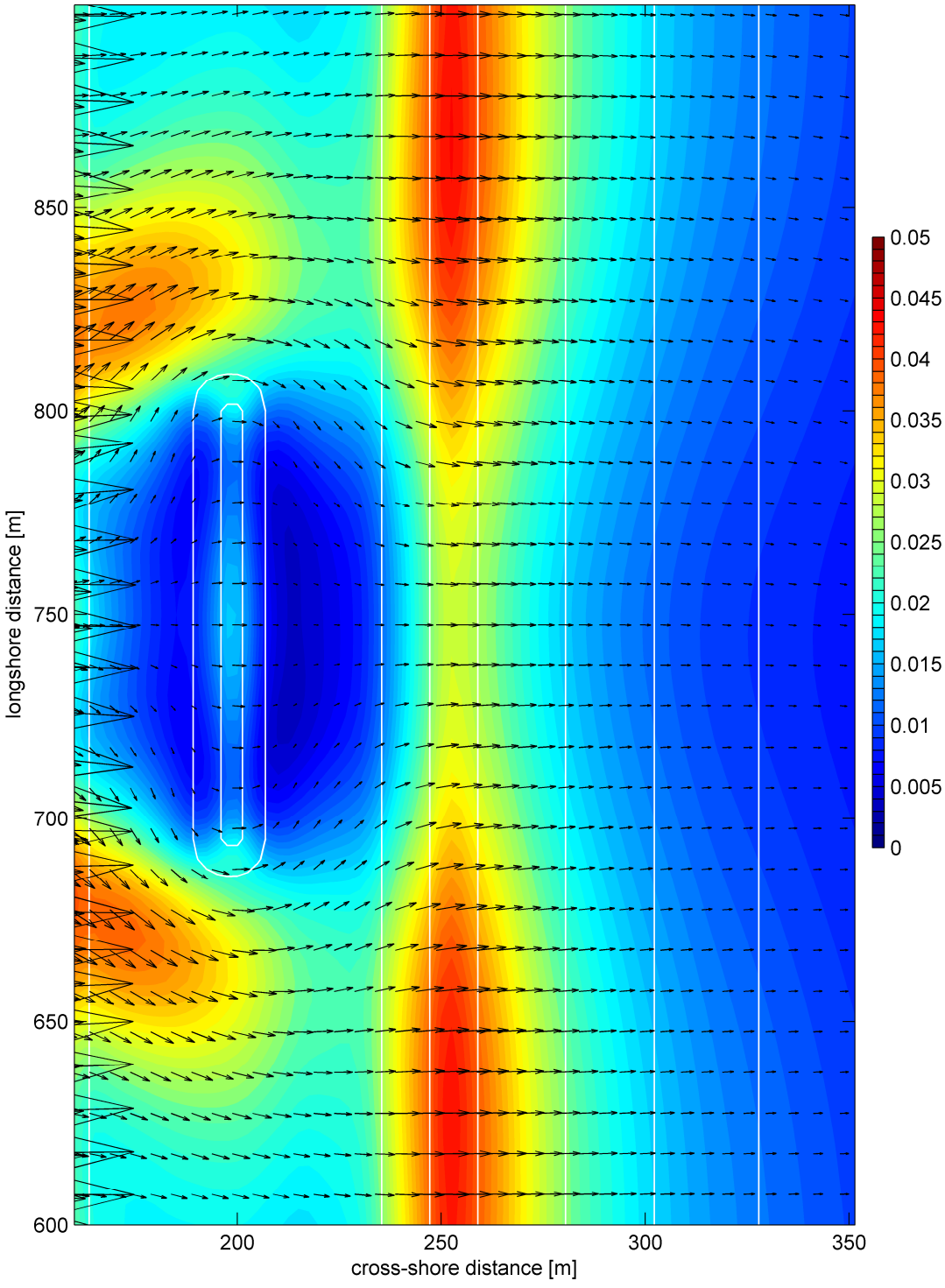

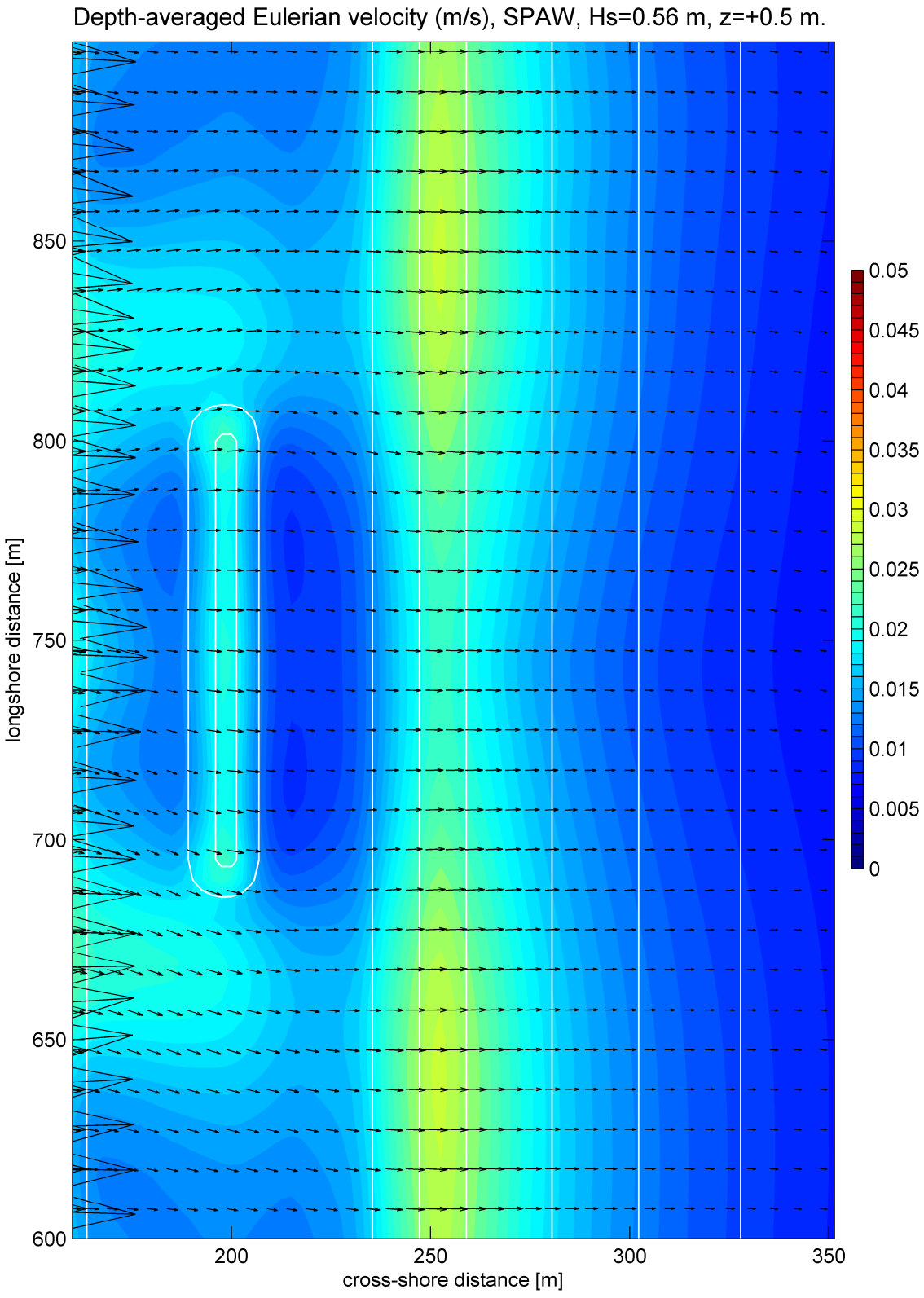
Depth-averaged Eulerian velocity (m/s), SPAW, Hs=0.56 m, z=+0.5 m.
longshore distance [m]
850
800
750
700
650
600
200
250
300
350
cross-shore distance [m]
0.05
0.045
0.04
0.035
0.03
0.025
0.02
0.015
0.01
0.005
0

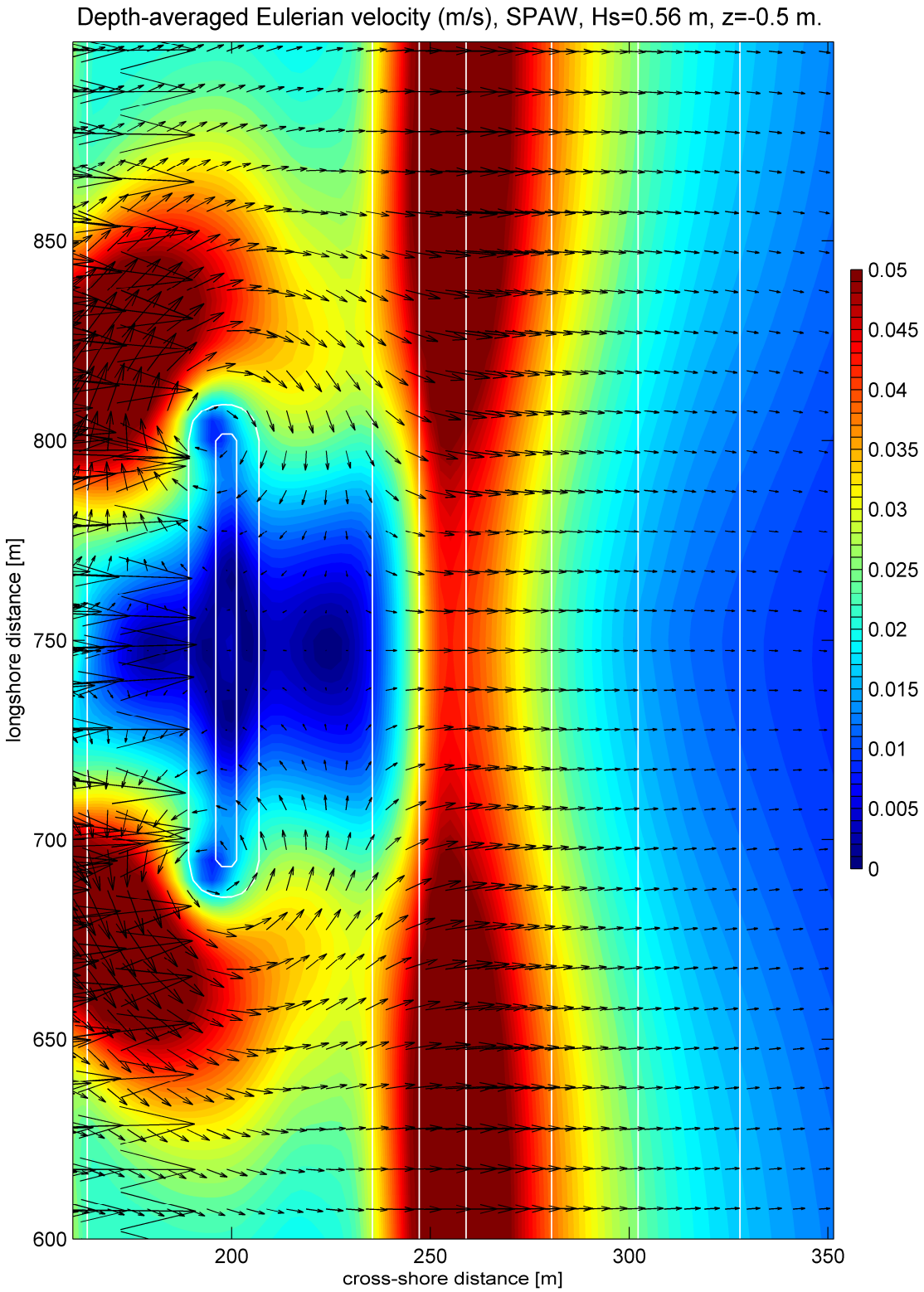
Depth-averaged Eulerian velocity (m/s), SPAW, Hs=0.56 m, z=-0.5 m.
longshore distance [m]
850
800
750
700
650
600
200
250
300
350
cross-shore distance [m]
0.05
0.045
0.04
0.035
0.03
0.025
0.02
0.015
0.01
0.005
0

Depth-averaged Eulerian velocity (m/s), SPAW, Hs=0.56 m, z=-0.5 m (test-version).

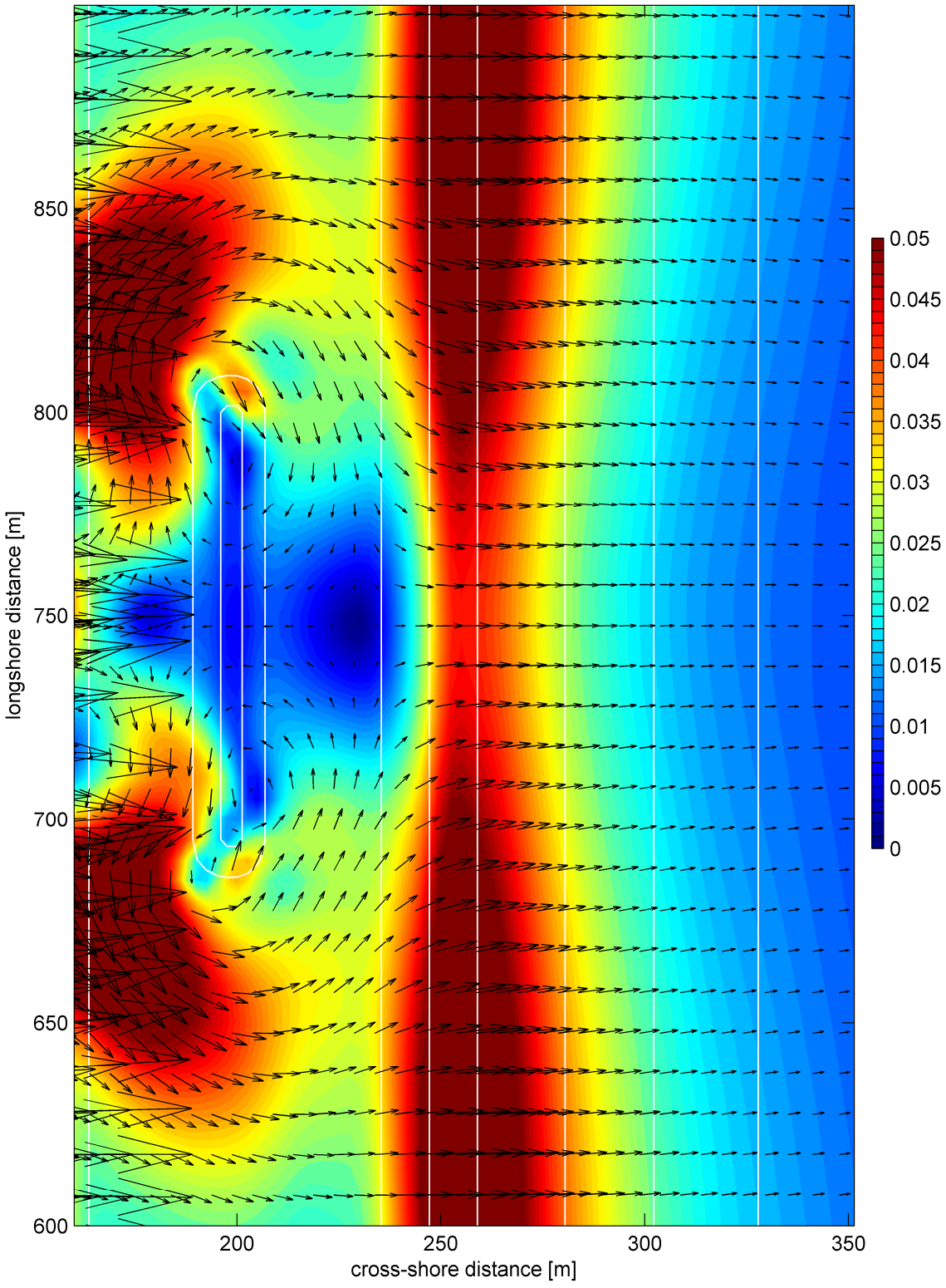

H Wave-driven depth averaged flow fields – morphometric changes

This Appendix shows the depth-averaged Eulerian velocity patterns around a SPAW for cases with different morphometric changes.

Depth-averaged Eulerian velocity (m/s), SPAW closer to shore, Hs=0.56 m, z=0 m.

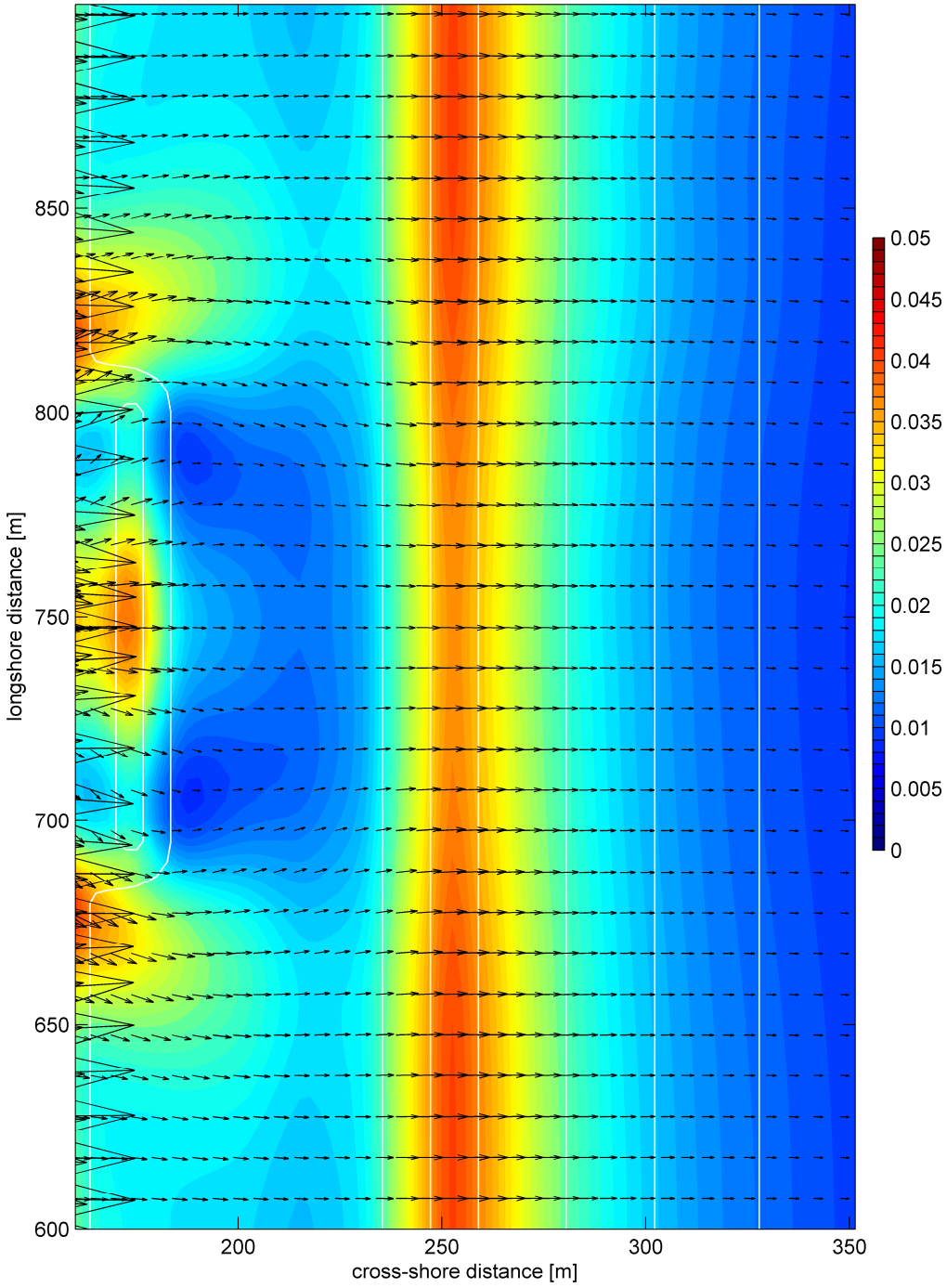

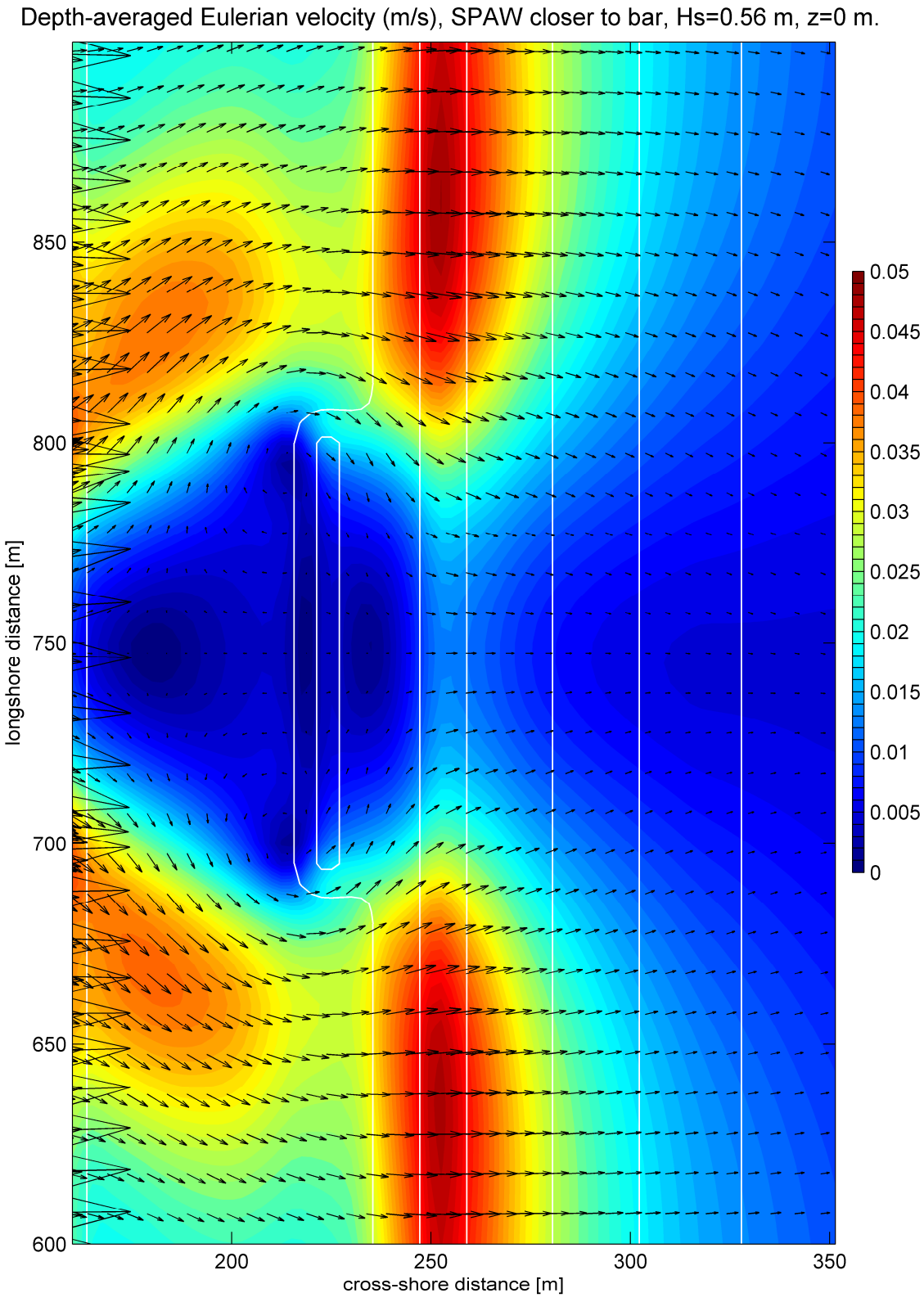
Depth-averaged Eulerian velocity (m/s), SPAW closer to bar, Hs=0.56 m, z=0 m.
longshore distance [m]
850
800
750
700
650
600
200
250
300
350
cross-shore distance [m]
0.05
0.045
0.04
0.035
0.03
0.025
0.02
0.015
0.01
0.005
0

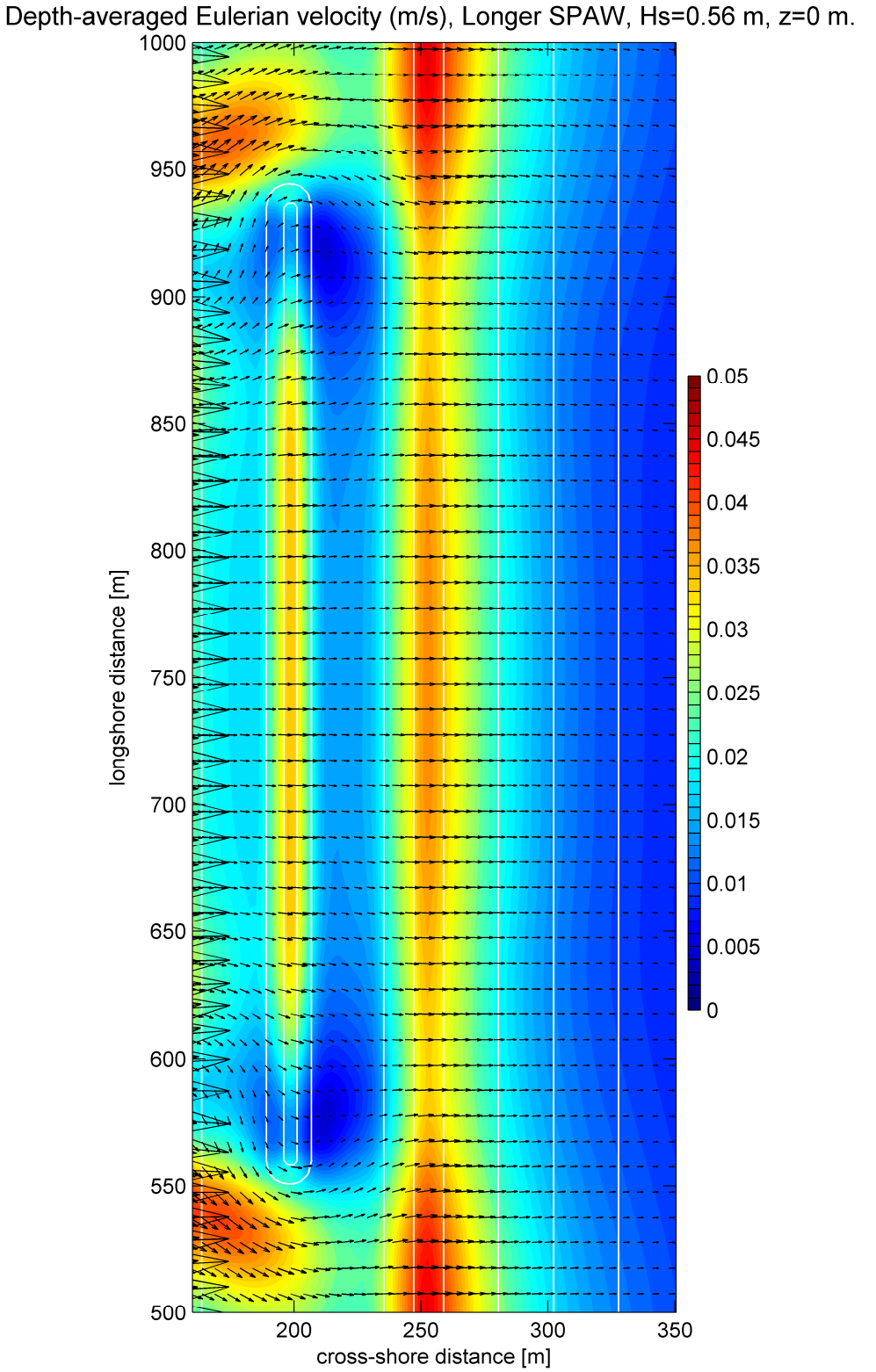
Depth-averaged Eulerian velocity (m/s), Longer SPAW, Hs=0.56 m, z=0 m.
longshore distance [m]
cross-shore distance [m]
1000
950
900
850
800
750
700
650
600
550
500
200
250
300
350
0.05
0.045
0.04
0.035
0.03
0.025
0.02
0.015
0.01
0.005
0

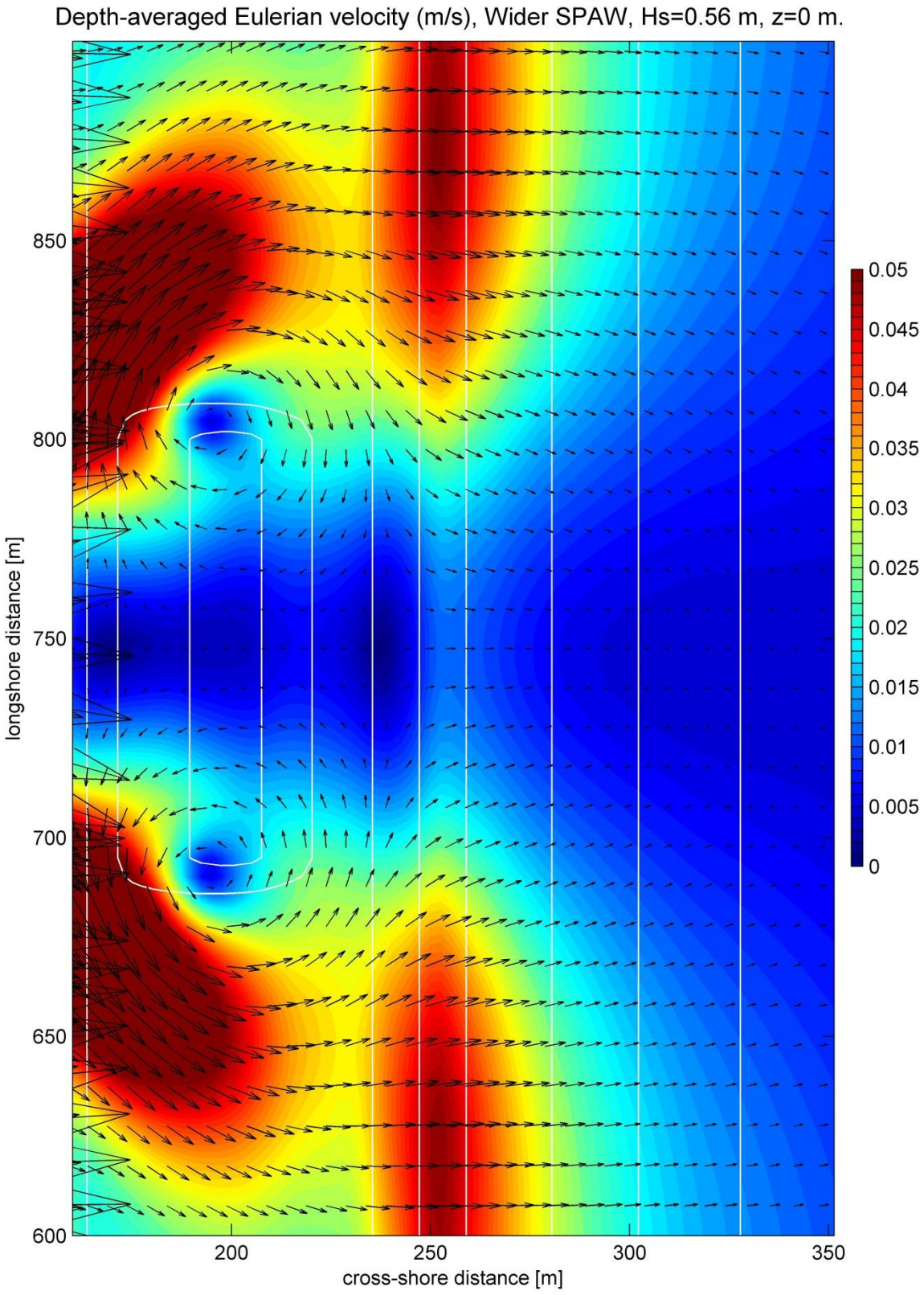
Depth-averaged Eulerian velocity (m/s), Wider SPAW, Hs=0.56 m, z=0 m.
longshore distance [m]
cross-shore distance [m]
850
800
750
700
650
600
200
250
300
350
0.05
0.045
0.04
0.035
0.03
0.025
0.02
0.015
0.01
0.005
0

Depth-averaged Eulerian velocity (m/s), Local Bathymetry change, Hs=0.56 m, z=0 m.

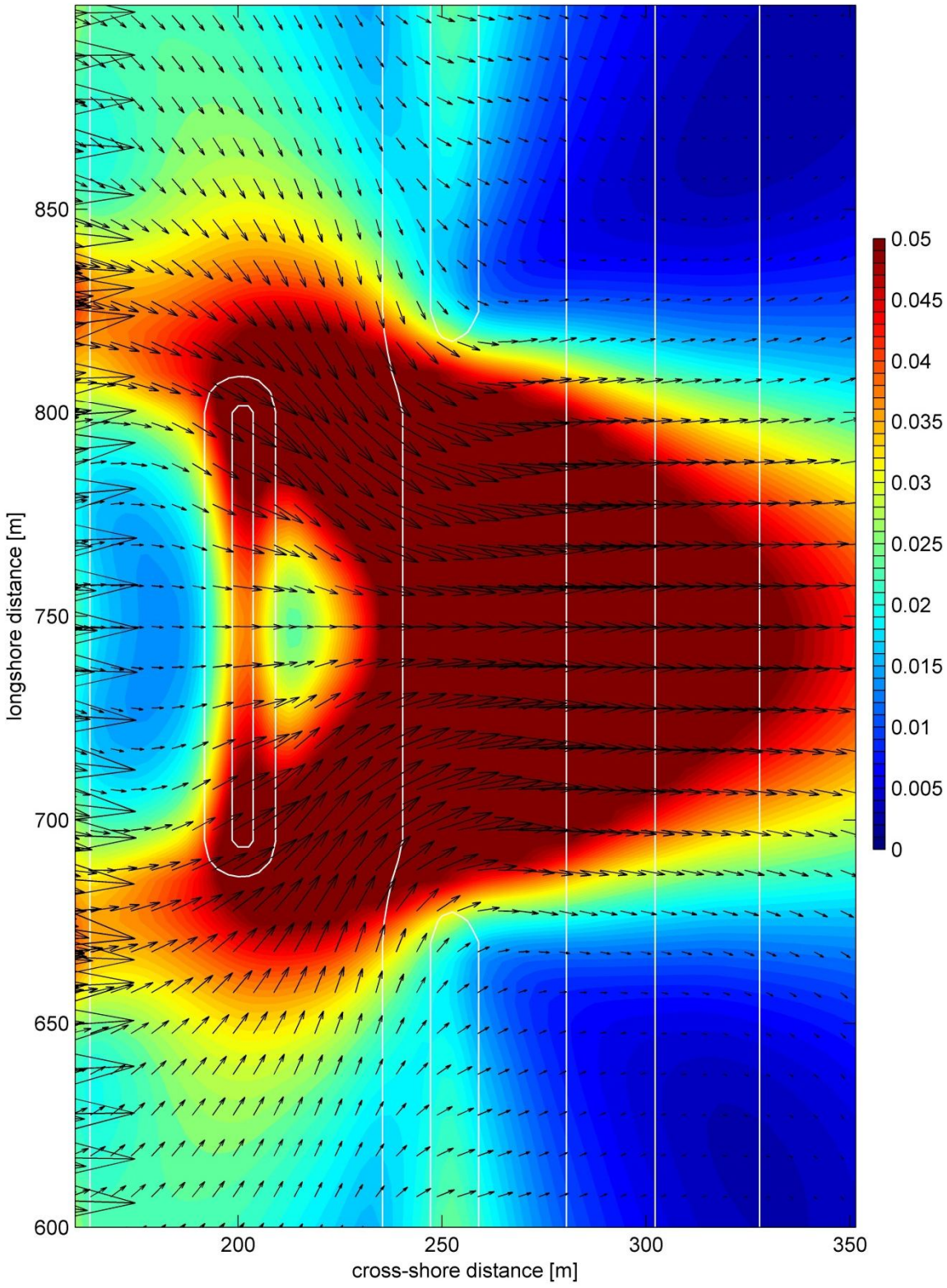

I Additional figures for H_s = 0.56 m with different water levels

In this Appendix additional figures are presented for the reader who is interested in more details of the runs with different water levels.

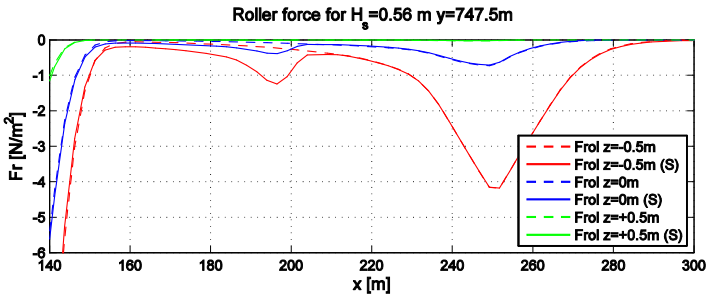

Figure 0.17. Cross-shore variations in roller forces for different water levels.

I.1 Sediment transport for z=+0.5 m

The sediment transport at the SPAW crest for the case of H_s=0.56 meter and a water level of z=+0.5m shows unrealistic results. Over the SPAW the transport is expected to be symmetric over the SPAW crest. However, the model results show a significant different transport on the northern and southern side of the SPAW (Figure 0.18 to 0.20).

These results are caused by some numerical issues, which can be seen in differences in vertical eddy viscosity (Figure 0.21). The profiles at the northern part of the SPAW show viscosity profiles with a large increase in the bottom layer, similar as was seen at a cross-shore distance x=280 meter (as discussed in paragraph 4.6). It would be very interesting to find out what exactly cause the differences in these profiles. However, this aspect falls outside the scope of this study. Unfortunately, the sediment transports for the case H_s=0.56 m and z=+0.5 m are therefore not discussed in more detail in this report.

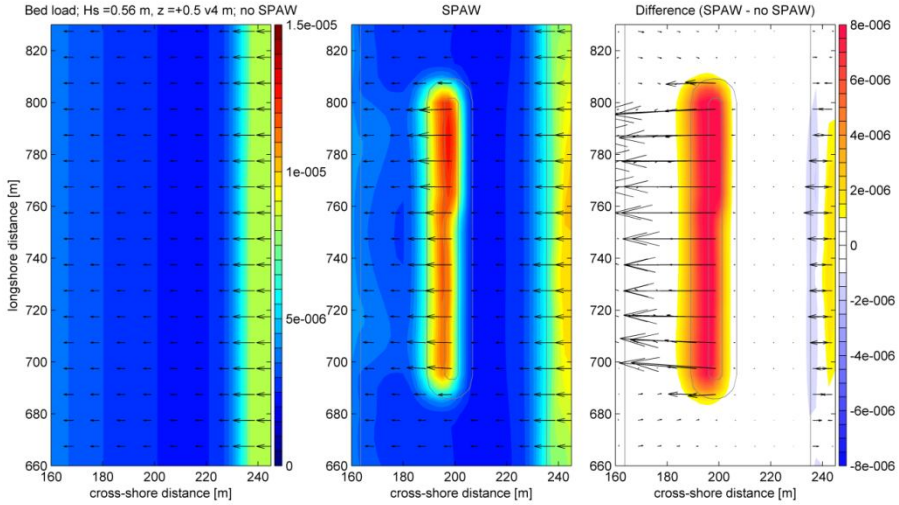

Figure 0.18. Top view of bed load transport showing reference situation (left), situation with a SPAW (middle) and the difference (right). The background colouring represents magnitude, vectors show directions, grey contour lines show bottom contours.

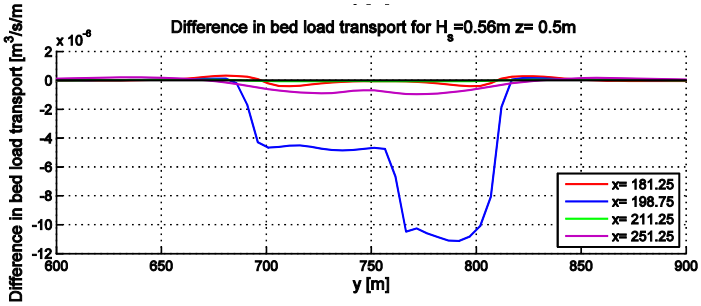

Figure 0.19. Longshore variation in bed-load transport load in x-direction (wave propagation) for different cross-shore transects. Negative values are onshore directed transports.

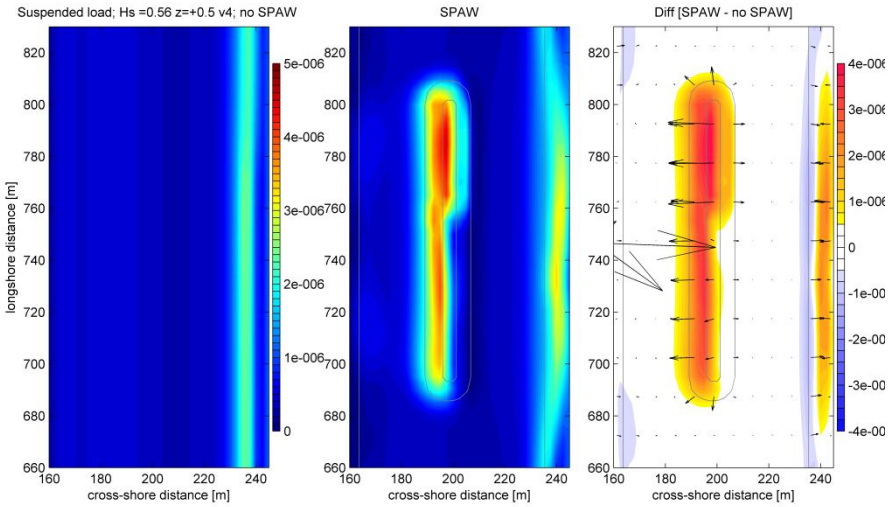

Figure 0.20. Top view of suspended load transport showing reference situation (left), situation with a SPAW (middle) and the difference (right). The background colouring represents magnitude, vectors show directions, grey contour lines show bottom contours.

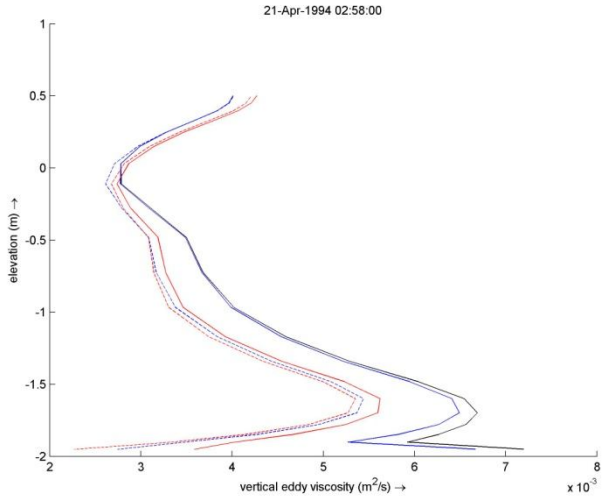

Figure 0.21. Vertical eddy viscosity profiles at longshore transect over crest of SPAW. The full lines indicate profiles at the north of the SPAW, dashed lines at the south. Black line in middle (y = 750m), blue line at quarter of SPAW (y = 775 and 825m), red line at tips of SPAW (y = 700 and 800m).